

Indoor cooling potential of trees under climate change

Coupling CityTree with building simulation to assess dynamics between shading and evapotranspiration

Wissenschaftliche Arbeit zur Erlangung des Grades
M.Sc. Ressourceneffizientes und Nachhaltiges Bauen
an der TUM School of Engineering and Design der Technischen Universität
München.

Betreut von Prof. Dr.-Ing. Werner Lang,
Roland Reitberger, M. Eng.
Lehrstuhl für energieeffizientes und nachhaltiges Planen und Bauen

Eingereicht von Juan Carlos Avalos Gutiérrez
juan.avalos@tum.de

Eingereicht am München, den 08.07.2024

Vereinbarung

zwischen

der Technischen Universität München, vertreten durch ihren Präsidenten,
Arcisstraße 21, 80333 München

hier handelnd der Lehrstuhl für Energieeffizientes und Nachhaltiges Planen und Bauen
(Univ.-Prof. Dr.-Ing. W. Lang), Arcisstr. 21, 80333 München

– nachfolgend TUM –

und

Herrn Juan Carlos Avalos Gutiérrez

– nachfolgend Autor –

Der Autor wünscht, dass die von ihr/ihm an der TUM erstellte Masterarbeit mit dem Titel

“Indoor cooling potential of trees under climate change: Coupling CityTree with
building simulation to assess dynamics between shading and evapotranspiration”

auf mediaTUM und der Webseite des Lehrstuhls für Energieeffizientes und
Nachhaltiges Planen und Bauen mit dem Namen der Verfasserin / des Verfassers, dem
Titel der Arbeit, den Betreuer:innen und dem Erscheinungsjahr genannt werden darf.

in Bibliotheken der TUM, einschließlich mediaTUM und die Präsenzbibliothek des
Lehrstuhls für Energieeffizientes und Nachhaltiges Planen und Bauen, Studierenden
und Besucher:innen zugänglich gemacht und veröffentlicht werden darf. Dies schließt
auch Inhalte von Abschlusspräsentationen ein.

mit einem Sperrvermerk versehen und nicht an Dritte weitergegeben wird.

(Zutreffendes bitte ankreuzen)

Zu diesem Zweck überträgt der Autor der TUM zeitlich und örtlich unbefristet das nichtausschließliche Nutzungs- und Veröffentlichungsrecht an der Masterarbeit.

Der Autor versichert, dass er alleiniger Inhaber aller Rechte an der Masterarbeit ist und der weltweiten Veröffentlichung keine Rechte Dritter entgegenstehen, bspw. an Abbildungen, beschränkende Absprachen mit Verlagen, Arbeitgebern oder Unterstützern der Masterarbeit. Der Autor stellt die TUM und deren Beschäftigte insofern von Ansprüchen und Forderungen Dritter sowie den damit verbundenen Kosten frei.

Eine elektronische Fassung der Masterarbeit als pdf-Datei hat der Autor dieser Vereinbarung beigelegt. Die TUM ist berechtigt, ggf. notwendig werdende Konvertierungen der Datei in andere Formate vorzunehmen.

Vergütungen werden nicht gewährt.
Eine Verpflichtung der TUM zur Veröffentlichung für eine bestimmte Dauer besteht nicht.

Der Autor hat jederzeit das Recht, die mit dieser Vereinbarung eingeräumten Rechte schriftlich zu widerrufen. Die TUM wird die Veröffentlichung nach dem Widerruf in einer angemessenen Frist und auf etwaige Kosten des Autors rückgängig machen, soweit rechtlich und tatsächlich möglich und zumutbar.

Die TUM haftet nur für vorsätzlich oder grob fahrlässig verursachte Schäden. Im Falle grober Fahrlässigkeit ist die Haftung auf den vorhersehbaren Schaden begrenzt; für mittelbare Schäden, Folgeschäden sowie unbefugte nachträgliche Veränderungen der veröffentlichten Masterarbeit ist die Haftung bei grober Fahrlässigkeit ausgeschlossen.

Die vorstehenden Haftungsbeschränkungen gelten nicht für Verletzungen des Lebens, des Körpers oder der Gesundheit.

Meinungsverschiedenheiten im Zusammenhang mit dieser Vereinbarung bemühen sich die TUM und der Autor einvernehmlich zu klären. Auf diese Vereinbarung findet deutsches Recht unter Ausschluss kollisionsrechtlicher Regelungen Anwendung. Ausschließlicher Gerichtsstand ist München.

München, den 08.07.2024

, den 08.07.2024

.....

.....

(TUM)

(Autor)

Erklärung

Ich versichere hiermit, dass ich die von mir eingereichte Abschlussarbeit selbstständig verfasst und keine anderen als die angegebenen Quellen und Hilfsmittel benutzt habe.

München, den 08.07.2024,

Ort, Datum, Unterschrift

Table of Content

Vereinbarung	I
Erklärung	III
Table of Content	V
Kurzfassung	1
Abstract	3
Abkürzungsverzeichnis	5
Glossary	7
1 Introduction	11
2 Research question.....	13
2.1 Objective of the project and hypothesis	13
2.2 Relevance of the research question.....	15
3 State of the art	17
3.1 Cooling potential through Shading	17
3.2 Cooling potential through Evapotranspiration	22
4 Methodology	31
4.1 Shading potential	32
4.2 Evapotranspiration potential.....	34
4.3 Tree features.....	37
4.4 Weather data	38
4.5 Key Performance Indicators.....	38
5 Case Study	39
5.1 Study area.....	39
5.2 Project Specifications.....	39
5.3 Weather	41
5.3.1 Weather of Munich.....	41
5.3.2 Weather Data.....	42
5.4 Data Validation.....	43
5.5 Proposal Design.....	46
5.6 Tree Species	46
5.7 Shading potential	48

Table of Content

5.8	Evapotranspiration potential	49
6	Results	53
6.1	Shading potential results	53
6.2	Evapotranspiration potential results.....	68
6.2.1	Cooling potential Evapotranspiration Outdoor.....	68
6.2.2	Cooling potential Evapotranspiration Indoor.....	73
6.3	Cooling potential Evapotranspiration and Shading.....	79
6.3.1	Share on the cooling potential	79
6.3.2	Cooling potential through shadow and evapotranspiration at $T_{air} \downarrow, 1.5^{\circ}C$	83
7	Discussion.....	89
7.1	Cooling potential through shading	89
7.2	Cooling potential through evapotranspiration	94
7.3	General.....	98
8	Conclusions.....	99
9	Acknowledgements	101
10	References.....	103
	List of figures.....	111
	List of Tables.....	113
	Appendix.....	115

Kurzfassung

Aufgrund der Folgen des Klimawandels ist in den kommenden Jahren weltweit eine repräsentative Steigerung des Kühlenergiebedarfs zu erwarten [1–3]. Verschattung- und Verdunstungskühlungspotenzial von Bäumen können die Außenlufttemperatur beeinflussen [4–11] und zum kühlenden Effekt des Mikroklimas beitragen [12]. Verschattung von Bäumen kann auch die Innentemperatur eines Raumes verbessern, indem sie ihn vor kurzwelliger Sonnenstrahlung schützt [13, 14] und somit dessen Kühlenergiebedarf reduziert [13–18]. Allerdings fehlt es noch eine dynamische Methode zur Integration vorhandener Verdunstungskühlungs-Daten in eine Simulation, sowie die Berücksichtigung der Auswirkungen von Baumwachstum, zur Untersuchung ihres Vorteils in Innenbereichen.

Ziel dieser Masterarbeit ist es, die Untersuchung des Einflusses des Kühlungspotenzials von Bäumen auf den thermischen Komfort eines Raumes durch ihre Verschattung und Verdunstungskühlung während der Sommersaison, wobei sie unter Bedingungen des Klimawandels wachsen. Die Ergebnisse haben dazu beigetragen, Möglichkeiten zur Verringerung der Notwendigkeit eines Kühlsystems zu ermitteln. Die Methode bestand darin, das Excel-Tool CityTree [19] mit einer thermischen Gebäudesimulation zu koppeln, um das Kühlungspotential von drei verschiedenen Bäumen auf den thermischen Komfort in einem bestehenden offenen Büro in München, Deutschland zu untersuchen. Die Studie wurde alle zehn Jahre von 2020 bis 2100 während der Sommersaison durchgeführt, wobei die Klimawandelprognosen RCP 4.5 und 8.5 berücksichtigt wurden. Die Verdunstungskühlungspotenzial wurde mittels einer Sensitivitätsanalyse untersucht, die auf der Verdunstung von Bäumen und ihrer Fähigkeit zur Senkung der Außenlufttemperatur, basiert.

Im Durchschnitt hat die Verschattung von Bäumen im Jahr 2100 ein Kühlungspotenzial von etwa 2°C aufzuweisen. Der größte Wert entsprach 2,4°C. Insgesamt wurde ein Kühlungspotenzial durch Verschattung und Verdunstungskühlung zwischen 2,8°C und 3,4°C beobachtet, wobei beide Klimawandelprognose berücksichtigt wurden. Die Verdunstungskühlung entsprach bis zu 21% (0,59°C) bzw. 38% (1,29°C) des gesamten Kühlungspotenzials. Insgesamt haben die Bäume dazu beigetragen, die Übertemperaturgradstunden (CDH) zwischen 45% und 55% im Vergleich zu denen ohne Bäume zu verringern. Zusätzlich entsprach die Häufigkeit der

Kurzfassung

Innenraumtemperaturen über 32°C etwa 7% bis 10% der Nutzungszeit, d.h., rund 30% weniger als ohne Bäume. Diejenigen, die unter 26°C lagen, sind von 10% auf zirka 30% bzw. 20% der Nutzungszeit gestiegen, unter Berücksichtigung der beiden Klimawandelprognosen. Im Falle der Installation eines Kühlsystems könnten Bäumen dazu beitragen, dessen Betriebszeit zu reduzieren.

Abstract

A significant increase in the cooling energy demand is expected worldwide in the next decades as a consequence of climate change [1–3]. Shading and evapotranspiration potential of trees can influence the outdoor air temperature [4–11] and contribute to the cooling effect of the microclimate [12]. Shading of trees contributes to enhancing indoor thermal comfort [13, 14] by protecting an interior space from shortwave radiation, and thus reducing the cooling energy demand of a space [13–18]. Nonetheless, a dynamic method for integrating existing evapotranspiration related data into a simulation as well as considering the effects of tree growth to study its benefits indoors are still missing.

The objective of this paper is to study the impact of cooling potential of trees on the indoor thermal comfort in a space through their shading and evapotranspiration potential during the summer season, as they grow under climate change conditions. The results contributed to identifying opportunities for reducing the need for an air conditioning system. The method consisted of coupling the excel tool CityTree [19] with a building simulation to assess the cooling potential of three different trees on the indoor thermal comfort in an existing open office space in Munich, Germany. The study was conducted every ten years between 2020 and 2100 during the summer season considering the climate change projection scenarios RCP 4.5 and RCP 8.5. The evapotranspiration potential was studied through a sensitivity analysis based on the transpiration of trees and their capacity to reduce the outdoor air temperature.

On average, by 2100, shading of trees showed a cooling potential of 2°C. The greatest value corresponded to 2.4°C. A total cooling potential through shading and evapotranspiration between 2.8°C and 3.4°C was observed, considering both climate change projections. Evapotranspiration accounted for up to 21% (0.59°C) and 38% (1.29°C), respectively, of the total cooling potential. Overall, trees contributed to reducing the cooling degree hours (CDH) between 45% and 55% compared to those without trees. Furthermore, the time frequency of operative temperatures above 32°C corresponded to about 7% to 10% of the occupancy time, i.e., about 30% less frequent than without trees. Those below 26°C increased from about 10% to almost 30% and 20% of the occupancy time under each climate change projection. In the event of installing a cooling system, trees could contribute to reducing its operating time.

Abstract

Abkürzungsverzeichnis

Hier bitte verwendete Abkürzungen auflisten.

CDR	Carbon dioxide removal
CFD	Computational fluid dynamics
COP	Conference of the Parties
CDD	Cooling degree days
CDH	Cooling degree hours
$T_{air\downarrow,daily\ average}$	Daily average outdoor air temperature reduction
$(T_{air\downarrow,Target})$	daily average outdoor air temperature reduction target
E_L , daily average	Daily average transpiration rate
E_L , daily average, 2060	Daily average transpiration rate in 2060
ENPB	Energy Efficient and Sustainable Design and Building (for its acronym in German)
EP	EnergyPlus
EPW	EnergyPlus Weather
EEA	European Environmental Agency
EU	European Union
$T_{air,f}$	Final outdoor air temperature
DIN	German Institute for Standardization (for its acronym in German)
DFG	German Research Foundation (for its acronym in German)
DWD	German Weather Service (for its acronym in German)
GWP	Global warming potential
GH	Grasshopper
GHG	Greenhouse gas
HB	Honeybee
$T_{air,i}$	Initial hourly outdoor air temperature
IPCC	Intergovernmental Panel on Climate Change
IEA	International Energy Agency
LB	Ladybug
MSL	Meters above sea level
T_{air}	Outdoor air temperature
$T_{air\downarrow}$	Outdoor air temperature reduction
PV	Photovoltaic
PIT	Point-in-time
RCP	Representative Concentration Pathways
RTG	Research Training Group
R^2	Coefficient of determination
SHGC	Solar heat gain coefficient
SDG	Sustainable Development Goals
TUM	Technical University of Munich
E_L	Transpiration
$E_L T_{air\downarrow,Target,Analysis\ Year}$	Transpiration-to-outdoor air temperature reduction ratio
UN	United Nations

Abkürzungsverzeichnis

UGI	Urban green infrastructure
VPD	Vapour pressure deficit
VLT	Visible light transmittance
WWR	Window-to-wall ratio

Glossary

Anisohydric behaviour refers to plants that have a daytime leaf water potential which markedly decreases with evaporative demand during the day and is lower in droughted than in watered plants. [20]

Anthropogenic heat is heat released to the atmosphere as a result of human activities, often involving combustion of fuels. [21]

Carbon sequestration is a phenomenon for the storage of CO₂ or other forms of carbon to mitigate global warming and its one of the important clause of Kyoto Protocol, through biological, chemical or physical processes; CO₂ is captured from the atmosphere. [22]

Cooling Degree Days (CDD) are a measure of how hot the temperature was on a given day or during a period of days [23]. It is an index used to estimate the amount of energy required for cooling during the warm season [24].

Cooling/Heating degree hours (CDH / HDH) represent the required energy to cool/warm the indoor environment to reach the comfort zone. [25]. The higher the degree hours, the higher the cooling/heating demand is, and the greater the energy required to maintain indoor thermal comfort conditions [26].

Degree days are measures of how cold or warm a location is. A degree day compares the mean (the average of the high and low) outdoor temperatures recorded for a location to a standard temperature, usually 65° Fahrenheit (F) in the United States. The more extreme the outside temperature, the higher the number of degree days. A high number of degree days generally results in higher energy use for space heating or cooling. [23]

Diameter at breast height (DBH) is the standard for measuring trees. DBH refers to the tree diameter measured at 4.5 feet (1.37 m) above the ground. [27]

Ecosystem services are the direct and indirect contributions ecosystems (known as natural capital) provide for human wellbeing and quality of life. [28]

Evapotranspiration is the loss of water from the soil both by evaporation from the soil surface and by transpiration from the leaves of the plants growing on it. [29]

Glossary

Operative temperature is the average of the air temperature and the mean radiant temperature weighted, respectively, by the convective heat transfer coefficient and the linearized radiant heat transfer coefficient for the occupant. [30]

Phenology is defined as the study of the timing of recurring biological events, the causes of their timing with regard to biotic and abiotic forces, and the interrelation among phases of the same or different species. [31]

It is the study of phenomena or happenings. It is applied to the recording and study of the dates of recurrent natural events (such as the flowering of a plant or the first or last appearance of a migrant bird) in relation to seasonal climatic changes. Phenology thus combines ecology with meteorology. [32]

Solar shading coefficient (C_m) is an index that allows determination of the performance of the solar protection at glazing. It corresponds to the fraction of the beam solar irradiation that impacts the glazing with and without the use of solar shadings. [33]

Street tree is a tree growing in a street (occasionally at the edge of the carriageway, usually in a verge or footway). [34]

Surface roughness refers to the irregularity of the three-dimensional shape of an area. In particular, it is related to the degree of irregularity of buildings. [35]

Thermal comfort is that condition of mind that expresses satisfaction with the thermal environment. Because there are large variations, both physiologically and psychologically, from person to person, it is difficult to satisfy everyone in a space. The environmental conditions required for comfort are not the same for everyone. [30]

Transpiration in botany, a plant's loss of water, mainly through the stomata of leaves. Stomatal openings are necessary to admit carbon dioxide to the leaf interior and to allow oxygen to escape during photosynthesis. [36]

It is the passage of water through a plant from the roots through the vascular system to the atmosphere. [37]

Urban green space means all green urban areas; broad-leaved forests; coniferous forests; mixed forests; natural grasslands; moors and heathlands; transitional woodland-shrubs and sparsely vegetated areas. [38]

Urban Heat Island (UHI) is a typical feature of the urban climate. It is characterised by the difference in air temperature between the hotter city and its cooler surrounding

countryside and reaches its maximum during nighttime under cloudless and calm weather conditions. This difference can be as much as 10 Kelvin in large cities. The air temperature in cities depends strongly in part on building geometry, the thermal properties of the building fabric, radiation properties of the urban surfaces and anthropogenic thermal release, e.g. domestic heating, traffic and industry. [39]

Vapor pressure deficit (VPD) is a measure of how dry or humid the air is. When it's hot outside, the air can hold a lot of water vapor. When it's cooler outside, the air can't hold as much water vapor. The difference between how much water vapor the air can hold and how much it actually contains is called the vapor pressure deficit, or VPD. [40] It is calculated as the difference between the amount of moisture that's actually in the air and the amount of moisture that air could hold at saturation. VPD is similar to relative humidity, which uses a percentage to describe how much moisture is in the air. But unlike relative humidity, temperature is always included in calculations of VPD. [41]

1 Introduction

Climate change is part of the consequences of carbon emissions, leading to an increase in global temperature [1]. A significant increase in the electricity demand for cooling is expected by 2050 worldwide [2, 3]. Climate neutrality is one of the main goals among countries [42]. It aims not only to reducing energy demand, but to reducing carbon emissions [43]. According to the climate change scenarios from the Intergovernmental Panel on Climate Change (IPCC) [44], at higher greenhouse gas emissions, the more difficult it will be to avoid global warming at temperatures below 2°C [45].

The search for passive strategies arises from the need to find solutions to face these challenges [46]. Urban green infrastructure (UGI), e.g., trees, provide several regulating ecosystem services [22, 47–51]. This paper focused on the cooling potential of trees, which is generated through their shading and evapotranspiration potential. On average, most of the cooling potential is attributed to the shading potential of trees. Both properties are interrelated [13, 15, 49, 51] and depend on tree species and climate conditions [52].

The impact of shading of trees in indoor environments has proved benefits by reducing operative temperatures [13, 14]. It also has the capacity to reducing the cooling energy demand of a space during the hot season in locations with different climate conditions [13–18]. The potential of evapotranspiration of trees to reducing the outdoor air temperature has been studied through on-site measurements and simulation studies [4–11]. However, information regarding its impact on indoor environments is limited. The capacity of evapotranspiration to reducing the indoor air temperature has been identified as part of the total cooling potential of a tree [53]. Results regarding its potential to modify the relative humidity in a space were not representative nor conclusive [16]. This property depends on several climatic conditions and environmental factors, that is usually suppressed in urban environments [5, 54–56].

The cooling potential of trees has been studied through on-site measurements and simulation studies. Evapotranspiration potential is not considered to be as representative as shading potential [48, 57]. However, a dynamic methodology to replicate [58] and integrate evapotranspiration related data into a simulation study is still missing. Furthermore, there is still room for analyzing their impact in a space as they grow over time.

Introduction

As part of the project Research Training Group of Urban Green Infrastructure (RTG-UGI), the objective of this topic is to couple the excel tool CityTree with a building simulation to study the cooling potential through shading and evapotranspiration of trees growing over time under climate change conditions. This way, their impact on indoor thermal comfort can be determined, as well as their capacity to mitigate climate change and reduce or even suppress the need for an air conditioning system. It is proposed to individually analyze each ecosystem service and then integrate them to determine the potential of each one. The results aim to support the benefits of UGI on a long-term basis and the cooling potential of trees in the indoor thermal comfort of a space.

2 Research question

Trees have always been present in the human environment. They have been used as ornamental, aesthetic, and delimitation elements. They contribute to the psychological wellbeing of humans, because of their biophilic effect. According to the European Environmental Agency (EEA) [47], trees provide several regulating ecosystem services such as solar protection radiation [47–49]; climate regulation [47, 50]; urban heat island (UHI) reduction [51]; air quality and runoff regulation [47]; and carbon sequestration [22].

2.1 Objective of the project and hypothesis

The RTG-UGI is a graduate program from the Technical University of Munich (TUM), Germany. It focuses on transdisciplinary research on urban green and blue infrastructure to understand the synergies of the ecosystem services. It aims to develop new solutions for UGI to enhance the quality of life, sustainability, and resilience of cities. It is funded by the German Research Foundation (for its acronym in German DFG). This topic aims to contribute to the research cluster 2, subproject 6: indoor comfort and energy consumption of buildings. [59]

Indoor thermal comfort is influenced by meteorological conditions such as outdoor temperature, solar radiation, relative humidity and wind speed [50]. Solar protection radiation and evapotranspiration of trees contribute to the cooling effect of a microclimate [12]. Trees can improve indoor temperature through their capacity to protect building and interior spaces from shortwave solar radiation [13]. These ecosystem services are interrelated and may play an important role in the interior thermal comfort of a space [13, 15, 49, 51].

International agreements aim to reduce carbon emissions and achieve climate neutrality by incorporating UGI [3, 38, 43, 46, 60, 61]. Researchers have analyzed the potential of UGI to minimize or even suppress the use of air conditioning systems [13, 15–17]. Thus, trees are a potential passive alternative to reduce heat island effect, improve the indoor temperature in a space, and contribute to climate change mitigation by reducing carbon emissions related to air conditioning systems.

The objective of this topic is to individually analyze the impact of the cooling potential through shading and evapotranspiration of street trees growing over time under climate change conditions on the interior space and address the following research questions:

Research question

- Can street trees contribute to improving indoor thermal comfort in buildings during the hot season in the long term, from 2020 to 2100?
- Can street trees contribute to mitigating climate change in the long term (2020-2100) by reducing or even suppressing the need for an air conditioning system?
- What is the potential contribution of the cooling effect through evapotranspiration of street trees to enhance indoor thermal comfort in a space?

After identifying the impact of each ecosystem service, they were combined to find synergies and support the results for the research questions.

2.2 Relevance of the research question

Because of the consequences of global warming, cooling is expected to have a greater electricity demand [62]. In 2016, the International Energy Agency (IEA) prognosed that, by 2050, the cooling degree days (CDD) would increase about 25% globally, posing a challenge for dealing with higher temperatures and covering the cooling energy demand [2]. For instance, the electricity demand in Texas has increased 4% as a reason of rising the average daily temperature above 24°C by 1°C [62]. About 2 billion air conditioning units worldwide account for one of the main electricity demands in buildings [46]. 70% of the whole cooling energy demand belongs to the residential sector [46]. Up to now, more than one-billion people have no access to cooling systems and they risk extreme heat [3]. Conventional cooling systems account for more than 7 % of the global greenhouse gas (GHG) emissions [3]. Actions are required, otherwise by 2050 the energy demand is highly expected to increase three times [3].

Energy use and climate change are high priority topics worldwide. Nowadays, 50% of the population live in cities and it is expected to increase up to 70% by 2050 [43]. Cities account for 60% to 80% of the total energy consumption and 75% of the total carbon emissions [43]. Since we spend on average 90% of the occupancy time in interior spaces [63, 64], energy use, indoor comfort, and their related carbon emissions are important topics to consider in building construction. According to the IEA, the building sector is responsible for 30% of the global final energy consumption as well as 26% of the carbon emissions from energy combustion and industrial processes [42].

Building energy codes and standards for new buildings have been established around the world to achieve environmental and energy goals, such as Net Zero Emissions Target by 2050 [42]. Some countries have established preliminary targets to be achieved by 2030 [42]. By reducing 25% of the energy consumption in buildings, fossil fuels consumption could be decreased by over 40% by 2030 [42]. According to the IEA, carbon emissions must be reduced by 2035, 80% in advanced economies and 60% in both emerging and developing countries, so the 1.5°C temperature goal can be achieved [44].

Despite these efforts, data shows a constant grow in energy consumption over time [42]. From 2021 to 2022 the total energy demand in the building sector grew 1%, cooling demand increased more than 3% while heating demand decreased 4% [42]. 20% of the total electricity consumption in buildings, which corresponds to 10% of the global

Research question

electricity consumption, is used for cooling purposes [2]. By 2050, two out of every three households around the world are expected to operate with air conditioning system, especially those in hot weather locations [2].

The IEA claims the efficiency of air conditioning systems to be a key solution, which could contribute to reducing the future energy demand by 50% [2]. However, both the implementation of energy efficiency standards and passive strategies are essential to overcome this challenge [46]. In 2023, the Conference of the Parties (COP) 28 integrated the topic of sustainable cooling into its agenda [3]. The actions focuses on energy efficiency and climate-friendly cooling solutions [3] .

The United Nations (UN) is addressing these challenges through the Sustainable Development Goals (SDG): they aim to reduce carbon emissions by reducing the electricity use and improving energy efficiency; as well as to reduce the global temperature by 1.5°C by 2030 in accordance with the Paris Agreement. Several nations have been working on promoting carbon offsets not only as an environmental benefit, but also as a business and economic strategy. [43]

The European Union (EU) has been working in the last decades on the European Green Deal, which aims to achieve climate neutrality by 2050 [60]. As part of this proposal, they created the EU's biodiversity strategy for 2030 to mitigate the effects of climate change concerning energy efficiency, building renovation, nature restauration, among other topics [60, 61]. Regarding nature, an EU Nature Restoration plan and a Nature Restoration Law were proposed [38]. The main target related to urban ecosystems is to increase the total area of urban green spaces by at least 3 % by 2040, and 5% by 2050 compared to those from cities, towns and suburbs in 2021 [38]. It also aims to incorporate green spaces into existing and new buildings as well as infrastructure developments [38].

The IPCC announced in its last report of 2023, that it is expected to exceed global warming temperature by 1.5°C in the near term of the 21st Century, by 2030, and, consequently, it will be difficult to avoid warming below 2°C by 2100. They have been working on different scenarios projections. One of the primary actions for this decade (2020-2030) consists of a deep global GHG reduction and achieving net zero GHG emissions. To achieve these goals, it is necessary to perform carbon dioxide removal (CDR) measures. Some of the mitigation measures for CDR comprise improving energy efficiency and forestry. [45]

3 State of the art

The presented literature compiles the findings of on-site measurements and calculations assisted with software simulations related to the cooling potential of trees through solar protection radiation and evapotranspiration in outdoor and indoor environments.

Outdoor air temperature in urban environments is influenced by, among other elements, the effect of trees on the solar radiation, evapotranspiration of trees and urban surface roughness [12]. These properties are interrelated and their results can vary depending on the approach, analysis period and climate location [12]. Trees contribute to reducing the solar radiation on horizontal and vertical surfaces. [65]. Indoor thermal comfort is influenced by meteorological conditions such as outdoor temperature, solar radiation, relative humidity and wind speed [50]. Since trees have a direct impact on outdoor environments, they are potential passive cooling strategies to improve indoor thermal comfort. Besides, they can contribute to reducing both cooling and heating energy demand [49].

3.1 Cooling potential through Shading

Outdoor environments

Solar protection radiation occurs as trees block, i.e., absorb, the incoming shortwave radiation from the sun. In a clear sky, the incoming shortwave radiation under a tree is lower. At night, the cooling exchange of outdoor exposed surfaces increases at a fast rate. Trees contribute to decreasing the cooling effect at night by emitting longwave radiation at a lower rate. On average, temperatures at night under a tree are higher than on exposed surfaces. Under an overcast sky, the effect on longwave radiation of trees is reduced. [65]

The solar radiation protection related to the tree crown density on horizontal surfaces can be about 5% higher than on vertical surfaces [17]. As a tree grows, both its crown and the shading area increase, nonetheless the shade density decreases because the leaf area density decreases over time [66]. Besides, due to seasonal phenology, the value for shading coefficient cannot be considered as a static value [67]. Contrary to evergreen trees, which provide shade and wind protection the whole year, deciduous trees provide most of the shade and wind speed reduction in summer [65]. The cooling effect of trees through shading also depends on the distance between trees, leaf area density, growth rate, water availability and shade density [48, 51, 66].

The higher is the leaf area density, the higher is the shadow potential. However, the lower the leaf area density, the more the leaves are exposed to solar radiation, which has an impact on the evapotranspiration of a tree. Manickathan observed through a computational fluid dynamics (CFD) study that the shading effect of trees contributed to reducing the air temperature at the bottom of a tree canopy. [51]

The study results of Shashua-Bar and Hoffman [48] showed that the shading potential of trees is more relevant than their evapotranspiration potential when it comes to cooling effect and outdoor thermal comfort: 80% of the cooling effect of trees was attributed to their shading effect in a surface with 61% of tree cover. [48]

It is suggested to prioritize the cooling potential of trees by shadow rather than by evapotranspiration in cities with high humidity and low temperature levels, where vapour pressure of air is near to saturation levels, which causes evapotranspiration of trees to decrease. Besides, shadow potential has a greater impact on cooling effect because it prevents from solar radiation, which significantly influences thermal comfort. [51]

A study performed in Melbourne, Australia, investigated the impact on exterior surface temperature of two different tree species at different distances from a building's façade. A building without tree cover was used as reference for the measurements. The shading coefficient for different tree species was calculated based on the amount of solar irradiation blocked by the tree and received on the exterior walls. During the day, the air temperature between the tree and the west facing exterior wall was lower than the wall without vegetation. At night, the air temperature of the west facing exterior walls was about 1°C warmer than the one without trees. The closer the trees are to exterior surfaces, the greater is the impact on the temperature reduction of the surfaces. [67]

Since streets represent a significant surface of an urban city, tree canopy cover can be a potential strategy to mitigating UHI effect and cool down the air temperature in urban areas. Such is the case for Tel-Aviv, where streets account for 25% of the urban city area. The cooling effect of trees in different urban environments in Israel during the summer season contributed to reducing the average air temperature about 2.8 °C. [48]

Nonetheless, a street with heavy traffic can diminish the cooling effect of trees about 2°C [68]. For instance, tree cover on a street with heavy traffic showed an air temperature reduction of about 1°C [48]. Meanwhile the air temperature of a 0.15-ha garden cooled down up to 4 °C [48]. Street shading using tree canopy cover can be a dynamic strategy, it can be regulated by proper selection and positioning of tree species in new green areas [48]. In existing areas, it can be controlled through adequate

maintenance and pruning [48]. Because of the time required for trees to grow, it is suggested to incorporate climbing plants to increase the shading potential on the required surfaces [67]. While a tree canopy contributes to reducing the UHI effect during the summer season, depending on the building height and orientation, it can limit the solar gains in an interior space during the cold season [68].

Indoor environments

Indoor thermal comfort in a space highly depends on the effectiveness of shading elements to prevent solar gains on exposed surfaces during the hot season [13]. Shading of trees can contribute to this end [13]. Besides, a proper combination of high albedo materials in conjunction with adequate species, number and position of trees can contribute to reducing cooling energy demand [15].

The synergies between daylight, shading, artificial lighting, cooling can have significant impacts on the energy demand of a space with direct access to daylight and UGI [69]. Cooling demand is influenced by the solar radiation that penetrates through windows [70]. Solar protection has an impact on the cooling and lighting demand of a space [33]. Solar shading coefficient is used to determine the solar protection efficiency of an element [33]. The visual performance through conventional solar shading devices is usually opposite to its cooling energy performance [33]. By reducing cooling loads, internal loads by artificial lighting increase [33]. Furthermore, depending on the material properties of a shading device, it can reach a temperature up to 60°C while exposed to solar radiation, limiting the possibility for natural ventilation [13]. The surface temperature at the top of a tree canopy also increases, but as observed by [71], it is not so different from the air temperature.

Tree size, geometry, leaf development and location related to the building orientation can have an impact on its cooling and heating energy performance. For instance, trees located on the south facade of a conditioned building in State College, Pennsylvania provided less solar protection and less cooling potential in comparison with trees located on the west and east facades. Tree shading on the south facade can make a lower contribution to reducing the cooling energy demand, while increasing the heating energy demand during the cold season. Nonetheless, it is suggested to use UGI to prioritize a higher cooling potential during the summer season over increasing the heating demand in winter. As exposed in the Section 2.2, cooling energy demand is expected to increase in the following decades because of the higher temperatures [2, 42]. This way the need to install an air conditioning system can be suppressed. Furthermore, deciduous trees

may contribute to reducing the thermal insulation requirements for winter, while increasing the cooling potential in summer. [17]

While tree cover can contribute to higher thermal comfort levels, energy for heating and lighting increases. Besides, the energy generation from a photovoltaic (PV) system can be decreased. This can be understood as a higher global warming potential caused by tree cover. Nonetheless, the study of Reitberger et. al. in [72] concluded that trees can contribute to steer the trade-offs between lifecycle-based global warming potential (GWP) and outdoor thermal comfort. [72]

The simulation study of a house in Montreal, Canada showed greater cooling savings in urban than in rural environments by incorporating vegetation cover and improving the albedo of exterior materials. The cooling demand was reduced by about 40% and 30% respectively by increasing the vegetation cover by 30% and improving the albedo by about 20%. Besides, greater cooling savings in urban environments were attributed to the impact of wind shielding of trees, which has a greater impact in open rural spaces than in dense urban environments. A slower wind speed reduces the cooling potential, while it contributes to reducing the heating demand. The cooling demand in a cold weather like Edmonton or Vancouver can be offset by incorporating trees without the need of high albedo materials. The cooling potential through shading and evapotranspiration of trees was observed, although it was not individually specified. [15]

A simulation study from Simpson et. al. [49] with weather data for cooler and warmer regions in California, USA, determined that trees placed on the west had the best performance on cooling potential. Those located on different orientations showed about 50% and 25% lower contribution. Cooling energy savings were proportional to the tree size and to the number of trees. Depending on the orientation, the benefit of adding a second tree resulted in an additional cooling savings of 80% with respect to the first tree. Cooler climates showed cooling energy savings between 40% and 50%. Whereas in warmer regions, savings oscillated from 10% to 20%. It was determined that solar gains have a representative share in the total heat gains of a building located in a cooler climate. Tree shape proved a more important specification than shading coefficient for maximizing shade on a façade. The ranges of shading coefficient for mature trees oscillated from 10% to 40%. In accordance with Gordon et. al. [17], trees placed to the south and southeast contribute to reducing cooling demand, while increasing the heating demand in winter. [49]

Szkordilis and Kiss [13] performed a simulation study for three tree species to determine the shading potential on a building facade with different material

specifications. The benefits of tree shading were expressed as savings in cooling energy demand. It was observed that window surfaces without tree cover were warmer both day and night. Trees contributed to the night cooling effect, preventing exterior surfaces from storing heat during the day and releasing it at night. This way, natural ventilation through windows with tree cover is feasible both day and night. During daytime, indoor temperature decreased about 0.8 °C for concrete and timber exterior walls, and 0.6°C for brick exterior walls. The interior temperature rose between 0.2°C and 0.3°C at night. Indoor temperature between 20°C and 25°C at night were observed without the need of an air conditioning system. [13]

A simulation study of a house in Morelos, Mexico showed that tree shading can contribute to decreasing the indoor temperature of a space about 4°C. They also contributed with energy savings up to 76.6% by reducing the cooling demand. [14]

Greater thermal insulation through construction materials can be achieved on roof surfaces rather than on exterior walls. Solar radiation protection of windows has the greatest impact on cooling potential of interior spaces. Nevertheless, the protection of opaque surfaces may also have an impact on the interior space, particularly in summer. For instance, the greatest cooling savings were observed in uninsulated buildings located in warmer climates [49]. Solar gains on opaque elements are not representative during the cold season because of convective heat losses through wind speed. [17]

As mentioned in the Section 3.1, wind speed can be reduced by trees [16, 17, 65]. Akbari [16] performed on-site measurements on specific surfaces shaded by trees at different periods. Lower wind speeds were registered when the surfaces were shaded. As observed by [16, 17, 65], wind speed reduction decreases the convective heat transfer between the outdoor air and the interior space, as well as the infiltration rate of outdoor air into the space. This physical effect can be a disadvantage in combination with high outdoor temperatures in summer, reducing the convective heat transfer between the exterior and the interior [16, 65]. Besides, it has an impact on the energy demand of air conditioning systems. Less convective heat transfer increases its cooling energy demand, while a lower infiltration into a space reduces it. In winter, heating energy demand decreases as both convective heat transfer and infiltration decrease. [16]

3.2 Cooling potential through Evapotranspiration

Outdoor environments

In natural environments, the net radiant energy absorbed by surfaces during the day is emitted back into the environment through three main mechanisms: by heating the air, by heating the surfaces, and by evaporating water [65]. Cooling through evapotranspiration is generated by the foliage of vegetation, e.g. trees, by absorbing the shortwave solar radiation and converting it from sensible to latent heat [12, 51]. Trees in natural environments, e.g. forests, contribute through evapotranspiration to dissipating the absorbed heat and prevent it to heat up the air and surrounding surfaces [51, 65], as well as to raising atmospheric humidity during the summer season [65].

Evapotranspiration of trees is influenced, but not limited, by the absorbed solar radiation of tree canopies and the ground [12]. It also depends on the tree species, morphology, growth and physiological conditions, such as soil properties [52]. In natural environments, evaporative demand of air, soil water content and stomatal process have an effect on the transpiration of trees [5, 73]. In urban environments, trees are exposed to higher surface and air temperatures [54], higher solar exposure of the surface [55], lower absolute humidity levels [55], and poor soil properties [5], which increase the evaporative demand of air [5, 54–56]. Evaporative demand is influenced by the combination effect of air temperature and humidity [5]. In absence of water for evaporation, such is the case of urban environments, sensible heat increases and dissipates into the ambient, increasing the air temperature [12, 51, 65]. Evapotranspiration also depends on the tree group arrangement. For instance, a tree within a tree canopy transpires less in contrast to an isolated tree [65]. The transpiration of isolated trees is proportional to their crown area exposed to solar radiation at the top of the canopy [65].

According to Federer [65], the impact on air temperature and humidity of a single tree in an urban environment is not representative compared to the exterior conditions and heat gains resulting from the UHI effect [65]. The greatest impact of a dense tree canopy in an urban environment would be to resemble the microclimate from the country side [65]. The air temperature difference between cities and forests is more significant in winter than in summer [65]. The cooling effect in urban environments is usually lower than in natural environments [57]. Cities have a slower cooling rate at night because the net longwave radiation emitted into the atmosphere is intercepted by the atmospheric

particles and reflected to the surface [65]. Besides, there is a higher net radiant energy in urban environments due to the anthropogenic heat [65]. Furthermore, the UHI effect usually reaches its maximum level 3 to 5 hours after sunset, both during summer and winter, reducing the night cooling effect [18]. Both contribute to increased heat waves, which represent human health risks, particularly during the day, as potential causes of diseases or mortality [74]. The short and longwave solar radiation flux of street trees placed on paved surfaces is higher than the one of trees located on green surfaces [55].

Taha [4] measured the air temperature and wind speed of an urban green area in Davis, California, over two typical days during the fall, i.e., October. The study consisted of two green areas: the first one comprised 5 m high trees and 25% tree canopy cover; the second one had 20 m high trees. The air temperature inside the canopy of each area was reduced up to 6°C and 4.5°C, respectively, during the daytime, and increased about 2°C and 1°C, respectively, at night. [4]

Konarska et. al. [5] investigated the transpiration levels for park and street trees during the day and in the afternoon in Gothenburg, Sweden. Transpiration levels were observed at sunset, demonstrating that the cooling effect through evapotranspiration does not necessarily occur during the day, when solar radiation is present. Differences on air temperature between day and night coincide with the observations of [4]. During daytime, transpiration levels of sunlit leaves were on average three times higher than those of shaded leaves. It was concluded that evapotranspiration depends on the percentage of leaves exposed to solar radiation along the vertically projected crown area. Park trees showed higher transpiration levels in comparison with street trees. Nonetheless, no representative cooling effect through evapotranspiration was observed during daytime. As exposed by Federer in [65], the resulting cooling effect through evapotranspiration during the day was suppressed by the greater amount of mixing air available in the environment. Nighttime was split in 2 phases to study the night cooling effect. Phase 1 comprised from 2 hours before sunset until 2 to 3 hours after sunset, and phase 2 started 2 to 3 hours after sunset until the rest of the night. A lower transpiration rate was observed about 2 to 3 hours before sunset, as solar radiation and vapour pressure deficit (VPD) decreased. A correlation between the transpiration rate, stomatal conductance and cooling effect of trees was observed, showing a greater cooling effect at sunset. Konarska et. al. determined that by increasing transpiration levels by $0.1 \text{ mmol m}^{-2}\text{s}^{-1}$, the cooling rate intensity increases by $0.25 \text{ }^{\circ}\text{C}$ per hour. This relationship depends on weather conditions. Due to an incomplete stomatal closure at night, some tree species showed increased transpiration levels after sunset. However,

about 2 to 3 hours after sunset no representative correlation between transpiration and night cooling was observed. At this period, similar cooling rate values were measured in both vegetated and non-vegetated areas. Similar to [12] and [58], it was concluded that trees may contribute to the nighttime cooling effect before and after sunset. [5]

A relation between transpiration, wind speed and air cooling potential was observed through a CFD study [51]. Similar to [5] and [9], the influence of transpiration was analyzed by calculating changes in air temperature along the vertical length of the tree crown. Like the results of [9], maximum transpiration levels were observed on top of the tree crown. On the bottom of the tree crown, the air temperature decreased about 0.9°C under the influence of transpiration. While it increased up to 6°C in absence of transpiration. Transpiration showed a minor influence under the shaded region by reducing the temperature around 0.4°C. There was a minor increase on air temperature in absence of transpiration. [51]

Mohammad et. al. [8] investigated the cooling potential of a tree canopy in an open space in Munich, Germany. The author observed an average reduction of the air temperature by about 1°C during the summer season. The canopy consisted of 60-year-old *Tilia C.* trees with a 4.5 m crown radius. The air temperature dropped up to 3.5°C in the afternoon and rose about 0.5°C at night. This observation is consistent with the observations from Konarska et. al [5], where trees showed a greater cooling effect at the sunset. Variations in the air temperature along the crown length were observed. Despite the difference in crown sizes and LAI of the trees, the temperature on the bottom of the tree crowns was similar. The transpiration and shadow effect were considered as part of the results for cooling potential. However, a distinction between each ecosystem service was not determined. It was concluded that by improving the transpiration rate, the daily air temperature could decrease up to 2.3 °C. [8]

In another study, Mohammad et al. [10] investigated the average daily air temperature reductions for *Tilia C.* and *Robina Pseudoacacia* in a region of northern Bavaria, Germany. The age of the trees ranged from 41 to 67 years and 38 to 55 years, respectively. The maximum peak air temperature reductions ranged from 1.4°C to 2.8°C. [10]

Table 1 summarizes the observed air temperature reduction through evapotranspiration of different tree species in urban environments in different locations.

Table 1 | Cooling potential through evapotranspiration | Outdoor air temperature reduction related to transpiration rate of trees

Study type and source	Season / Period	Tree species	Location	Outdoor air temperature reduction [°C]
On-site measurements Taha et. al. [4]	October	Not specified	Davis, California	daytime Reduction between 6°C and 4.5°C night increase from 2°C to 1°C
On-site measurements Konarska et. al. [5]	Summer	Several ¹	Gothenburg, Sweden	Reduction of 0.25°C per hour by increasing transpiration levels by 0.1 mmol m ⁻² s ⁻¹
On-site measurements Myrup, L.O.[6]	Summer solstice (1 day)	Not specified	Davis, California	Reduction of 3.5°C
CFD study Dimoudi et al. [7]	Not specified ²	Not specified ³	Athens, Greece	Reduction from 0.5 °C to 4.0 °C
On-site measurements Mohammad et al.[8]	Summer	60-year-old Tilia C.	Munich, Germany	1°C daily average reduction Reduction of 3.5°C in the afternoon increase of 0.5°C at night
On-site measurements Mohammad et al. [10]	hottest week (end July)	54-year-old Tilia C. Robina Pseudoacacia	Würzburg, Germany	Reduction from 1.4°C to 2.8°C

Study type and source	Season / Period	Tree species	Location	Outdoor air temperature reduction [°C]
On-site measurements Kurn et al. [11]	September	Not specified	Southern California	Reduction from 1°C to 2°C

- 1- *Tilia C. europea*, *Quercus robur*, *Betula P.*, *Acer platanoides*, *Aesculus*, *Fagus sylvatica* and *Prunus serrulata* [5]
- 2- Specific values for air temperature and wind speed were part of the analyzed scenarios [7].
- 3- Species with different evapotranspiration rates were analyzed [7].

Since the greatest solar radiation absorption takes place on the top of a tree, the air temperature and the transpiration are usually higher in this zone. However, according to the results of Manickathan [51], despite the influence of solar radiation on both transpiration rate and the energy balance by increasing the latent heat, no representative relation between solar radiation and cooling through evapotranspiration was observed. At high solar radiation, the sensible heat increased with a higher transpiration rate, reducing the cooling rate. The transpiration rate was not high enough to cool down the leaves. The absorbed radiation on the horizontal surface remained constant as the tree height increased. However, on the vertical surface, as observed by [5], sensible and latent heat levels increase as the tree length increases, because the leaf area is proportional to the length, influencing the transpiration rate. While the measured temperatures along the vertical crown length increased with higher solar radiation exposure, the transpiration rate at different heights was similar. Shading effect accounted for the decreased air temperatures. The air temperature was lower on the bottom of the trees as there was less solar radiation, reducing the sensible heat and promoting the cooling effect through evapotranspiration. Evapotranspiration has a direct impact on outdoor thermal comfort as long as the bottom of the tree is within 3 m of a person. A combination of high tree cover and dense vegetation on the bottom can contribute to cooling through shadow and evapotranspiration. [51]

Rötzer developed the excel tool CityTree [19], which assists with the calculation of tree morphology and data related to cooling potential of different tree species at specific age considering weather conditions [66]. In contrast with the study of Meili et.al. [12] and

Konarska et al [5], the calculations of Rötzer [66] for cooling potential by evapotranspiration, e.g. latent heat, only accounts during the day, when solar radiation is available [66].

Regarding tree morphology, both latent and sensible heat are reduced as leaf size increases. The cooling effect reduces as heat flux decreases. The smallest the leaf area is, the more efficient is the convective factor, so the highest the cooling effect is. Leaf area density influences the absorbed solar radiation of the leaf surface. While a high leaf area density contributes to a higher shadow potential, at a low leaf area density more leaf surface is exposed to solar radiation. This ratio increases the air temperature and reduces the transpiration rate, which prevents the leaves from cooling. [51]

Mohammad et al. [9] analyzed the impact of both the cooling effect of trees through shading effect and their transpiration rate on the air temperature under the canopy of two tree species. These were *Tilia C.* and *R. Pseudoacacia* with an average age of 36 and 32 years old, respectively. The study was performed in an open space in Munich, Germany. Air temperatures were recorded along the crown length of trees during four summer days with different temperature conditions. Trees with higher transpiration rate showed a greater air temperature reduction potential within the canopy. The air temperature of *Tilia C.* decreased while its transpiration rate got dispersed as the distance between the ground and the crown increased. It showed a daily average air temperature reduction of around 1.1°C at 1.5 m above the ground, and 1.8°C at 4.5 m above the ground. [9]

The greatest cooling effect on the ground area on a hot day was attributed to the moisture content of the grass surface. This observation agrees with the conclusions of Manickathan et. Al. [51]. Species with less water consumption have greater moisture content on the ground, which allows a greater transpiration rate of the grass, and therefore, a greater air temperature reduction. Furthermore, green areas covered with trees require less water and have a greater air-cooling potential than green uncovered surfaces. For instance, despite *Tilia C.* showed a transpiration rate three times greater within the canopy than *R. Pseudoacacia*, the latter presented a greater air-cooling potential through evapotranspiration of the grass cover, at about 1.5 m above the ground because it has less water requirements. As recommended by Manickathan in [51], it was suggested to plant trees with dense canopies on grass surfaces to promote air cooling effect. [9]

It is to be noted that this effect depends between species and ground properties. If trees were planted on paved surfaces, *P. Pseudoacacia* would allow more solar radiation on

State of the art

the ground, sensible heat would increase, so the air temperature would be higher on the ground. Thus, Tilia C. would provide a higher cooling effect through shadow and evapotranspiration effect. [75]

Water supply for trees in urban environments is key for their evapotranspiration process [65]. Street trees are susceptible to water stress, the transpiration and leaf growth are negatively affected by water deficiency [65]. However, in the study of Konarska et. al [5] it was observed that street trees with the highest water loss during the day had the greatest night-time transpiration levels [5]. Isolated trees have greater water needs, because the surface has a higher solar radiation exposure [55].

The relation between vegetated and non-vegetated area, and the influence on a microclimate level in urban environments has been studied. According to on-site measurements performed by Kurn et al. [11], the temperature in urban environments in southern California can be reduced about 1°C by increasing the vegetation area. A daily air temperature reduction of about 2°C was observed in areas with tree canopies. [11]

Myrup [6] determined in his study that the air temperature of a space in Davis, California can be reduced up to 3.5°C by increasing the existing vegetated area at least from 20% to 30% [6]. Conversely, as observed by Federer [65], the changes in vegetated area does not imply a direct increment of evapotranspiration, and thus, a reduction in air temperature by heat removal from trees. It was concluded that the benefit of increasing vegetated area may have a greater impact on urban areas without preexisting vegetation [65].

It was also observed in a CFD study [7] with weather data from Athens, Greece that air temperature can be reduced by about 1°C by adding 100 m² of vegetation area on a space. Moreover, as well as Myrup [6], a relation between vegetated area and built area was defined: air temperature can be reduced about 0.8°C for every 10% of additional vegetated area. Changes in air temperature when contrasting the performance of species with different evapotranspiration rates were not representative, resulting in variations lower than 0.5°C. [7]

Depending on weather conditions, urban environment, as well as tree shape, type and density, the cooling effect provided by trees can still have an impact with lower intensity in the surrounding area [48]. In the measurements of Taha [4] it was concluded that a tree canopy can influence the air temperature of the surrounding environment on a distance about five times the tree height in the south direction [4]. For instance, the

cooling effect at -3°C in an urban park in the region of Tel-Aviv, Israel could be extended up to 0.5 km with a cooling effect of about -1.5°C [48]. As observed by Shashua-Bar et al [48] and Konarska et. al. [5], lower transpiration levels and lower cooling rates were observed on trees located on heavy traffic streets and on paved surfaces. Dimoudi et. al [7] concluded that the extension and intensity of the cooling effect was reduced on streets due to the surface temperatures of the surrounding built environment and the surface roughness [7].

The presence of high VPD in urban environments leads to alterations in the evapotranspiration process of vegetation, e.g., trees [12]. High levels of VPD causes plants to release water and eventually dry out, endangering the vegetation [41]. Air vapor pressure depends on the relative humidity and the air temperature. Therefore, these latter have a direct impact on the evapotranspiration potential of a tree. At high humidity levels, transpiration rate is reduced to such an extent that it is no longer representative for cooling; leaf temperature increases, causing the air temperature to heat up. At this stage, air vapour pressure reaches its saturation point, limiting the capacity of the air to absorb additional humidity from the leaves. Thus, shadow effect accounts for most of the cooling effect. At low humidity levels, as transpiration increases, the heat flux does, so the cooling effect through evapotranspiration increases. In this case, there is a lower vapour pressure because the air has a lower temperature, preventing the air from taking additional humidity from the leaves. The greatest cooling effect through transpiration was observed during the hot season in presence of low relative humidity levels, assuming that trees are well irrigated. [51]

Wind speed directly influences heat convective transfer of leaves and the evapotranspiration effect [7, 17, 65]. It was observed that cooling potential through evapotranspiration increases both at outdoor air temperatures above 25°C with high wind speeds, as well as at temperatures below 25°C with lower wind speeds [7]. Depending on tree species and weather conditions, a dense tree cover can contribute to reducing wind speed by promoting a greater wind flow resistance [51, 65]. However, because wind influences transpiration of tree leaves, low wind speed reduces transpiration cooling effect of air due to a lower transpiration of the leaves [51]. The maximum heat absorption by trees occurs at high wind speeds [51]. High wind speed contributes to reducing UHI effect, while human sensibility to evapotranspiration cooling is higher at low wind speed in the direct surrounding of a tree [51]. Outdoor comfort temperature levels decrease as height increases because wind speed increases as height does [51].

Indoor environments

A simulation study assisted with ENVI-met was performed by Pastore and Rosella [53] to analyze the effect of vegetation on indoor thermal comfort of residential spaces in Palermo, Italy. The study considered air temperature at different heights, one study for each floor building level, being 15 m the maximum height. It was determined that trees can contribute to reducing the indoor operative temperature up to 3.4°C. Shading and evapotranspiration of vegetation were both considered in the analysis. Nonetheless, evapotranspiration approach for trees was not described in the study. Besides, the available database for vegetation of the software was a limitation for the study. [53]

Marx et. al. [76] analyzed the performance of different UGI elements in the operative temperature of a residential building in Kempten, Germany during a hot day in July. Compared to green walls, trees provided less cooling potential. It was about 0.44°C less than the maximum operative temperature of the scenario without trees. Green walls reported a cooling potential of about 1.6°C. [76]

Akbari [16] analyzed the influence of evapotranspiration of trees by calculating hourly changes on humidity level in an interior space through measurements of air temperature and relative humidity. Despite the results were not representative, the influence of evapotranspiration was not discarded to have an influence in the interior space. [16]

4 Methodology

The methodology consisted of an indoor adaptive thermal comfort simulation to individually analyze the impact of the cooling potential of street trees through shadow and evapotranspiration in a space. After this process, both variables were integrated to identify synergies.

Trees were analyzed as they grew over time considering two climate change scenarios with different Representative Concentration Pathways (RCP). The study was performed every 10 years, from 2020 to 2100, between April and October, from Monday to Sunday, the 24 hours per day, using weather data projection from Meteonorm [77].

The simulation was assisted with Grasshopper (GH) [78] using the Ladybug (LB) [78] and HoneyBee (HB) [78] tools.

The study comprises a baseline case to compare the impact of trees on different scenarios:

- The baseline case refers to a study site with existing conditions, i.e., without trees on the sidewalk of the building. It is referred to as “No trees” in the results.
- The scenarios consist of adding trees on the sidewalk of a study site considering different tree species, number, position, size, transparency level. One tree species per scenario was proposed to better understand its performance.

Material properties and specifications of the building envelope, orientation, as well as representative urban context were defined. Growing development data of trees at specific age was calculated with the excel tool CityTree [19].

No changes in the surroundings such as new buildings were assumed in the study. Although ground properties [12, 51, 52] as well as albedo of trees and exterior construction materials [15] can influence the thermal balance of trees, variations in these properties were not taken into account. Water availability for tree growth was considered under ideal conditions. Wind speed rate was specified according to the weather files, no further changes on wind speed that may influence the performance of trees [16, 50] were considered in the study.

4.1 Shading potential

Trees were integrated into the thermal simulation as exterior context geometry. The tree geometry was modelled based on the data calculated with the excel tool CityTree [19] and exported to GH. Since the simulation time and effort depend on the geometry complexity [69], trees were modelled as simply as possible. Parametric design tools from GH in combination with HB components were used to generate the tree geometry, which was updated for each analyzed year according to the data imported from CityTree. Vertical faces following the crown shape were defined to analyze the shading potential of trees on the building façade. To account for the shadow potential of trees, a transparency value for each month of each analysis year was specified. The maximum transparency value was applied both when the leaves start to unfold and when they reach the senescence period, and the minimum transparency level when the leaves reach their maximum unfolding size. As mentioned in Section 3.1, as the crown of a tree increases over time, so does the shading area. Nonetheless, the shade density of the tree decreases over time [79]. The transparency values for each tree species were calculated with CityTree [19], according to the solar radiation blocked by the crown on a horizontal surface on the ground for each analysis period (month and year). The values were compared for validation purposes with those from the *Table H1: Transparencies of tree crowns to solar radiation* from [80]. It is important to note that the calculated values correspond to a horizontal surface, while the projected shadow on a building is on the vertical surface. As observed by Gordon M. in [17], an increasing factor of 5% was considered for the transparency values of trees, based on the ratio between solar radiation protection on a vertical surface and the crown leaf density on a horizontal surface.

The simulation was performed with EnergyPlus (EP) assisted with HB components. Data was imported from excel data sheets for each analysis period and each tree species. Finally, LB components were used for the indoor adaptive thermal comfort simulation. Figure 1 shows the simulation process.

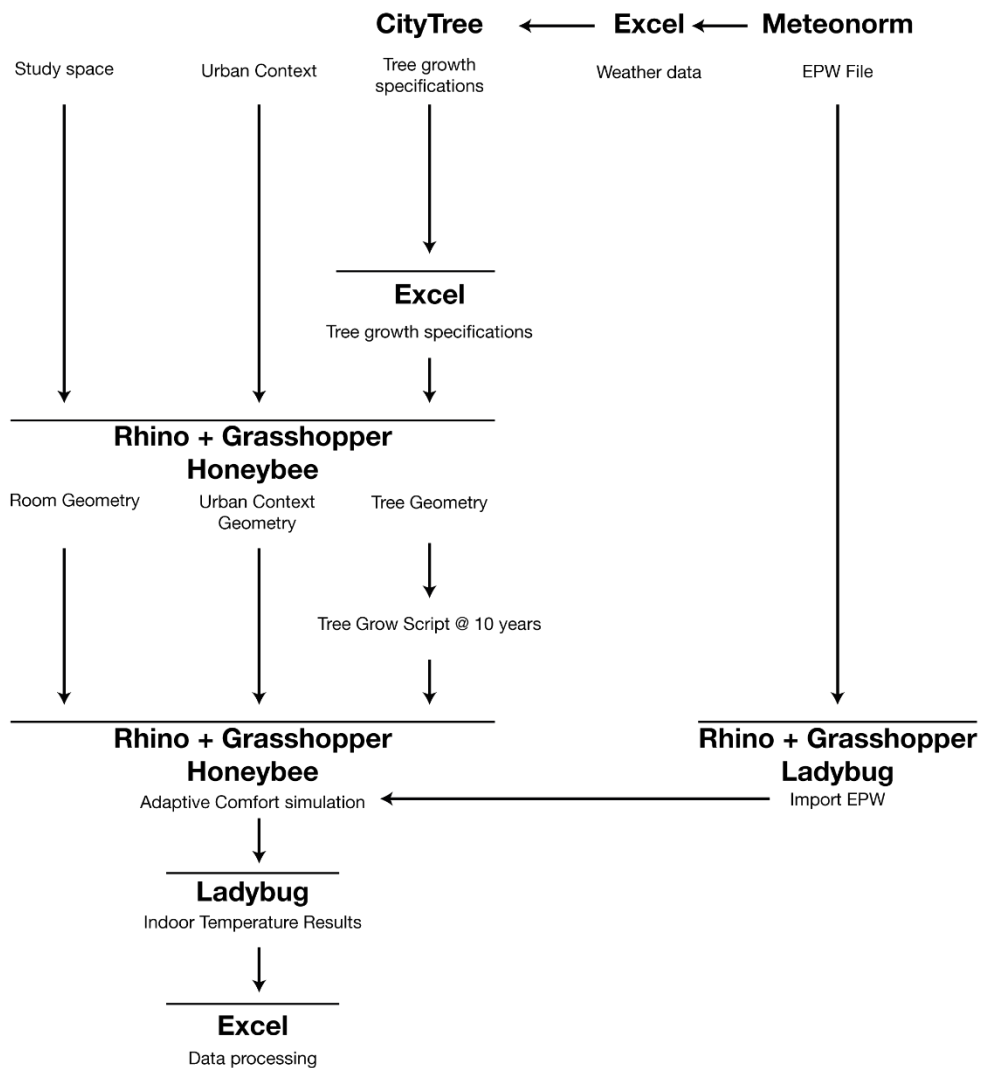


Figure 1 | Simulation process - Shading potential

4.2 Evapotranspiration potential

According to the studies exposed in section 3.2, evapotranspiration is affected, among several factors, by the transpiration rate of trees [5]. Transpiration is related to the size and age of trees [52, 58, 66]. Depending on tree species, morphology, location, context and microclimate conditions, trees can reduce the daily average outdoor air temperature based on their transpiration rate [5, 8, 9, 51]. However, as exposed in [58], it is not clear whether cooling potential through evapotranspiration is limited to a minimum tree size or age. Besides, despite the cooling effect can be extended on a horizontal distance from a tree canopy [4, 7, 48], many studies have considered existing and specific conditions that make their results difficult to replicate [58]. Furthermore, specific data related to the relation between distance and tree size to generate a specific cooling effect [58] and the air volume that can be influenced for the energy balance are missing.

For that reason, a sensitivity analysis was performed to study the influence of transpiration of trees (E_L) on the outdoor air temperature (T_{air}). The daily average outdoor air temperature reduction ($T_{air\downarrow,daily\ average}$) was related to the daily average transpiration rate ($E_{L,daily\ average}$) per tree species. A microclimate considering the outdoor air temperature reduction ($T_{air\downarrow}$) through E_L was calculated. The final outdoor air temperature ($T_{air,f}$) was integrated in the weather file of each thermal simulation to study its impact on the indoor thermal comfort of a space. Based on the daily average outdoor air temperature reductions from 0.5°C to 4°C summarized in Table 1, it was proposed to work with ranges between 0.25°C and 1.5°C. The sensitivity analysis comprised six thermal simulations per scenario, i.e., per tree species. Each one considered a daily average outdoor air temperature reduction target ($T_{air\downarrow,Target}$), i.e., from 0.25°C to 1.5°C, every 0.25°C. It was assumed that the outdoor conditions were given [5, 12, 41, 54–56, 73] for the trees to transpire.

PANDO is a parametric tool for tree modeling and analysis in GH. It works in conjunction with MAESPA for calculation data of transpiration rate, absorbed near infrared radiation, average foliage temperature, etc. It requires tree morphology and weather data from for the calculations. [81]

Since E_L is related to tree size and age [52, 58], and based on the data from the study of [10], a 60-year-old tree was selected as the reference age for the specified $T_{air\downarrow,Target}$. The calculation was performed as follows:

1. The hourly E_L for each tree species was calculated with PANDO components using the weather files from Meteonorm.
2. The daily average transpiration rate ($E_{L, \text{daily average}, 2060}$) during July 2060 was calculated. This value was considered as the baseline value for the hourly transpiration calculations of each analysis period.
3. Based on the $E_{L, \text{daily average}, 2060}$, a Transpiration-to-outdoor air temperature reduction ratio ($E_L | T_{air\downarrow, Target, Analysis Year}$) for each outdoor air temperature reduction target and each analysis period was calculated.

$$E_L | T_{air\downarrow, Target, Analysis Year} = \frac{E_{L, \text{daily average}, Analysis Year}}{E_{L, \text{daily average}, 2060}} \quad (1)$$

4. The initial hourly outdoor air temperature ($T_{air, i}$) was obtained from the EnergyPlus Weather (EPW) files and imported into excel.
5. The calculated $E_L | T_{air\downarrow, Target, Analysis Year}$ was related to the $T_{air\downarrow, Target, Analysis Year}$ to determine the outdoor air temperature that can be reduced per unit of transpiration rate.

$$T_{air\downarrow, Target, Analysis Year} = E_L | T_{air\downarrow, Target, Analysis Year} \times T_{air\downarrow, Target, 2060} \quad (2)$$

6. The hourly E_L per tree calculated with PANDO was used to define the proportion of transpiration as follows:

$$E_{L, \text{daily Average}, Analysis Year} | E_{L, PIT, Analysis Year} = \frac{E_{L, PIT, Analysis Year}}{E_{L, \text{daily average}, Analysis Year}} \quad (3)$$

7. The hourly $T_{air\downarrow}$ was calculated as follows:

$$T_{air\downarrow} = (E_L | T_{air\downarrow, Target, A. Year} \times E_{L, \text{daily Average}, A. Year} | E_{L, PIT, A. Year}) \quad (4)$$

8. The $T_{air, f}$ was obtained by suppressing the hourly $T_{air\downarrow}$ to the hourly $T_{air, i}$.

$$T_{air, f} = T_{air} - T_{air\downarrow} \quad (5)$$

9. The hourly $T_{air, f}$ was exported back to GH and integrated in the simulation using LB components to modify a EPW file.

Methodology

The tree geometry data was calculated with the excel tool CityTree[19] and imported into GH for each analysis period and each tree species. The transpiration rate was calculated with PANDO + MAESPA [81] components. The required data for the calculation comprised weather data from the EPW file, tree geometry and morphology data. The calculated transpiration rate from PANDO was imported into excel for the calculation of outdoor air temperature reduction. The information was imported back into GH and integrated into the weather file to generate a microclimate. The modified weather files were used to run the different scenarios. Figure 2 shows the simulation process. The study was performed every 10 years, from 2020 to 2100, between April and October, from Monday to Sunday, 24 hours per day, using weather data projection of Meteonorm [77].

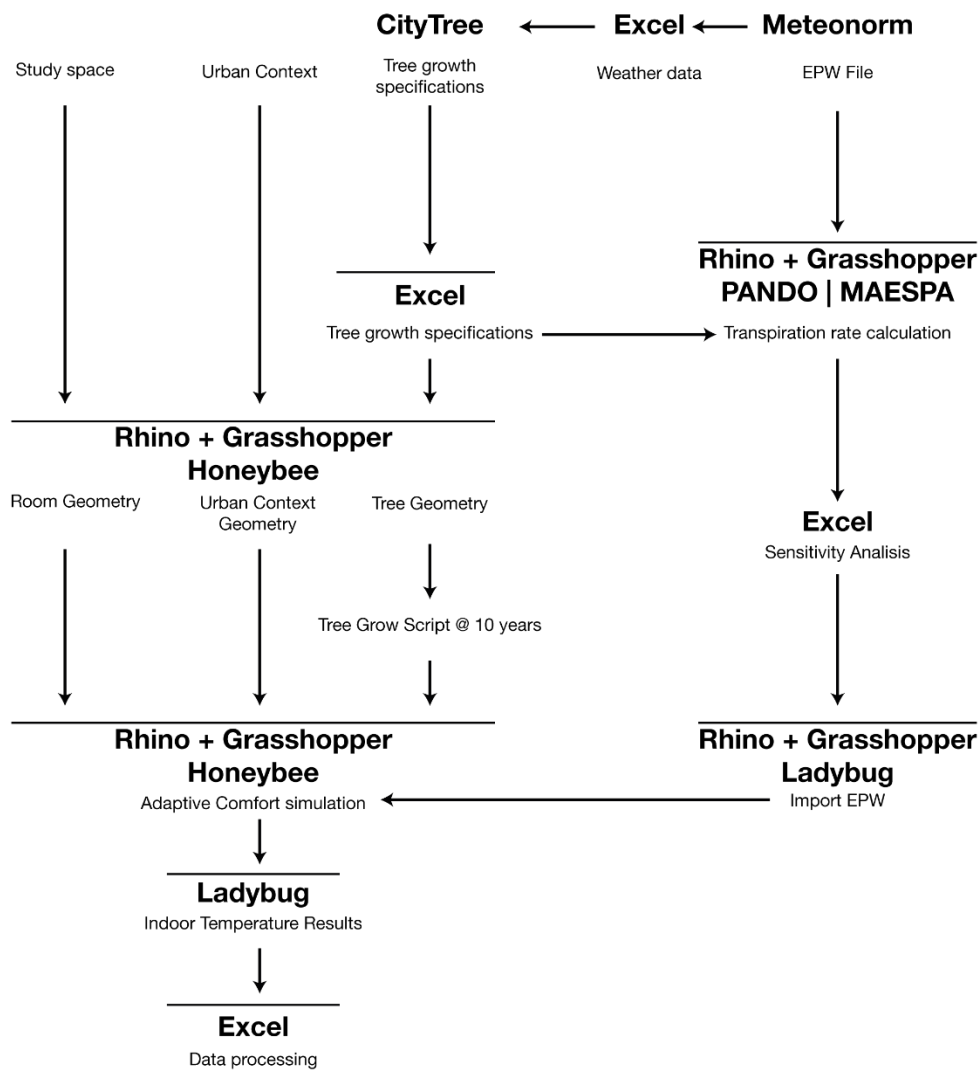


Figure 2 | Simulation process - Evapotranspiration potential

The study was performed in two stages. The first stage did not consider the shading potential of trees within the simulation study. In a second stage, outdoor air temperature reduction was integrated in the simulation process for shadow potential of trees described in the section 4.1.

4.3 Tree features

The following tree specifications for urban trees were considered for the analysis:

- Species type
- number of trees
- Morphology (trunk diameter, tree height, crown diameter and height)
- position related to the building (separation distance and separation between trees)

Information regarding growth rate, dimensions and tree development were gathered from CityTree tool [19] and the German catalogue of street trees [82].

The excel tool CityTree developed by Rötzer [66] provides information about the growth development of several tree species typical of Europe considering urban conditions [66]. CityTree tool takes into consideration the influence of urban conditions, climate change, e.g. carbon emissions, changing soil and weather conditions for the growth calculation of tree species [66]. The required inputs regarding weather data for the tree development calculation are monthly values of air temperature, relative humidity, solar incident radiation, precipitation, and wind speed [19]. This data was provided from the weather files from Meeonorm. Output data for a selected tree can be obtained every ten years, starting at age younger than 10 years up to older than 90 years [19]. Different values for soil properties as well as tree competition can be adjusted [19]. The changes on tree development related to soil properties were neglected in the study because the results from CityTree are related for one year only [19]. Thus, the influence on a long-term from one analysis period to another could not be considered. The tool delivers data regarding tree dimensions, e.g. diameter at breast height, tree height, crown length and crown diameter; cooling potential, e.g. evapotranspiration potential; plant development, e.g. LAI, beginning of leaf unfolding and leaf senescence; solar radiation on the horizontal surface of the tree canopy and the ground [19].

4.4 Weather data

Weather data was obtained from the EPW files from Meteonorm [77]. The data was imported into GH and City Tool to process the information and perform calculations. Weather files with RCP 4.5 and RCP 8.5 were used in the simulation process.

RCP 4.5 refers to an intermediate climate change scenario, with an increase in the global mean surface temperature by the end of the 21st century, i.e., from 2081 to 2100, from 1.1°C to 2.6°C. RCP 8.5 consists of a scenario with high GHG emissions, with temperatures between 2.6°C and 4.8°C. [83]

4.5 Key Performance Indicators

The key performance indicators (KPI) for the indoor thermal comfort results are:

- Cooling potential: Average operative temperature reduction (°C)
- Cooling degree hours [CDH] (Kh) based on DIN 4108-2:2013

According to table 9 of the DIN 4108-2:2013, CDH for office spaces must be calculated using the hourly operative temperature from Monday to Friday, from 7 to 18 hours. The reference value for the operative temperature ($\theta_{b,op}$) used to analyze the thermal comfort in a space is based on the climate region of a given location. The maximum CDH allowed for offices in new building is 500 Kh/a. [84]

The CDH were calculated with the following equation:

$$CDH_{b,op} = \sum_{i=1}^{4380} (\theta_i - \theta_{b,op}) \times 1h|_{pos} \quad (6)$$

*The formula was adapted from [26].

Additionally, the time frequency of the hourly operative temperature is presented in five ranges: <26°C, >26°C and <28°C, >28°C and <30°C, >30°C and < 32°C and >32°C. It must be noted that for this study, the CDH were calculated from April to October.

5 Case Study

5.1 Study area

The office of the Energy Efficient and Sustainable Design and Building (for its acronym in German ENPB) of the TUM was selected for this analysis. The office is located on the second floor of the south building “Bestelmeyer” of the Main Campus, at the corner of Arcisstraße and Gabelsbergerstraße. Figure 3 shows its location.

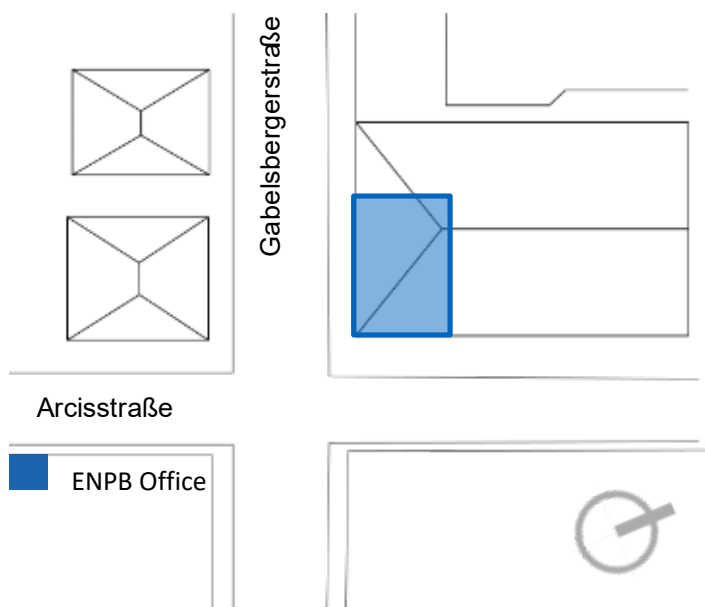


Figure 3 | Case Study - Site location

5.2 Project Specifications

The building was built in 1927 and is labelled as a monumental protection building [85]. The main construction consists of massive construction material and box-type windows [85]. Table 2 summarizes the building material specifications considered in the simulation process. The U-Values were specified according to the Table 12 – Thermal transmittance coefficient according to building age classes from the Federal Ministry for Economic Affairs and Energy Federal Ministry of the Interior, Building and Community [86].

Table 2 | Building construction specifications

Building element	Material description	U-Value [W/m ² K]
Exterior walls	Massive construction	1.7
Roof	Steep roof	1.4
Windows	Box-type window	2.7

The building is about 21 m high and has 4 levels. The office is located on the second floor, about 11.6 m above the sidewalk. The sidewalk on Gabelsbergerstraße is 3 m wide, and the street has a total section of about 17 m. Further information can be consulted in the Appendix | Figure VI. Gabelsbergerstraße comprises a parking lane, a cycling lane, two car lanes, and one partial parking lane, which ends about 50 m before the corner on Arcisstraße. From that point on, it continues as a car lane. The building is oriented 23° clockwise to the north. The southwest and southeast oriented facades are exposed to outdoors. Buildings located in front of the building office do not provide representative shade during the summer season on the southwest façade of the office. These provide partial shade on the ground and floor levels. A park with trees and green areas is located on the southeast side of the building. Nonetheless, these do not protect the southeast façade of the office from solar radiation during the summer season because of the distance and height related to the office space.

Since the analyzed space is on the second floor, both floor and ceiling were considered as adiabatic surfaces. The study comprises only the open office space. It has an internal floor area of 150.5 m², a floor-to-ceiling height of 3.18 m and a window-to-wall ratio (WWR) of 25%. All the windows are operable. Nonetheless, night cooling ventilation is limited because of the actual window design [85]. The center of the windows is 1.8 m above the office level. Window specifications were defined through a solar heat gain coefficient (SHGC) of 80% [87] and a visible light transmittance (VLT) of 64%. There are no exterior nor interior solar protection devices on the windows [85]. The office includes a heating system and ceiling fans. The latter were not included within the cooling strategies of the simulation study to show only the impact of UGI in the interior space. Interior loads comprise a lighting power density of 6.5 W/m², plug loads of 9.4 W/m² and 17 people. Occupancy schedule was assigned for a typical office, from Monday to

Friday, from 7 to 18 hours. A window opening schedule related to the outdoor and indoor temperature setpoints was defined through HB components. Natural ventilation is only feasible during the occupancy time when outdoor temperature is above 21°C.

5.3 Weather

5.3.1 Weather of Munich

The weather of Munich is warm and temperate [8]. Both air temperature and solar radiation vary considerably along the year. Because of the annual average temperature, natural ventilation is a feasible strategy throughout the year. In summer, the air temperature increases considerably, and because of the swing in the air temperature at night, night ventilation is a feasible cooling strategy. The amount of direct solar radiation is greater than the diffuse solar radiation. In summer, most of the solar radiation is incident on the east and west facades of a building, especially from June to July. In winter, the south façade receives an increased amount of solar radiation, which can contribute to heat gains. [88]

The total cooling days in the city have increased because the UHI effect keeps rising [89]. Monthly mean UHI intensity up to 6°C has been registered in the city [89]. It is expected the annual mean temperature to increase about 0.6°C and the annual precipitation to slightly decrease in the coming years [66]. According to the German Weather Service (for its acronym in German DWD), the annual average temperature in 2023 was 11.6°C, with 76 summer days [90].

The weather of Munich is highly influenced by the Alpina Pumpen, about 20 to 60 days during the summer season, especially at night and in the mornings, contributing to the cooling effect. Due to climate change, the ratio of summer days in the Alpina Pumpen are expected to increase from 35% to 40% by 2050. These can be duplicated in the worst-case scenario. In 2018, it showed an increased average annual temperature of around 1.9°C in comparison with the reference data from 1971-2000. [91]

The maximum solar altitude corresponds to 65° on June 21st at noon. According to [88], exterior shading devices and night cooling ventilation in combination with materials with high thermal mass capacity are some of the cooling strategies for buildings in Munich. These can contribute to enhancing indoor thermal comfort and reducing the need for an air conditioning system. [88]

5.3.2 Weather Data

EPW data was collected from the station “Munich GM”, which is located in the city, at 48.13° N 11.58° E, at 536 m above sea level [77]. Projection weather data from 2020 to 2100, considering the climate change scenarios RCP 4.5 and RCP 8.5, was obtained from Meteonorm. [77]

Weather Data – RCP 4.5

RCP 4.5 refers to a future intermediate climate change scenario [83]. It prognoses higher average outdoor temperatures around 0.2 to 0.4°C per year, increasing in Munich from 11.81°C in 2020 to 13.94°C in 2100 [77]. Temperature is expected to increase about 2.2°C by 2100 [77]. This represents an average increase of 2.4°C during the summer season, about 2.3°C and 2.5°C in July and August, respectively. Annual precipitation is expected to increase about 3 mm from 2020 to 2100 [77]. Relative humidity levels is prognosed to rise about 0.6% by 2100 [77]. Further information regarding outdoor temperature can be consulted in the Appendix | Table II.

Weather Data – RCP 8.5

RCP 8.5 consists of a scenario with high GHG emissions [83]. It prognoses higher average outdoor temperatures around 0.4 to 0.7°C per year, increasing from 11.81°C in 2020 to 16.8°C in 2100 [77]. Temperature is expected to increase about 5°C by 2100 [77]. This represents an average increase of 7.1°C during the summer season, 6.8°C and 7.4°C, in July and August respectively [77]. In contrast to RCP 4.5, annual precipitation is expected to decrease about 3 mm from 2020 to 2100 [77]. Relative humidity levels is expected to rise about 0.5% by 2100 [77]. Further information related to the average outdoor air temperature per year can be consulted in the Appendix | Table III.

5.4 Data Validation

On-site indoor air temperature measurements from 2021 to 2023 were provided by the Department of ENPB [92]. The data was used to calibrate the temperature setpoints as well as the ventilation control schedule of the simulation study. It is to note that partial data from April to October 2022 was not available, so an hourly average indoor air temperature for 2021 and 2022 was used to compare it with the simulation results. Besides, no information was available from October 8th to October 15th, so this period was suppressed to maintain consistency with the results. Weather data from DWD [93] was used in the simulation study.

Figure 4 illustrates the prediction quality of the simulation study related to the on-site measurements of the hourly air temperature through the coefficient of determination (R^2). The presented data illustrates the monthly average indoor air temperature, from April to October 2022. R^2 corresponds to 0.76.

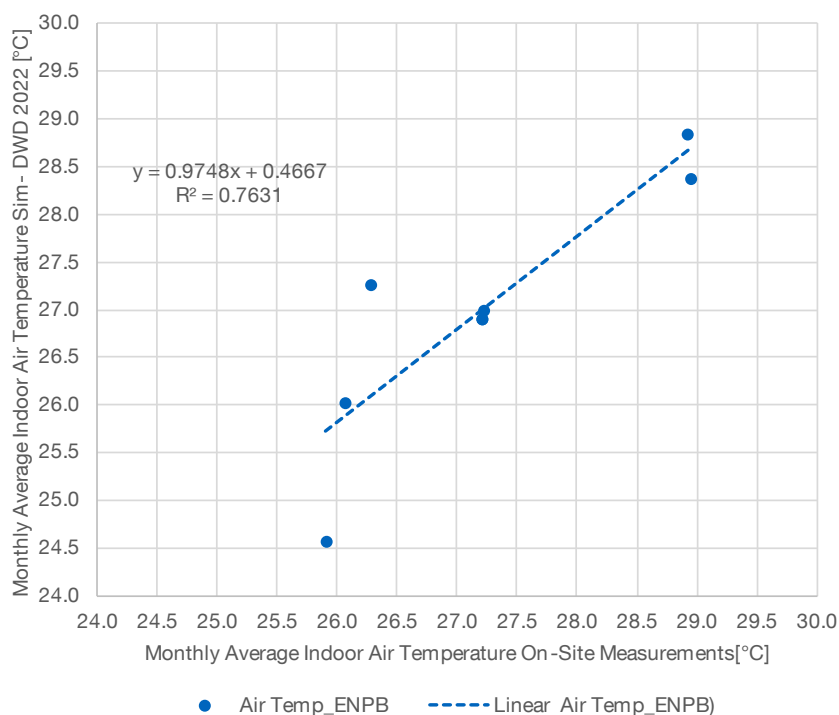


Figure 4 | Data Validation | Monthly average indoor air temperature | On-site measurements and simulation results.

Case Study

Table 3 illustrates the indoor air temperature of both the on-site measurements and the simulation results between April and October 2022. It can be observed that the greatest difference between the data occurred in April, about 1.32°C. And the least differences were observed in July and October, with 0.06°C and 0.03°C, respectively.

Table 3 | Average monthly indoor air temperature per scenario

Monthly average indoor air temperature [°C]	April	May	June	July	Aug	Sep	Oct	Summer Average
On-site M. ENPB [92]	25.9	26.3	28.9	28.9	27.2	27.2	26.1	27.2
Sim-DWD	24.6	27.3	28.4	28.8	26.9	26.9	26.0	27.0
Difference	1.32	-1.00	0.56	0.06	0.28	0.28	0.03	0.22

As stated in the DIN 4108-2:2013, Munich is located on the climate region B, so the reference value for the operative temperature ($\theta_{b,op}$) is 26°C. [84]

The CDH were calculated using the equation 6, as follows:

$$CDH_{26} = \sum_{i=1}^{1,764} (\theta_i - \theta_{26}) \times 1h|_{pos} \quad (6)$$

It must be noted that for the validation procedure, the CDH were calculated based on the indoor air temperature. Furthermore, the analysis period comprised from April to October. Therefore, the total hours for each study corresponded to 1,848 hours. Nonetheless, as mentioned above, the hours from October 8th to October 15th between 7 and 18 hrs. were suppressed from the validation results. So, the total hours summed 1,764 hours. The results are shown in the Figure 5. Besides, the time frequency of the hourly operative temperatures is presented in five ranges: <26°C, >26°C and <28°C, >28°C and <30°C, >30°C and <32°C, and >32°C.

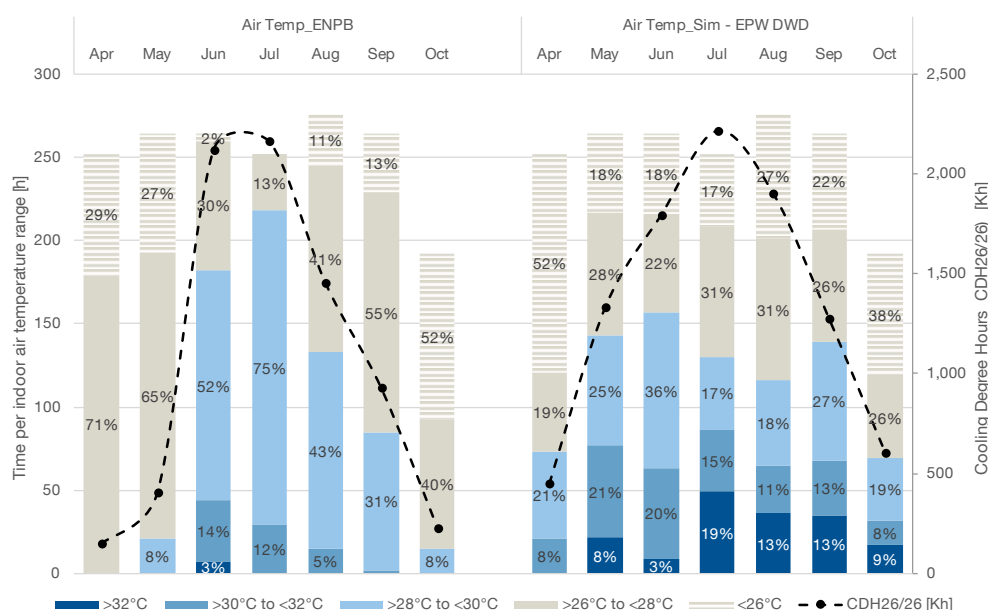


Figure 5 | CDH for Data Validation | On-site measurements and Simulation results

It can be observed in the simulation results that indoor air temperatures above 32°C occurred over twice as much of the occupancy time compared to the on-site measurements. Those occurred about 6% of the occupancy time. Moreover, more than 50% of the air temperatures from the on-site measurements occurred between 26°C and 28°C. Whereas almost 70% of those from the simulation results were observed between the ranges 26°C to 28°C and 28°C to 30°C. Overall, the total CDH from the simulation results were 29% higher than those from the on-site measurements. And indoor air temperatures above 26°C from the simulation results were observed for over 10% of the occupancy time less compared to the on-site measurements (see Table 4).

Table 4 | CDH results for Data Validation | On-site measurements and Simulation results

Scenario	ENPB On-site measurements [92]	Sim - DWD 2022	Difference
Cooling Degree hours (CDH _{26/26}) [Kh]	7,446	9,576	+29%
Hours when average Operative Temp is above 26°C [h]	1,450 (82% of the time)	1,289 (73% of the time)	-11%

5.5 Proposal Design

According to on-site measurements [92], indoor air temperatures above 26°C have been recorded in the office space more than 80% of the occupancy time (see Table 4). Since the building is labelled as a monumental protection building, there are several restrictions for the adaptation of measures to protect the interior space from solar radiation. Thus, UGI, i.e., street trees could be a feasible solution to reduce overheating in the space [13, 14]. A section of street trees is proposed to be placed on the sidewalk of the southwest façade, along the Gabelsbergerstraße. It is proposed to transform the partial car and parking lane into a pedestrian path, extending the section of the sidewalk from 3m to 6m. Trees are proposed to be placed about 5 m from the building (see Appendix | Figure II and Appendix | Figure VII). It is proposed to plant 10-year-old trees, once they have reached a minimum size and are not endangered as they grow. Depending on the tree species, maintenance and pruning may be required as the trees grow. The separation distance between the trees depends on each tree species (see Table 5). According to the infrastructure Atlas from Munich [94], there are no underground infrastructures related to transportation systems, water sewage nor district heating that could prevent the placement of trees.

This proposal is intended to contribute to the Mobility plan for 2035 of Munich [95], which aims to maximize the use of the public space and reduce the use of cars in the city [95]. It is proposed to work with a 2-phase transition:

- Phase 1: Extend the size of the sidewalk to place trees and locate parking lots between the trees, including infrastructure for e-cars and bicycle pots.
- Phase 2: Replace the parking lots with urban infrastructure, e.g., bicycle pots and urban equipment. Replace the ground cover with a material that contributes to reducing UHI effect and increasing the moisture content of the ground.

5.6 Tree Species

Three street tree species with different morphologies were selected to study their cooling potential.

- *Betula Pendula*, also known as silver birch, is a street tree with a loose, high arched crown shape. It has a high growth rate, low cultivation, and development pruning requirements. It is not recommended to be planted on paved surfaces

because it tends to lift surface coverings. Besides it does not resist urban climates. [82]

- *Tilia Cordata*, also known as small leaved lime, has a high growth rate [82]. It has mostly an oblique shape [82]. In contrast with other species, it has a high cultivation and development pruning requirements [82] as well as a greater transpiration rate [9].
- *Populus nigra* “italica”, also known as Lombardi poplar, has a high growth rate. It has a pillar shape. It resists urban climates. [82]

Both *Tilia C.* and *Lombardi P.* trees can be found in different open areas in Munich, e.g., Bordeauxplatz and Dollmannstraße, respectively. Existing trees in the city were used to validate the data obtained with CityTree. Further information can be found in the Appendix | Table I. Table 5 shows the tree geometry data for each tree species, both at the beginning and at the end of the analysis period, i.e., 2020 and 2100. It must be noted that no representative differences in the tree development were observed between the climate scenarios RCP 4.5 and RCP 8.5.

Table 5 | Morphology per tree species from 2020 to 2100

Species	<i>Betula P.</i>	<i>Tilia C.</i>	<i>Lombardi P.</i>
Height (min-max) [m] ^A	11 to 28	8.8 to 21.3	14.9 to 30
Crown length (min-max) [m] ^A	9 to 21.5	5.9 to 17	11.8 to 27.3
Crown radius (min-max) [m] ^A	2.5 to 8	2.5 to 7.5	1.5 to 3.6
Leaf area (min-max) [m ²] ^A	22.8 to 469.2	43.2 to 597.2	13.4 to 118.0
Shape ^{A,B}	half-ellipsoid	ovoid	cylindrical
Separation between trees [m]	15	14	7

A – CityTree [19]

B – German catalogue of street trees [82]

5.7 Shading potential

For the study of shading potential, a group of trees per scenario with the morphology data described in Table 5 was used. As exposed in the section 3.1, shade density of trees decreases over time [66]. Therefore, a transparency value per month and per analysis year was calculated assisted with CityTree (see Table 6). The maximum value was assigned when the leaves started to unfold (in April) and when they reached the senescence period (in October). A minimum value was used when the leaves reached their maximum unfolding size (in July). It can be observed that the grow development remained the same for both scenarios. Slight changes in leaf area can be observed in 2100, but it did not have a representative impact on the transparency calculations.

Table 6 | Leaf development and seasonal transparency per tree species for the climate change projections RCP 4.5 and RCP 8.5

Species	Betula P.	Tilia C.	Lombardi P.
Leaf area (min -max) RCP 4.5 [m ²]	22.8 – 469.2	43.2 – 597.2	13.4 - 118
Leaf area (min -max) RCP 8.5 [m ²]	22.8 – 475.7	43.2 – 618	13.4 – 119.7
Begin leaf unfolding [DOY]	93 to 104	98 to 106	93 to 104
Leaf senescence [DOY]	280	280	280
Initial Transparency 2020 (min-max)	0.64 to 0.98	0.41 to 0.93	0.47 to 0.94
Final Transparency 2100 (min-max)	0.41 to 0.93	0.26 to 0.87	0.33 to 0.90

A hypothetical office on both the first and ground floor of the building were used to study the shading potential of trees in spaces at different building levels as they grow. These were located at 6.3 m (Appendix | Figure VIII) and 1.05 m (Appendix | Figure IX) above the sidewalk level, respectively. The material and project specifications were the same from the initial study specified in section 5.2.

5.8 Evapotranspiration potential

The sensitivity analysis for the three tree species was performed considering six possible daily average air temperature reduction targets ($T_{air\downarrow,Target,Analysis\ Year}$), i.e., from 0.25°C to 1.5°C, every 0.25°C as exposed in the section 3.2. The study consisted of the analysis of the influence of transpiration rate of trees (E_L) on the air temperature (T_{air}) to define a microclimate. The air temperature reduction ($T_{air\downarrow}$) was calculated following the steps described in section 4.2. Table 7 summarizes the calculation procedure for the air temperature reduction target at 0.25°C for each analysis year ($T_{air\downarrow,0.25^\circ C,Analysis\ Year}$). A 60-year-old Betula P. was used as benchmark for the transpiration-to-outdoor air temperature reduction ratio ($E_L|T_{air\downarrow,Target,Analysis\ Year}$) for the different analysis years as well as for the calculations of the other two tree species.

Table 7 | Data for average air temperature calculations | Daily average air temperature reduction target of 0.25°C ($T_{air\downarrow,0.25^\circ C}$) | RCP 4.5

Analysis Year	2020	2030	2040	2050	2060	2070	2080	2090	2100
Daily average Transpiration rate (E_L , daily average) ¹	36.2	70.6	138.1	234.7	399.0	572.3	653.8	835.3	979.1
Transpiration ratio-to-Outdoor air temperature reduction ratio $E_L T_{air\downarrow}$	0.09	0.18	0.35	0.59	1.00	1.43	1.64	2.09	2.45
Average daily Outdoor air temperature reduction target $T_{air\downarrow,0.25^\circ C}$	0.02	0.04	0.09	0.15	0.25	0.36	0.41	0.52	0.61

1 – Calculation during July, considering that the daily air temperature reduction occurs in the summer season.

Case Study

For instance, in 2050, the highest transpiration rate was observed on 24th July at 17 h, about 913.83 mmol per tree s⁻¹. The data was calculated with the PANDO + MAESPA components. The following procedure was performed to calculate the ($T_{air\downarrow,0.25^{\circ}C}$) at this point-in-time (PIT) using the data from Table 7 at target 0.25°C.

The first step consisted of calculating the Transpiration-to-Outdoor air temperature reduction ratio for 2050 ($E_L|T_{air\downarrow,0.25^{\circ}C,2050}$) with the following formula:

$$E_L|T_{air\downarrow,Target,Analysis\ Year} = \frac{E_{L,daily\ average,Analysis\ Year}}{E_{L,daily\ average,2060}} \quad (1)$$

$$E_L|T_{air\downarrow,0.25^{\circ}C,2050} = \frac{E_{L,daily\ average,2050}}{E_{L,daily\ average,2060}}$$

$$E_L|T_{air\downarrow,0.25^{\circ}C,2050} = \frac{234.7\ mmol\ /tree - s}{399\ mmol\ /tree - s} = 0.59$$

Once the ratio was defined, it was related to the outdoor air temperature reduction target, i.e., 0.25°C for 2050 ($T_{air\downarrow,0.25^{\circ}C,2050}$) as follows:

$$T_{air\downarrow,Target,Analysis\ Year} = E_L|T_{air\downarrow,Target,Analysis\ Year} \times T_{air\downarrow,Target,2060} \quad (2)$$

$$T_{air\downarrow,0.25^{\circ}C,2050} = E_L|T_{air\downarrow,0.25^{\circ}C,2050} \times T_{air\downarrow,0.25^{\circ}C,2060}$$

$$T_{air\downarrow,0.25^{\circ}C-2050} = 0.59 \times 0.25^{\circ}C = 0.15 \frac{^{\circ}C}{mmol\ per\ tree - s}$$

The ratio of 0.15 °C means that for every 234.7 mmol per tree s⁻¹, the outdoor air temperature can be reduced by 0.15°C. Considering the E_L of 913.83 mmol per tree s⁻¹ on 24th July 2050 at 17 h calculated with PANDO + MAESPA, the proportion to the average transpiration rate ($E_{L,daily\ Average,Analysis\ Year} | E_{L,PIT,Analysis\ Year}$) was calculated as follows:

$$E_{L,daily\ Average,Analysis\ Year} | E_{L,PIT,Analysis\ Year} = \frac{E_{L,PIT,Analysis\ Year}}{E_{L,daily\ average,Analysis\ Year}} \quad (3)$$

$$E_{L,daily\ Average,2050} | E_{L,24.07.2050\ at\ 17\ h} = \frac{E_{L,24.07\ at\ 17h,2050}}{E_{L,daily\ average,2050}}$$

$$E_{L,daily\ Average,2050} | E_{L,24.07.2050\ at\ 17\ h} = \frac{913.83\ mmol\ per\ tree - s}{234.7\ mmol\ per\ tree - s} = 3.89$$

The outdoor air temperature reduction ($T_{air\downarrow}$) was calculated with the following formula:

$$T_{air\downarrow,Target,PIT} = (E_L | T_{air\downarrow,Target,A. Year} \times E_{L,daily Average,A. Year} | E_{L,PIT,A. Year}) \quad (4)$$

$$T_{air\downarrow,Target,PIT} = (E_L | T_{air\downarrow,0.25^\circ C,2050} \times E_{L,daily Average,2050} | E_{L,24.07 at 17 h,2050})$$

$$T_{air\downarrow,0.25^\circ C,PIT} = (0.15^\circ C \text{ per } mmol / tree - s \times 3.89 \text{ } mmol / tree - s) = 0.58^\circ C$$

Finally, the final outdoor air temperature ($T_{air,f}$) was obtained by suppressing the hourly outdoor air temperature reduction ($T_{air\downarrow}$) to the initial hourly outdoor air temperature ($T_{air,i}$).

$$T_{air,f} = T_{air,i} - T_{air\downarrow} \quad (5)$$

$$T_{air,f} = 31.4^\circ C - 0.58^\circ C = 30.82^\circ C$$

This procedure was performed for every hour of each analysis period for each air temperature reduction target and for both climate scenarios, i.e., RCP 4.5 and RCP 8.5.

6 Results

The results refer to the cooling potential of trees, i.e., the summer average operative temperature reduction compared to the baseline scenario, i.e., without trees.

6.1 Shading potential results

The cooling potential of trees through shading in an office space on 3 different levels considering the climate change scenarios RCP 4.5 and RCP 8.5 was analyzed.

RCP4.5 Scenarios

The average outdoor temperature increased about 13.4% (2.3°C) from 2020 to 2100, i.e., from 16.9°C to 19.1°C respectively [77].

Office space | 2nd Floor | EPW RCP4.5

The summer average operative temperature of the baseline scenario increased 1.4°C (4.7%), i.e., from 28.4°C, in 2020, to 29.8°C, in 2100. Figure 6 summarizes the cooling potential per tree species per analysis year. By placing trees on the sidewalk, the summer average operative temperature decreased from 2040. In 2040, the summer average operative temperature of the baseline scenario was about 29°C. Lombardi P. showed the highest cooling potential in that year, about 0.8°C. Betula P. showed a cooling potential of 0.3°C. The one from Tilia C. was minimal, it was about 0.1°C. By 2100, the summer average operative temperature of the baseline scenario increased up to 29.8°C. The highest cooling potential in 2100 was achieved by Betula P. and Lombardi P. trees, about 2.2°C and 2.1°C, respectively. Tilia C. remained as the less

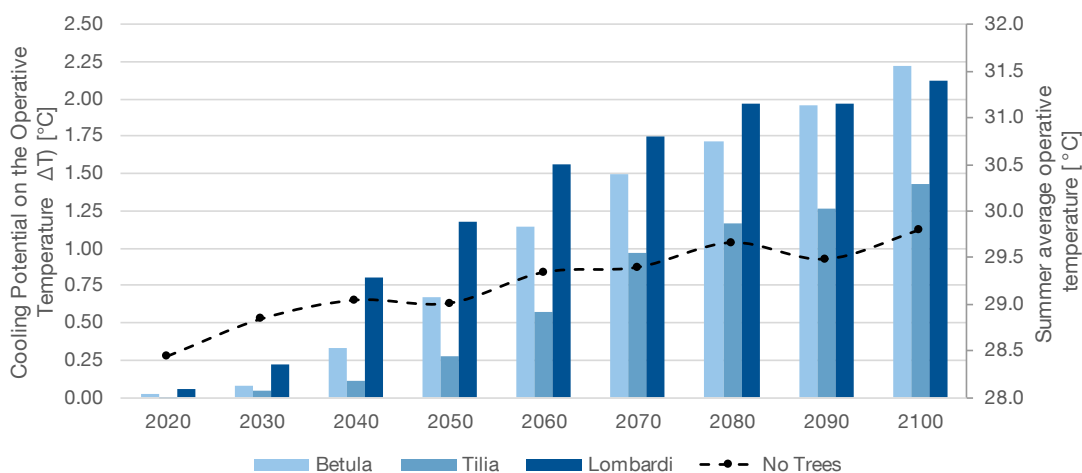


Figure 6 | Cooling Potential per Tree – Summer average temperature reduction per analysis year | 2nd Floor | RCP 4.5

Results

effective scenario, with a cooling potential of about 1.4°C. Further data can be found in Appendix | Table IV.

For the CDH calculation, as described in the Section 5.4, the reference value for the operative temperature ($\theta_{b,op}$) was 26°C [84]. The calculation was based on 1,848 hours for each analysis year, i.e., from Monday to Friday from 7 to 18 hours. Equation 6 was used for the CDH calculations as follows:

$$CDH_{26} = \sum_{i=1}^{1848} (\theta_i - \theta_{26}) \times 1h|_{pos} \quad (6)$$

Table 8 summarizes the CDH per scenario between 2020 and 2100. Figure 7 illustrates the time frequency per operative temperature range as well as the total CDH for each scenario in 2100. The total CDH of the baseline scenario in 2020 accounted for 6,350 Kh. By 2100, these increased up to 8,700 Kh. Betula P. and Lombardi P. contributed to reducing them by around 45% and 44%, respectively. These were reduced about 31% by placing Tilia C. trees.

Table 8 | Cooling degree hours per analysis year per scenario | 2nd Floor | RCP 4.5

CDH26/26 [Kh]	2020	2030	2040	2050	2060	2070	2080	2090	2100
No Trees	6,350	7,313	7,588	6,976	7,718	7,901	8,398	8,232	8,701
Betula P.	6,320	7,155	6,932	5,698	5,612	5,068	5,300	4,694	4,744
Tilia C.	6,368	7,225	7,359	6,463	6,612	6,065	6,230	5,877	6,046
Lombardi P.	6,259	6,898	6,131	4,871	4,967	4,656	4,897	4,693	4,915

In 2020, the scenario without trees showed operative temperatures above 26°C more than 80% of the occupancy time. Operative temperatures on each range were observed about 20% (+/- 3%) of the occupancy time. By 2100, operative temperatures above 26°C increased up to 88% of the occupancy time. Those above 32°C were observed more than 30% of the occupancy time. Operative temperatures from 28°C to 30°C and from

30°C to 32°C occurred about 20% of the occupancy time each. By placing *Betula P.* and *Lombardi P.* trees, operative temperatures above 26°C occurred less than 80% of the occupancy time. They decreased about 10% compared to those from the baseline scenario. Operative temperatures above 32°C significantly decreased by about 25% less time than in the scenario without trees. Those between 26°C and 28°C and between 28°C and 30°C were observed more than 50% of the occupancy time. By placing *Tilia C.* trees, operative temperatures above 26°C occurred more than 80% of the occupancy time. It can be noted that the total hours above 26°C of *Tilia C.* scenario were the same as those from the baseline scenario in 2020. However, the total CDH were about 5% lower than in the baseline scenario in 2020. In the *Tilia C.* scenario, operative temperatures above 32°C occurred more than 15% of the occupancy time. Operative temperatures between 28°C and 30°C were observed more than 25% of the occupancy time. It is to be noted that those between 30°C and 32°C occurred around 20% of the occupancy time in all the scenarios, including those from the baseline scenario in 2020 and 2100. The time frequency of operative temperatures between 26°C and 28°C was around 20% in all the tree scenarios by 2100 and in the baseline scenario from 2020.

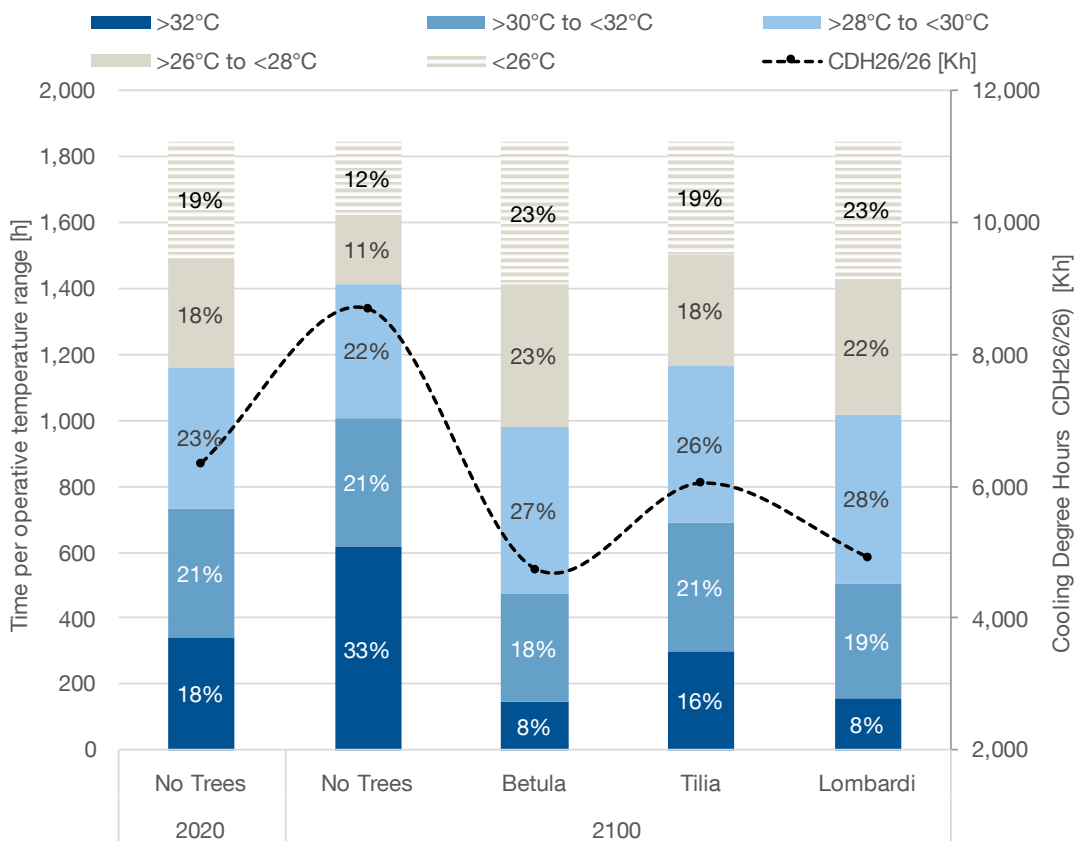


Figure 7 | Time per operative temperature range and CDH per scenario by 2100 | 2nd Floor | RCP 4.5

Results

Office space | 1st Floor | EPW RCP4.5

In 2030, the summer average operative temperature of the baseline scenario was about 28.7°C. In contrast with the results on the second floor, trees showed slightly lower summer average operative temperatures than the baseline scenario between 2020 and 2030 (see Figure 8). Lombardi P. showed a cooling potential of about 0.4°C and 0.9°C, respectively. In 2030, that of Betula P. and Tilia C. was about 0.4°C and 0.3°C, respectively. The cooling potential remained active at a lower rate from 2020 until 2040. Lombardi P. remained as the scenario with the highest cooling potential of about 1.4°C. From 2070 until 2100, the summer average operative temperature of the baseline scenario increased from 29.3°C to 29.7°C, respectively. The cooling potential of trees contributed to keeping a summer average operative temperature between 27.4°C and 27.2°C. Overall, by 2100, Lombardi P. and Tilia C. species reached a similar cooling potential, about 2.35°C. Betula P. scenario showed a slightly higher cooling potential, about 2.4°C. Further information can be consulted in the Appendix | Table V.

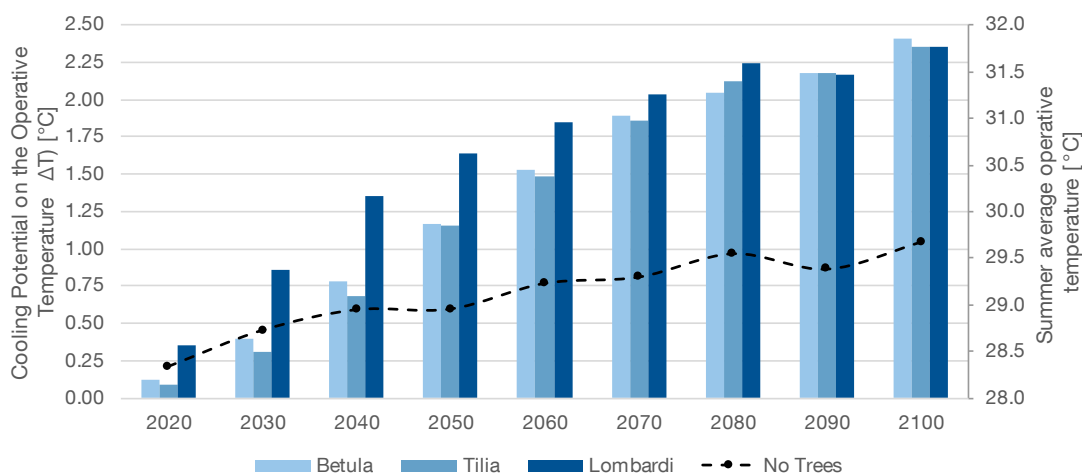


Figure 8 | Cooling Potential per Tree – Summer average temperature reduction per analysis year | 1st Floor | RCP 4.5

The CDH from the baseline scenario increased 38% from 2020 to 2100, i.e., from 6,146 Kh to 8,468 Kh, respectively. As observed in the operative temperature performance, by 2100, the three species contributed to reducing the CDH around 49% compared to those from the baseline scenario. It must be noted that by 2100, the CDH from the three species were about 30% lower than those from the scenario without trees in 2020. See Table 9 for more information.

Table 9 | Cooling degree hours per analysis year per scenario | 1st Floor | RCP 4.5

CDH26/26 [Kh]	2020	2030	2040	2050	2060	2070	2080	2090	2100
No Trees	6,146	7,114	7,385	6,863	7,501	7,713	8,210	8,045	8,468
Betula P.	5,945	6,351	5,945	4,763	4,839	4,263	4,610	4,243	4,284
Tilia C.	6,003	6,556	6,150	4,797	4,949	4,349	4,507	4,256	4,354
Lombardi P.	5,532	5,530	4,993	4,016	4,369	4,025	4,312	4,250	4,365

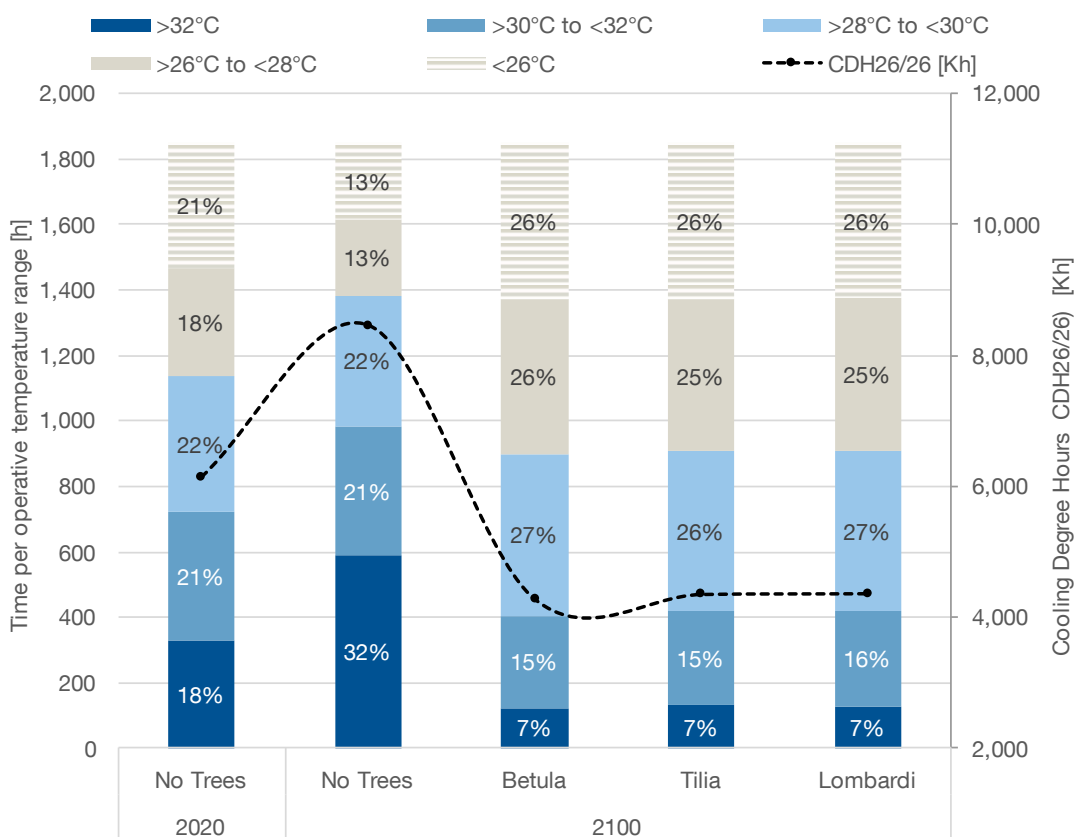


Figure 9 | Time per operative temperature range and CDH per scenario by 2100 | 1st Floor | RCP 4.5

As described in the Figure 9, in 2020, the operative temperature of the office was above 26°C almost 80% of the occupancy time. Operative temperatures at each range occurred about 20% of the time. By 2100, the baseline scenario showed temperatures above 26°C about 90% of the occupancy time, this was 8% more than in 2020. As

Results

mentioned above, the three tree species showed a similar performance. Operative Temperatures above 26°C decreased 13% of the occupancy time, compared to those without trees. Compared to the baseline scenario, operative temperatures above 32°C and from 30°C to 32°C decreased up to 7% and 15% of the occupancy time, respectively. Operative Temperatures from 26°C to 28°C and from 28°C to 30°C were observed more than 25% of the occupancy time at each temperature range.

Office space | Ground Floor | EPW RCP4.5

Figure 10 summarizes the cooling potential per tree species on each analysis year for the office located on the ground floor. In 2020, the summer average operative temperature of the baseline scenario corresponded to 28.1°C. The cooling potential of Lombardi P. scenario was about 0.7°C. From 2030, Betula P. and Tilia C. showed a cooling potential of about 0.6°C and 0.8°C, respectively. The cooling potential of all the tree species kept increasing from 2020 until 2040, especially that of Lombardi P. and Tilia C. These were about 1.4°C and 1.2°C, respectively. The one from Betula P. corresponded to 0.9°C. By 2070, the summer average operative temperature of the baseline scenario was about 29°C. The cooling potential of Tilia C. and Lombardi P. was about 1.9°C. The one from Betula P. corresponded to 1.8°C. From 2080 to 2100, the cooling potential of Tilia C. increased at a higher rate. By 2100, with a summer average operative temperature of 29.4°C for the baseline scenario, Tilia C. showed the highest cooling potential of 2.3°C. The one from Lombardi P. was about 2.2°C. Betula P. remained as the scenario with the lowest cooling potential of about 2°C. See Appendix | Table VI for further information.

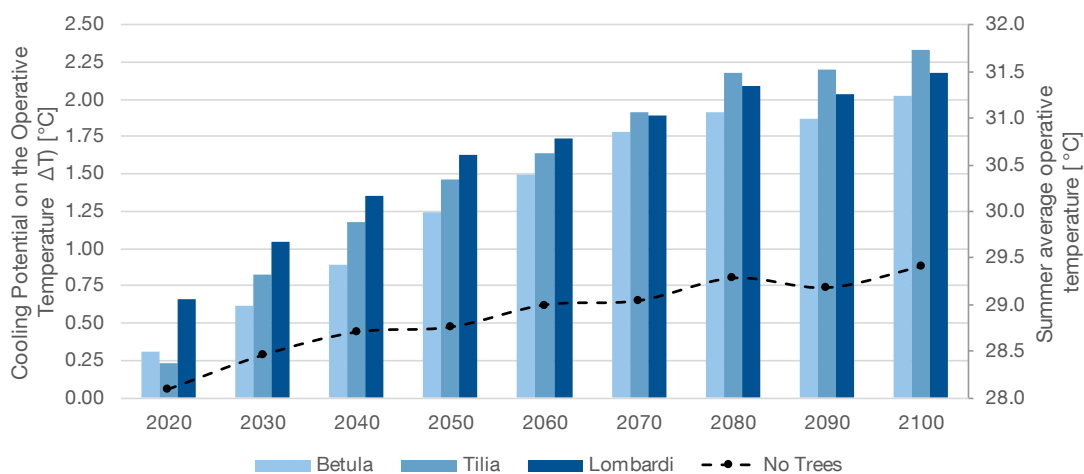


Figure 10 | Cooling Potential per Tree – Summer average temperature reduction per analysis year | Ground Floor | RCP 4.5

Table 10 summarizes the CDH per analysis period and per scenario. CDH for the office without street trees increased 37% from 2020 to 2100, i.e., from 5,791 Kh to 7,921 Kh, respectively. Shading of trees contributed to reducing CDH by 2100 about 50%, 47% and 44% through Tilia C., Lombardi P. and Betula P. trees, respectively. When comparing them to the initial CDH in 2020, street trees contributed to reducing these by 31%, 27% and 23% through Tilia C., Lombardi P. and Betula P., respectively.

Table 10 | Cooling degree hours per analysis year per scenario | Ground Floor | RCP 4.5

CDH26/26 [Kh]	2020	2030	2040	2050	2060	2070	2080	2090	2100
No Trees	5,791	6,677	6,973	6,513	7,111	7,285	7,740	7,693	7,921
Betula P.	5,245	5,532	5,378	4,355	4,588	4,053	4,389	4,378	4,444
Tilia C.	5,399	5,188	4,927	4,024	4,392	3,870	4,009	3,930	3,993
Lombardi P.	4,632	4,783	4,614	3,747	4,227	3,876	4,131	4,166	4,208

Figure 11 summarizes the total hours per operative temperature range for each scenario in 2100. In 2020, operative temperatures above 26°C were observed almost 80% of the occupancy time. Similar to the results of the office on the first floor, operative temperatures at each temperature range occurred about 20% of the occupancy time. By 2100, the operative temperatures above 32°C from the baseline scenario occurred almost a third of the occupancy time. Operative temperatures between 28°C to 30°C and between 30°C to 32°C were observed about 20% of the occupancy time at each range. Operative temperatures below 26°C and between 26°C and 28°C occurred about 15% of the occupancy time, respectively. The three tree species showed a similar performance, Tilia C. was the one with the slightly highest performance. Operative temperatures above 32°C were observed 23% less of the occupancy time than in the baseline scenario, i.e., between 6% and 7% of the occupancy time. Operative temperatures below 26°C occurred between 12% and 15% of the occupancy time more than without trees. Operative temperatures from 26°C to 28°C and from 28°C to 30°C were observed about 50% of the occupancy time, i.e., around 25% on each range.

Results

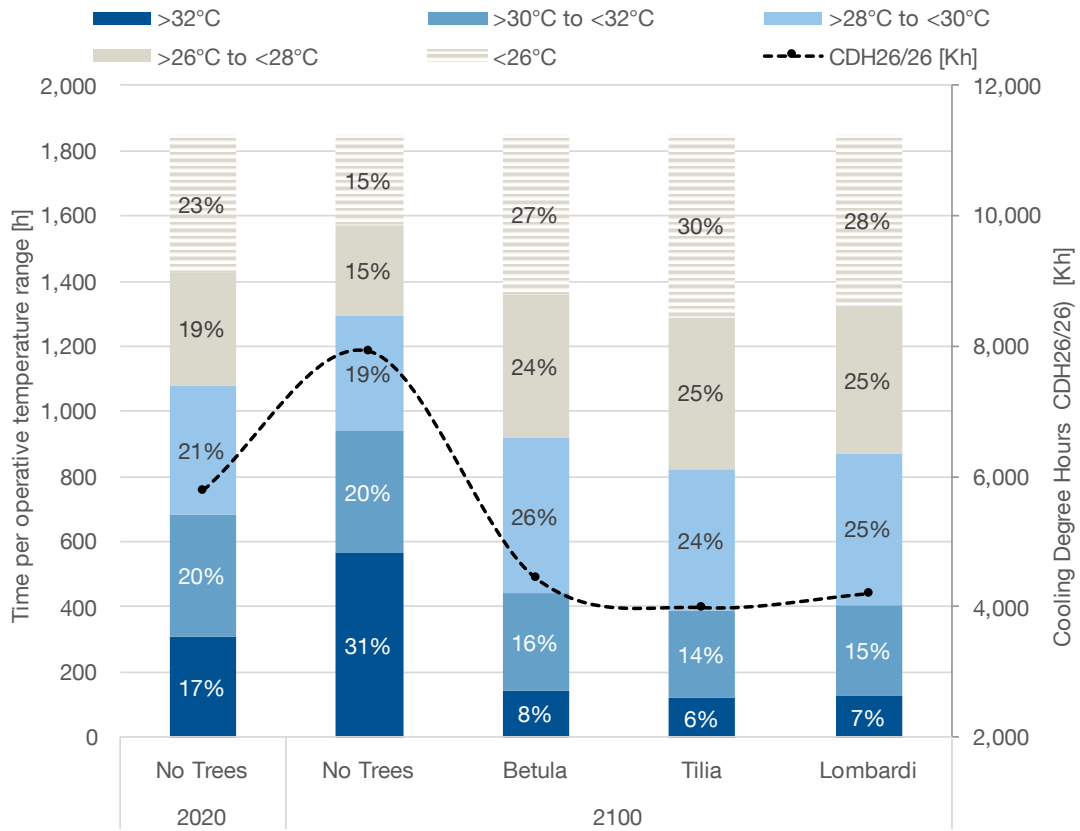


Figure 11 | Time per operative temperature range and CDH per scenario by 2100 | Ground Floor | RCP 4.5

RCP 8.5 Scenarios

The average outdoor temperature increased about 32% from 2020 to 2100, i.e., from 16.9°C to 22.3°C respectively [77]. This corresponded to an increase of 5.4°C, 3.2°C higher than the one from RCP 4.5 scenario.

Office space | 2nd Floor | EPW RCP8.5

Without considering trees, the summer average operative temperature increased around 10% (2.9°C) from 2020 to 2100, i.e., from 28.7°C to 31.6°C, respectively. Figure 12 shows the cooling potential through shadow for each tree species. From 2020 to 2040, no representative benefits from street trees were observed. In 2040, the summer average operative temperature was 29.2°C. The cooling potential of the Lombardi P. scenario corresponded to about 0.8°C. The ones from Betula P. and Tilia C. were lower, around 0.3°C and 0.1°C, respectively. From 2050 to 2070, the cooling potential of Betula P. and Lombardi P. increased at a higher rate than the one from Tilia C. By 2070, with a summer average operative temperature of about 30.2°C in the baseline scenario, Lombardi P. and Betula P. scenarios showed a cooling potential of about 1.7°C and 1.5°C, respectively. The one from Tilia C. corresponded to 0.9°C. From 2070 to 2100, the cooling potential of Betula P. increased at a higher rate than the other tree species. The one from Lombardi P. kept increasing at a lower rate. By 2100, the baseline scenario reached a summer average operative temperature of 31.6°C. Betula P. and Lombardi P. showed a cooling potential of about 2.1°C and 2.0°C, respectively. The one from Tilia C. was about 1.34°C. Further data can be found in Appendix | Table VII.

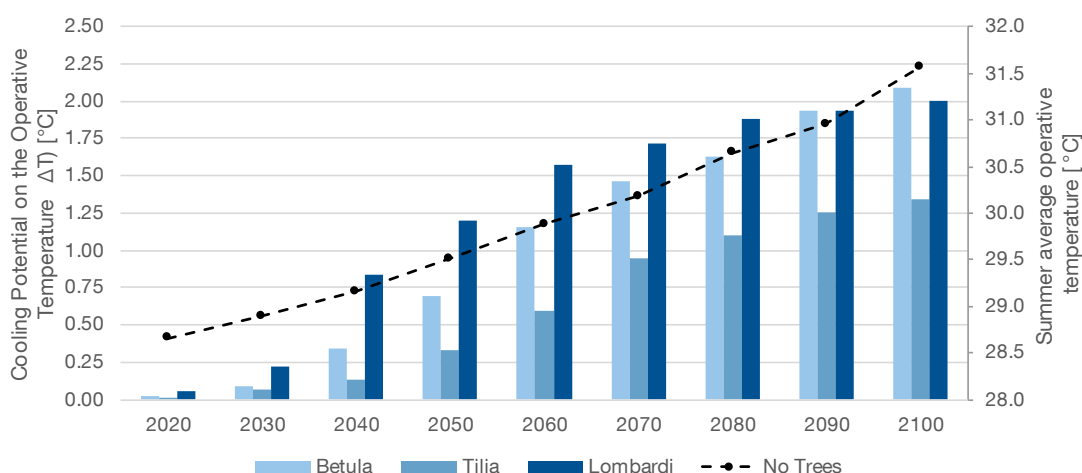


Figure 12 | Cooling Potential per Tree – Summer average temperature reduction per analysis year | 2nd Floor | RCP 8.5

Results

As described in the Table 11, the CDH increased 64% from 2020 to 2100, i.e., from 7,050 Kh to 11,566 Kh, respectively without considering shading cover of trees. In 2100, the greatest reduction in the total CDH was observed in the Betula P. and Lombardi P. scenarios. These were about 33% and 31% lower, respectively, than the baseline scenario. Tilia C. contributed to reducing them by about 21%.

When comparing the CDH from the tree species from 2100 with those from the baseline scenario in 2020, by placing Betula P. and Lombardi P. trees, these increased up to 11% and 13%, respectively.

Table 11 | Cooling degree hours per analysis year per scenario | 2nd Floor | RCP 8.5

CDH26/26 [Kh]	2020	2030	2040	2050	2060	2070	2080	2090	2100
No Trees	7,050	7,164	7,509	8,172	8,871	9,233	9,843	10,418	11,566
Betula P.	7,032	7,005	6,845	6,852	6,716	6,601	6,788	6,891	7,801
Tilia C.	7,042	7,046	7,255	7,566	7,739	7,505	7,747	8,045	9,109
Lombardi P.	6,955	6,763	6,035	6,010	6,020	6,216	6,359	6,896	7,945

Figure 13 summarizes the hours per operative temperature range for the different scenarios. In 2020, operative temperatures above 26°C were observed about 84% of the occupancy time. Operative temperatures at each temperature range were observed about 20% of the occupancy time. Those above 32°C were slightly superior, about 23% of the occupancy time. By 2100, operative temperatures above 26°C occurred more than 90% of the occupancy time, i.e., about 9% more hours than in 2020. Operative temperatures above 32°C occurred more than 40% of the occupancy time. Betula P. and Lombardi P. trees contributed to reducing the time with operative temperatures above 26°C around 10% less than in the baseline scenario. These above 32°C were observed about 30% of the occupancy time, which corresponded to 13% less hours than in the baseline scenario. Tilia C. showed operative temperatures above 26°C almost 90% of the occupancy time. These above 32°C were observed about 35% of the occupancy time. Compared to the baseline scenario in 2100, operative temperatures between 30°C and 32°C occurred about 5% to 7% less time in all the scenarios. Those

between 28°C and 30°C remained almost constant in all the scenarios, including the baseline scenario, about 20% of the occupancy time. Operative temperatures between 26°C and 28°C remained almost constant in all the tree species scenarios, about 20% of the occupancy time. These occurred 8% more often than without trees.

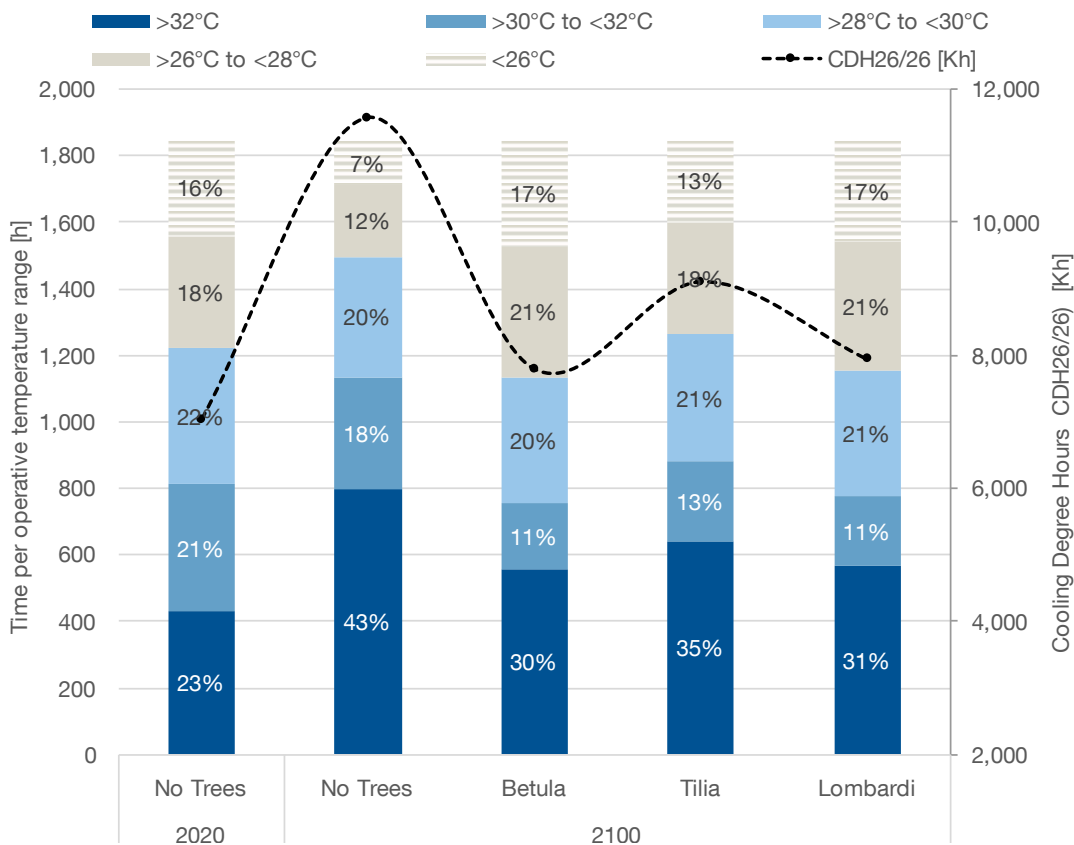


Figure 13 | Time per operative temperature range and CDH per scenario by 2100 | 2nd Floor | RCP 8.5

Office space | 1st Floor | EPW RCP8.5

The summer average operative temperature in the scenario without trees increased about 10% (2.9°C), i.e., from 28.5°C to 31.4°C respectively. In contrast to the scenario RCP4.5, the operative temperature reduction through Betula P. and Tilia C. trees was not representative from 2020 to 2030. In 2030, the summer average operative temperature of the baseline scenario was about 28.7°C. Lombardi P. showed a cooling potential of 0.8°C. From 2040 to 2070, the cooling potential of all the tree species increased. That of Betula P. and Tilia C. did it at a higher rate. Their cooling potential was similar on each analysis year. Lombardi P. remained as the scenario with the highest colling potential. For instance, in 2060, the summer average operative temperature of the baseline scenario was 29.7°C. The cooling potential of Lombardi P.

Results

trees was 1.8°C. That from Betula P. and Tilia C. trees was 1.5°C and 1.4°C, respectively. From 2070 to 2100, the cooling potential of the three scenarios increased at a lower rate. By 2100, all the tree species reached a cooling potential between 2.2°C and 2.1°C. Tilia C. showed a slightly lower cooling potential. The summer average operative temperature without trees was about 31.4°C. See Figure 14 and Appendix | Table VIII for further information.

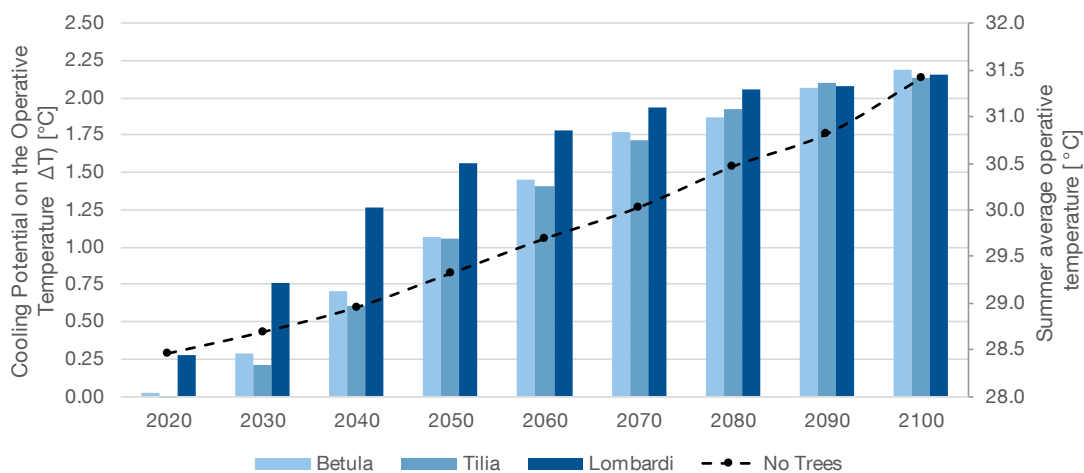


Figure 14 | Cooling Potential per Tree – Summer average temperature reduction per analysis year | 1st Floor | RCP 8.5

The CDH increased 68% from 2020 to 2100 in the scenario without trees, i.e., from 6,691 Kh to 11,264 Kh, respectively. By 2100, the three tree scenarios showed CDH about 34% less than in the baseline scenario. See Table 12 for further information.

Table 12 | Cooling degree hours per analysis year per scenario | 1st Floor | RCP 8.5

CDH26/26 [Kh]	2020	2030	2040	2050	2060	2070	2080	2090	2100
No Trees	6,691	6,790	7,142	7,822	8,500	8,946	9,496	10,112	11,264
Betula P.	6,665	6,240	5,882	5,884	5,886	5,876	6,076	6,448	7,392
Tilia C.	6,737	6,408	6,089	5,935	5,970	5,975	6,009	6,416	7,496
Lombardi P.	6,177	5,475	5,011	5,067	5,329	5,612	5,757	6,436	7,429

A summary of the hours per operative temperature range can be consulted in Figure 15. In 2020, operative temperatures above 26°C occurred more than 80% of the occupancy time. On average, operative temperatures within each temperature range occurred about 20% of the occupancy time. By 2100, operative temperatures above 26°C occurred more than 90% of the occupancy time. Those above 32°C were observed about 42% of the occupancy time. The three tree species had a similar performance by 2100. On average, trees contributed to reducing the time when operative temperatures were above 26°C. These were observed about 19% of the occupancy time, more than 10% less compared to those from the baseline scenario. Operative temperatures above 32°C occurred less than 30% of the occupancy time, about 13% less than in the baseline scenario. Operative temperatures between 28°C and 30°C in all the scenarios, including those from the baseline scenario in 2020 and 2100, were observed about 20% of the occupancy time. Operative temperatures between 30°C and 32°C in all the tree species scenarios occurred about 10% of the occupancy time. This corresponded to almost half of those from the baseline scenario. Moreover, those between 26°C and 28°C occurred more than 20% of the occupancy time in all the scenarios with trees. This is about twice the operative temperatures of the baseline scenario.

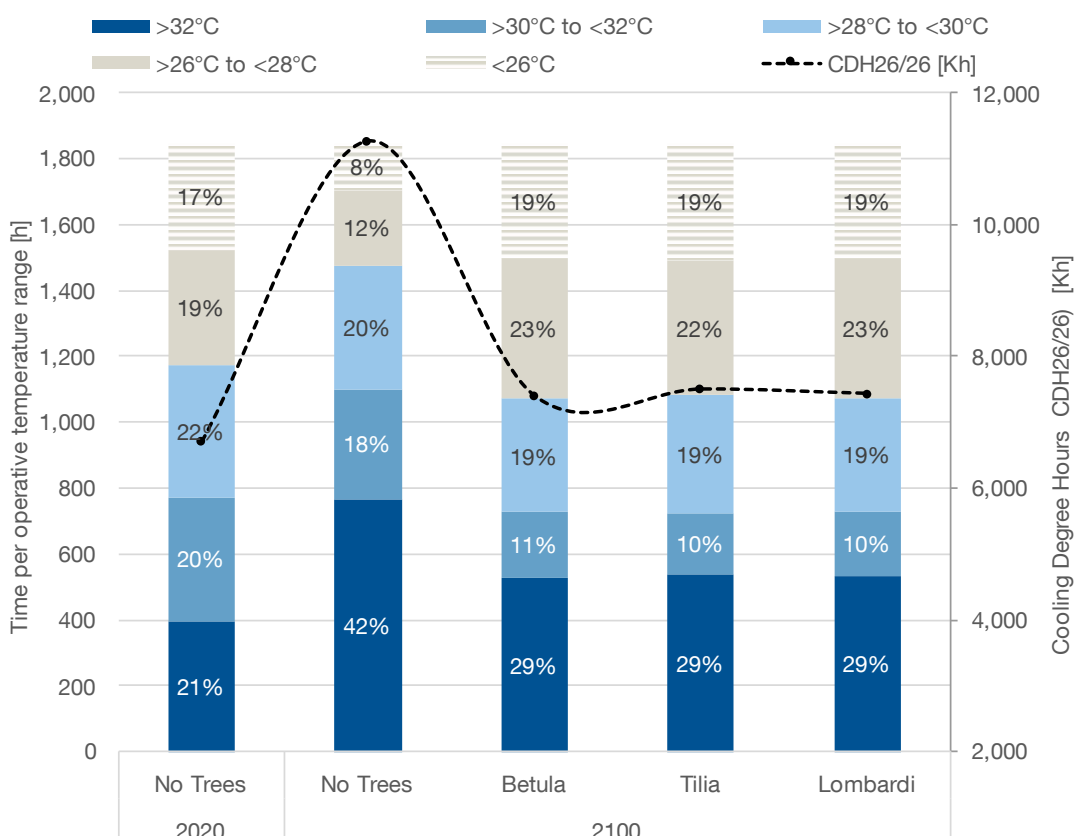


Figure 15 | Time per operative temperature range and CDH per scenario by 2100 | 1st Floor | RCP 8.5

Office space | Ground Floor | EPW RCP8.5

Like the office located on the first floor, the summer average operative temperature without trees increased around 10% (3°C) from 2020 to 2100, i.e., from 28.2°C to 31.2°C respectively. Figure 16 summarizes the cooling potential through shadow for each tree species per analysis year. In 2020, Lombardi P. showed the largest cooling potential, it was about 0.6°C. From 2030 to 2060, the cooling potential of Betula P. and Tilia C. increased at a higher rate. However, Lombardi P. remained as the scenario with the highest cooling potential. For instance, in 2060, the summer average operative temperature from the scenario without trees was about 29.4°C. The cooling potential of Lombardi P. scenario was 1.7°C. That from Betula P. and Tilia C. corresponded to 1.4°C and 1.6°C, respectively. In 2070, all the tree scenarios showed a comparable cooling potential. These were about 1.8°C for Tilia C. and Lombardi P., and about 1.7°C for Betula P. The summer average operative temperature from the baseline scenario was about 29.8°C. From 2080 to 2100, the cooling potential of Tilia C. trees increased at a higher rate than the other tree species. By 2100, the scenario without trees reported a summer average operative temperature of about 31.2°C. Tilia C. reached a cooling potential of about 2.2°C. That from Betula P. and Lombardi P. trees was about 1.9°C and 2.0°C, respectively. See Appendix | Table IX for further details.

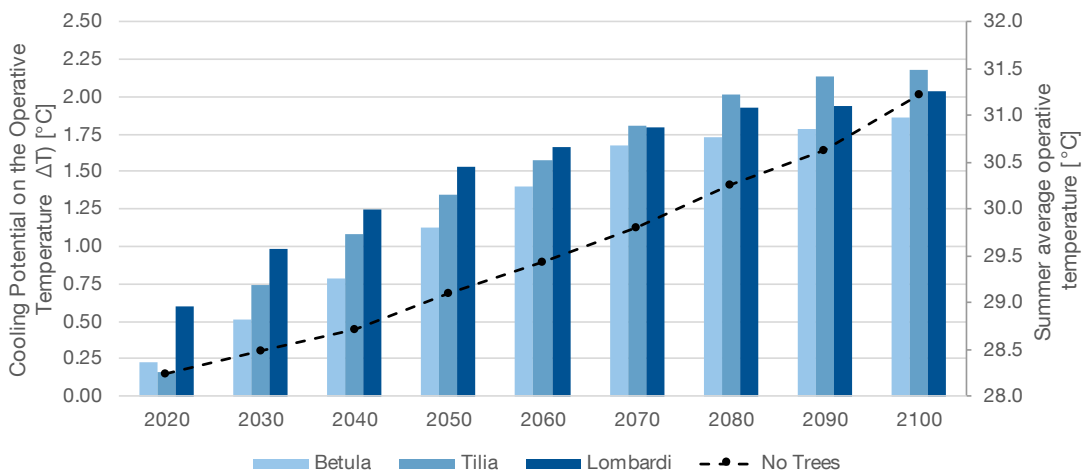


Figure 16 | Cooling Potential per Tree – Summer average temperature reduction per analysis year | Ground Floor | RCP 8.5

The CDH increased 73% from 2020 to 2100 in the scenario without trees, i.e., from 6,329 Kh to 10,970 Kh, respectively. Tilia C. trees contributed to reducing the total CDH by about 35% by 2100. Lombardi P. and Betula P. trees contributed to reducing them around 33% and 31%, respectively. See Table 13 for further information.

Table 13 - Cooling degree hours per analysis year per scenario | Ground Floor | RCP 8.5

CDH26/26 [Kh]	2020	2030	2040	2050	2060	2070	2080	2090	2100
No Trees	6,329	6,437	6,802	7,458	8,064	8,579	9,156	9,756	10,970
Betula P.	5,899	5,540	5,444	5,446	5,588	5,718	6,015	6,614	7,617
Tilia C.	6,036	5,167	4,986	5,097	5,313	5,527	5,577	6,086	7,136
Lombardi P.	5,236	4,741	4,709	4,775	5,158	5,521	5,693	6,374	7,346

Regarding the time frequency at different operative temperature ranges, Figure 17 summarizes the performance of the different scenarios. It can be observed that in 2020, operative temperatures above 26°C occurred about 80% of the occupancy time. The time frequency at each temperature range was about 20% at each one.

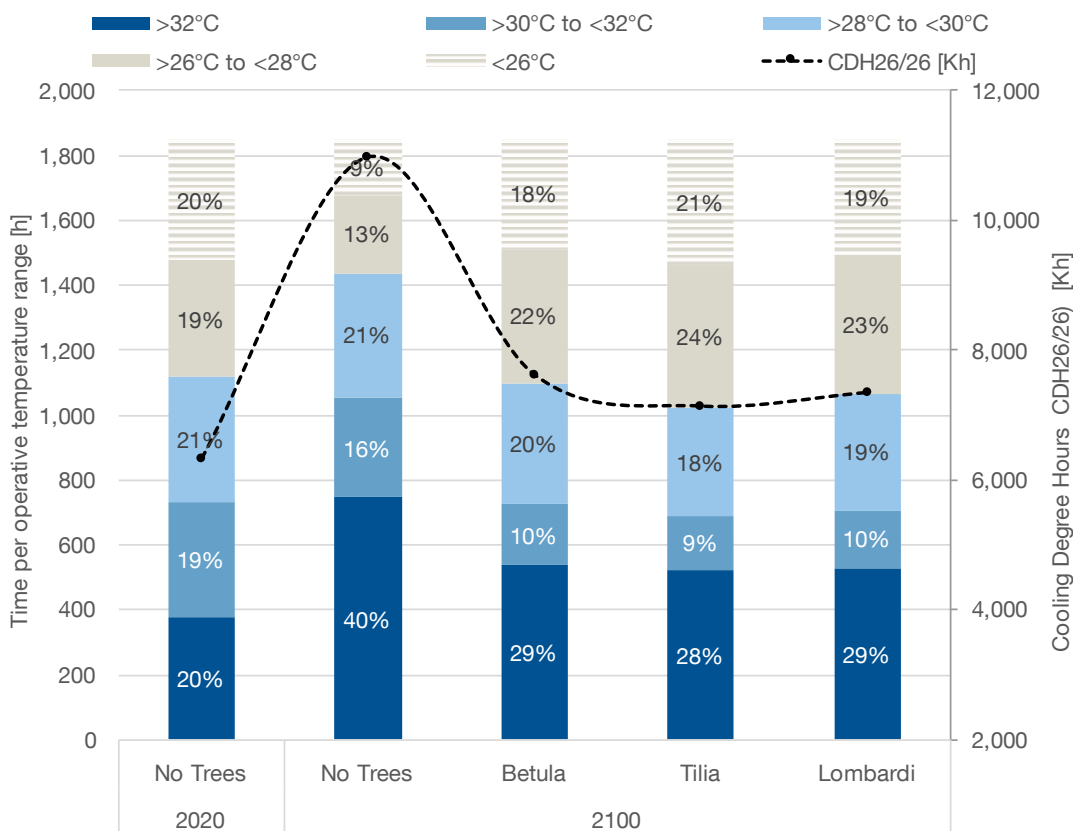


Figure 17 | Time per operative temperature range and CDH per scenario by 2100 | Ground Floor | RCP 8.5

Results

By 2100, operative temperatures above 26°C increased 10% more than in 2020, which corresponded to more than 90% of the occupancy time. Those above 32°C were observed about 40% of the occupancy time. Operative temperatures between 30°C and 32°C occurred about 16% of the occupancy time. The three tree species showed a similar performance, nonetheless, *Tilia C.* showed a slightly higher performance. On average, operative temperatures above 26°C were observed around 80% of the occupancy time. Those above 32°C occurred less than 30% of the occupancy time, this is about 10% less than in the baseline scenario. Temperatures between 30°C and 32°C were observed no more than 10% of the occupancy time. This corresponded to almost half of those from the baseline scenario in 2020. Operative temperatures between 26°C to 28°C were observed about 20% of the occupancy time. These were about the same from the baseline scenario in 2020. Moreover, these were almost two times more frequent than in the baseline scenario in 2100. Finally, operative temperatures between 28°C and 30°C occurred about 20% of the occupancy time in all the scenarios, including those from the baseline scenario in 2020 and 2100.

6.2 Evapotranspiration potential results

The evapotranspiration potential study was performed in two stages for each tree species. The first stage considered only the cooling potential through evapotranspiration of trees following the calculation procedure described in Section 4.2. For the second stage, the evapotranspiration potential was integrated to the shading potential described in Section 4.1. The results show the cooling potential, i.e., the summer average operative temperature reduction observed in the office located on the second floor.

6.2.1 Cooling potential | Evapotranspiration | Outdoor

Outdoor air temperature reduction | EPW RCP 4.5

Figure 18 illustrates the box plot of the cooling potential through evapotranspiration of trees on the summer average outdoor air temperature considering the daily average outdoor air temperature targets ($T_{\text{air}\downarrow, \text{Target}}$) from 0.25°C ($T_{\text{air}\downarrow, 0.25^\circ\text{C}}$) to 1.5°C ($T_{\text{air}\downarrow, 1.5^\circ\text{C}}$). Further details can be found in the Appendix | Table XVI to Appendix | Table XVIII.

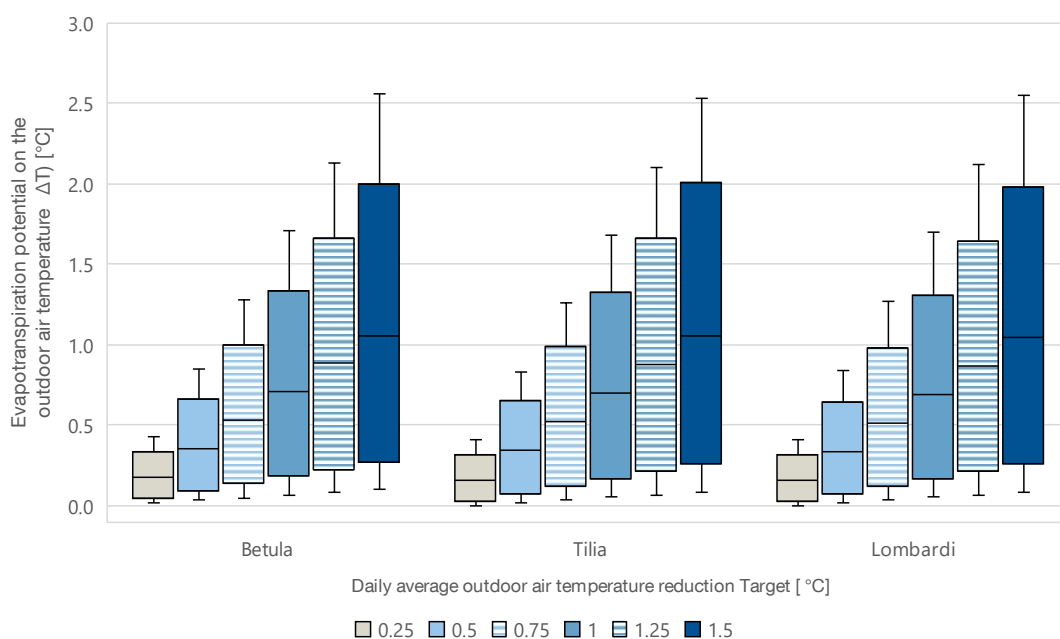


Figure 18 | Box plot of the cooling potential through evapotranspiration per tree species in the summer average outdoor air temperature at each $T_{air\downarrow,Target}$ | 2020-2100 | RCP 4.5

It can be observed that all the tree species showed a similar cooling potential at each $T_{air\downarrow,Target}$. Betula P. was the only scenario with perceptible results from 2020. Those from Tilia C. and Lombardi P. were noticeable from 2030. Table 14 summarizes the observed results. The increase in cooling potential rate between 2020 and 2100 depended on each $T_{air\downarrow,Target}$. It must be noted that these rates were not constant from one analysis year to another, the presented value are averages from 2020 to 2100.

Figure 19 illustrates the evapotranspiration potential per tree species at each $T_{air\downarrow,Target}$ in 2050 and 2100. Lombardi P. and Tilia C. tree species showed similar cooling potentials. By 2050, cooling potentials from about 0.09°C to 0.64°C for $T_{air\downarrow,0.25^\circ C}$ and $T_{air\downarrow,1.5^\circ C}$, respectively, were observed. Those from Betula P. ranged between 0.11°C and 0.65°C, respectively. By 2100, all tree species reached a similar cooling potential, Betula P. was the one with the slightly highest cooling potential. It ranged from around 0.41°C to 2.56°C for $T_{air\downarrow,0.25^\circ C}$ and $T_{air\downarrow,1.5^\circ C}$, respectively.

Results

Table 14 | Summary - Evapotranspiration rate in the summer average outdoor air temperature per tree species at each $T_{air,Target}$ between 2050 and 2100 | RCP 4.5

Cooling potential [°C]	0.25	0.5	0.75	1.0	1.25	1.5
Min- Max	0.002 to 0.41	0.02 to 0.85	0.03 to 1.28	0.05 to 1.71	0.07 to 2.13	0.08 to 2.56
Median	0.05 to 0.33	0.09 to 0.67	0.14 to 1.00	0.18 to 1.33	0.23 to 1.66	0.27 to 2.00
Average ¹	0.05 (+/- 0.04)	0.10 (+/- 0.07)	0.15 (+/- 0.11)	0.21 (+/- 0.15)	0.26 (+/- 0.19)	0.31 (+/- 0.22)

1 – Average cooling potential increase per analysis year, i.e., from 2020 to 2100.

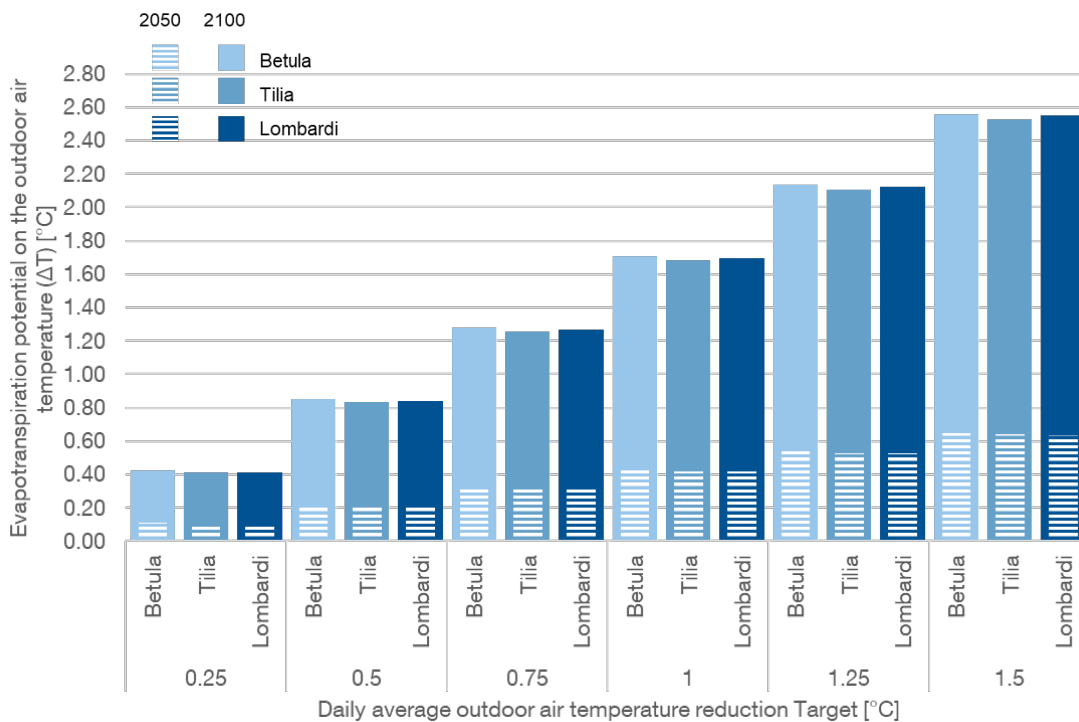


Figure 19 | Evapotranspiration potential on the outdoor air temperature per tree species | 2050 -2100 | RCP 4.5

Outdoor air temperature reduction | EPW RCP 8.5

Like the results with the climate projection RCP 4.5, the evapotranspiration effect of the three tree species considering the projections of RCP 8.5 showed a similar cooling potential on each $T_{air\downarrow,Target}$. Figure 20 illustrates the box plot of the cooling potential through evapotranspiration of trees on the summer average outdoor air temperature considering the $T_{air\downarrow,0.25^{\circ}C}$ to $T_{air\downarrow,1.5^{\circ}C}$. Further information can be consulted in the Appendix | Table XIX to Appendix | Table XXI.

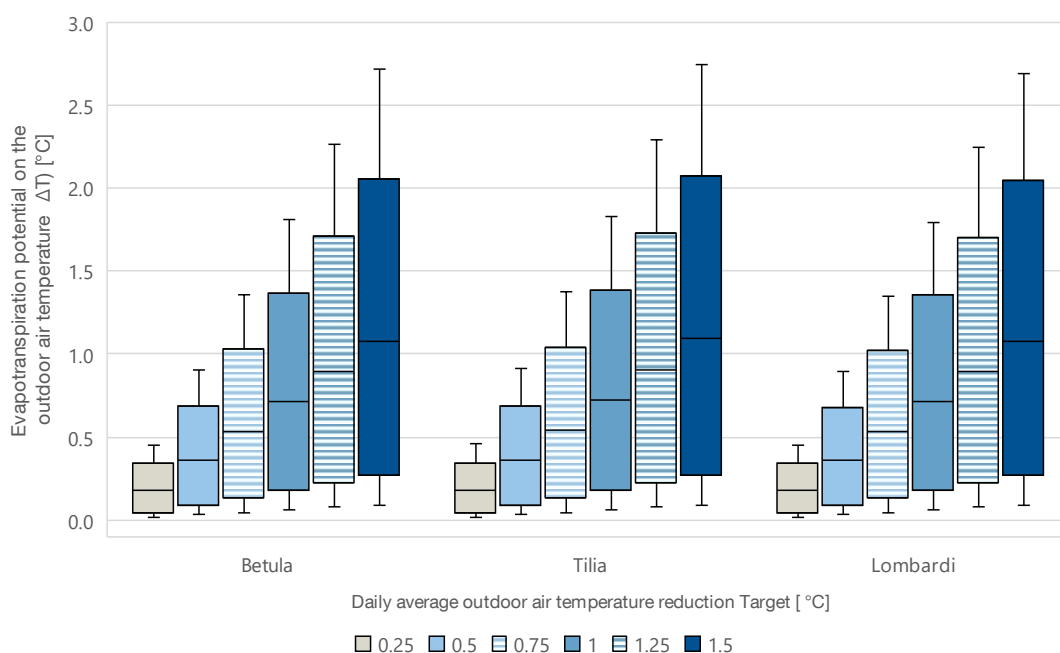


Figure 20 | Box plot of the cooling potential through evapotranspiration per tree species in the summer average outdoor air temperature at each $T_{air\downarrow,Target}$ | 2020-2100 | RCP 8.5

A summary of the results can be consulted in Table 15. From 2020 to 2050 all scenarios showed the same cooling potential at each $T_{air\downarrow,Target}$. It can be observed that the cooling potential increased at different rates at each $T_{air\downarrow,Target}$. For instance, it increased about $0.05^{\circ}C$ per year at $T_{air\downarrow,0.25^{\circ}C}$ and about $0.33^{\circ}C$ per year at $T_{air\downarrow,1.5^{\circ}C}$. It must be noted that these increase rates were not constant from one analysis year to another, the presented value are average values from 2020 to 2100.

Figure 21 shows the evapotranspiration potential per tree species per $T_{air\downarrow,Target}$ in 2050 and 2100. All tree species showed the same cooling potential in 2050 at each $T_{air\downarrow,Target}$. In 2050, a cooling potential from about $0.11^{\circ}C$ to $0.65^{\circ}C$ for $T_{air\downarrow,0.25^{\circ}C}$ and $T_{air\downarrow,1.5^{\circ}C}$, respectively, was observed. By 2100, Tilia C. showed the highest cooling

Results

potential from about 0.46°C to 2.75°C at $T_{air\downarrow,0.25^{\circ}C}$ and $T_{air\downarrow,1.5^{\circ}C}$, respectively. Those from Betula P. and Lombardi P. were between 0.45°C and around 2.70°C, respectively.

Table 15 | Summary - Evapotranspiration rate in the summer average outdoor air temperature per tree species at each $T_{air\downarrow,Target}$ between 2050 and 2100 | RCP 8.5

Cooling potential [°C]	0.25	0.5	0.75	1.0	1.25	1.5
Min- Max	0.02 to 0.45	0.03 to 0.92	0.05 to 1.37	0.06 to 1.83	0.08 to 2.29	0.09 to 2.75
Median	0.02 to 0.35	0.09 to 0.69	0.13 to 1.04	0.18 to 1.38	0.22 to 1.73	0.27 to 2.08
Average ¹	0.05 (+/- 0.04)	0.11 (+/- 0.08)	0.16 (+/- 0.12)	0.22 (+/- 0.16)	0.27 (+/- 0.20)	0.33 (+/- 0.24)

1 – Average cooling potential increase per analysis year, i.e., from 2020 to 2100.

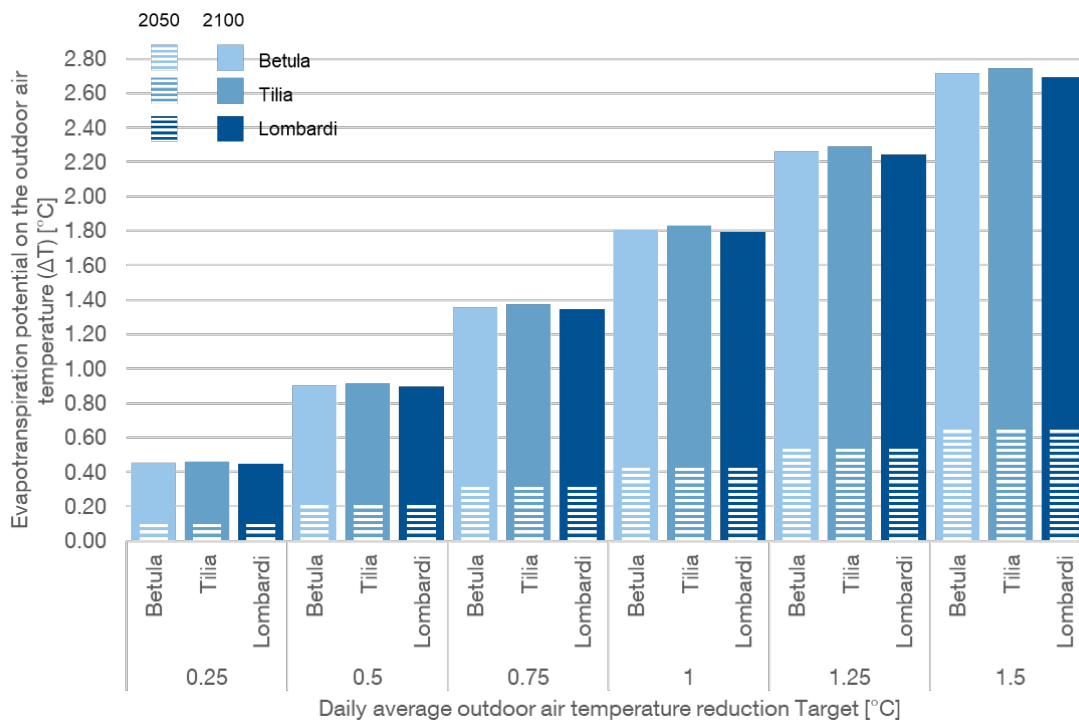


Figure 21 | Evapotranspiration potential on the outdoor air temperature per tree species | 2050 -2100 | RCP 8.5

6.2.2 Cooling potential | Evapotranspiration | Indoor

The results refer to the cooling potential through evapotranspiration of trees, i.e., the summer average operative temperature reduction compared to the baseline scenario, i.e., without trees at each $T_{air\downarrow,Target}$.

Office space | 2nd Floor | EPW RCP4.5

Figure 22 illustrates the box plot of the cooling potential through evapotranspiration per tree species in the summer average operative temperature of the office on the second floor at each $T_{air\downarrow,Target}$.

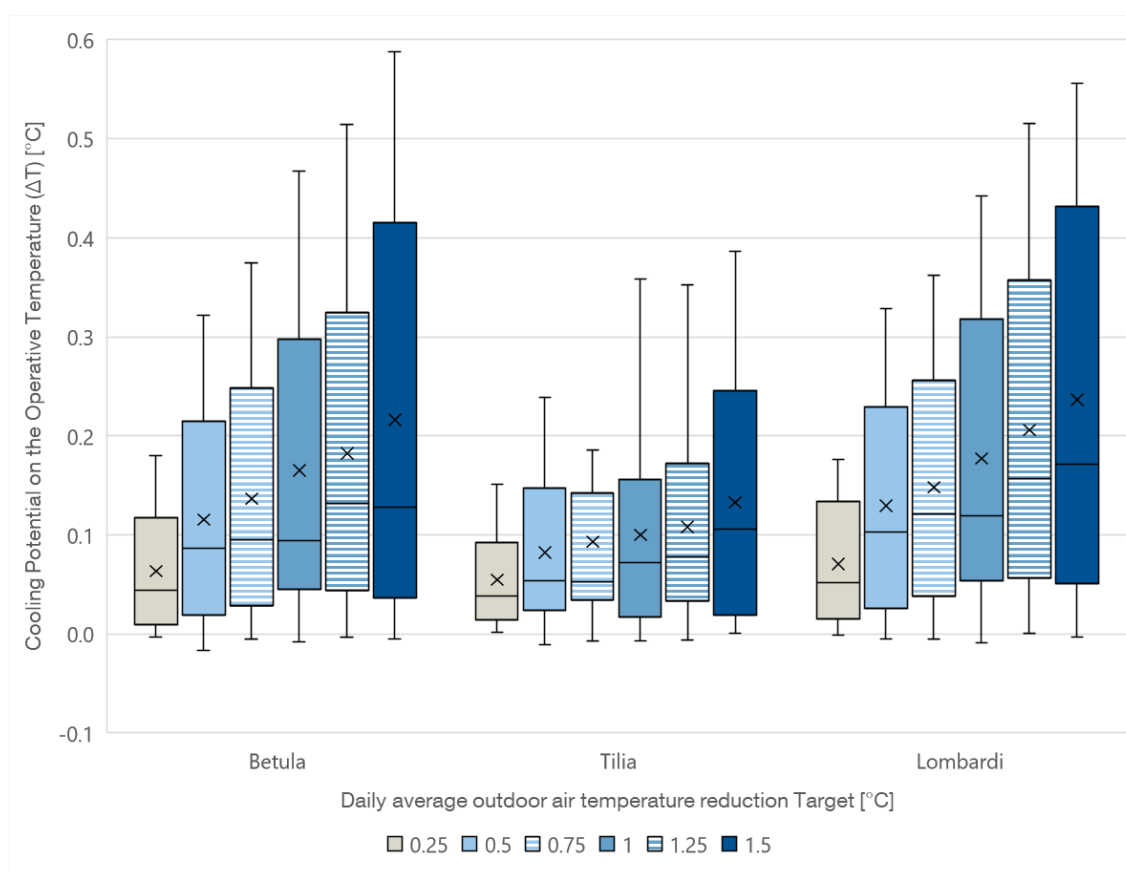


Figure 22 | Box plot of the cooling potential through evapotranspiration per tree species in the summer average operative temperature of the office at each $T_{air\downarrow,Target}$ | 2020-2100 | RCP 4.5

Betula P. and Lombardi P. showed the greatest cooling potential through evapotranspiration. At $T_{air\downarrow,0.25^{\circ}C}$, the median of both scenarios cooling potential stood above 0.1°C. At $T_{air\downarrow,1.5^{\circ}C}$, both scenarios reached a median cooling potential of about 0.4°C. On average, the median values from Lombardi P. trees were slightly greater than those from Betula P. trees. The maximum cooling potential of Betula P. trees at

Results

$T_{air\downarrow,0.75^{\circ}C}$ was slightly higher than that from Lombardi P. trees. The increase rate of the cooling potential per analysis year was greater for Betula P. than for the Lombardi P. scenario. That from Tilia C. was less consistent. On average, the cooling potential of Tilia C. scenario was lower than expected. Limitations on the simulation process caused inconsistent results in the cooling potential. Further details are explained in the Section 7.2. The median operative temperature reduction was below $0.2^{\circ}C$ from $T_{air\downarrow,0.25^{\circ}C}$ to $T_{air\downarrow,1.5^{\circ}C}$. It reached a median temperature reduction of almost $0.25^{\circ}C$ at $T_{air\downarrow,1.5^{\circ}C}$.

On average, changes in the summer average operative temperature were not noticeable between 2020 and 2040. Table 16 summarizes the observed cooling potential per tree species in 2050 and 2100 at each $T_{air\downarrow,Target}$. Further information at each outdoor air temperature reduction target can be found in Appendix | Table XXII to Appendix | Table XXIV.

Table 16 | Cooling potential through evapotranspiration per tree species per $T_{air\downarrow,Target}$ | 2050 to 2100 with RCP 4.5

Cooling potential [$^{\circ}C$]	0.25	0.5	0.75	1.0	1.25	1.5
Betula P.	0.04 to 0.13	0.08 to 0.32	0.09 to 0.33	0.09 to 0.40	0.13 to 0.47	0.13 to 0.59
Tilia C.	0.06 to 0.09	0.08 to 0.21	0.08 to 0.19	0.09 to 0.19	0.10 to 0.25	0.13 to 0.36
Lombardi P.	0.05 to 0.14	0.10 to 0.33	0.11 to 0.34	0.12 to 0.40	0.16 to 0.47	0.17 to 0.53

From 2050, Betula P. showed a cooling potential from $0.04^{\circ}C$ to $0.13^{\circ}C$ from $T_{air\downarrow,0.25^{\circ}C}$ to $T_{air\downarrow,1.5^{\circ}C}$, respectively (see Figure 23). Those from Lombardi P. trees ranged from $0.05^{\circ}C$ to $0.17^{\circ}C$, respectively. The cooling potential of Tilia C. oscillated between $0.06^{\circ}C$ and $0.13^{\circ}C$ from $T_{air\downarrow,0.25^{\circ}C}$ to $T_{air\downarrow,1.5^{\circ}C}$, respectively. A cooling potential of almost $0.1^{\circ}C$ were observed from $T_{air\downarrow,0.5^{\circ}C}$ for all tree species. These from Betula P. and Tilia C. trees were $0.02^{\circ}C$ lower than that from Lombardi P. By 2100, Betula P. and Lombardi P. showed the greatest cooling potential through evapotranspiration (see Figure 24). At $T_{air\downarrow,1.5^{\circ}C}$, cooling potentials of $0.59^{\circ}C$ and $0.53^{\circ}C$ were observed for Betula P. and Lombardi P., respectively. Tilia C. reached a cooling potential of $0.36^{\circ}C$.

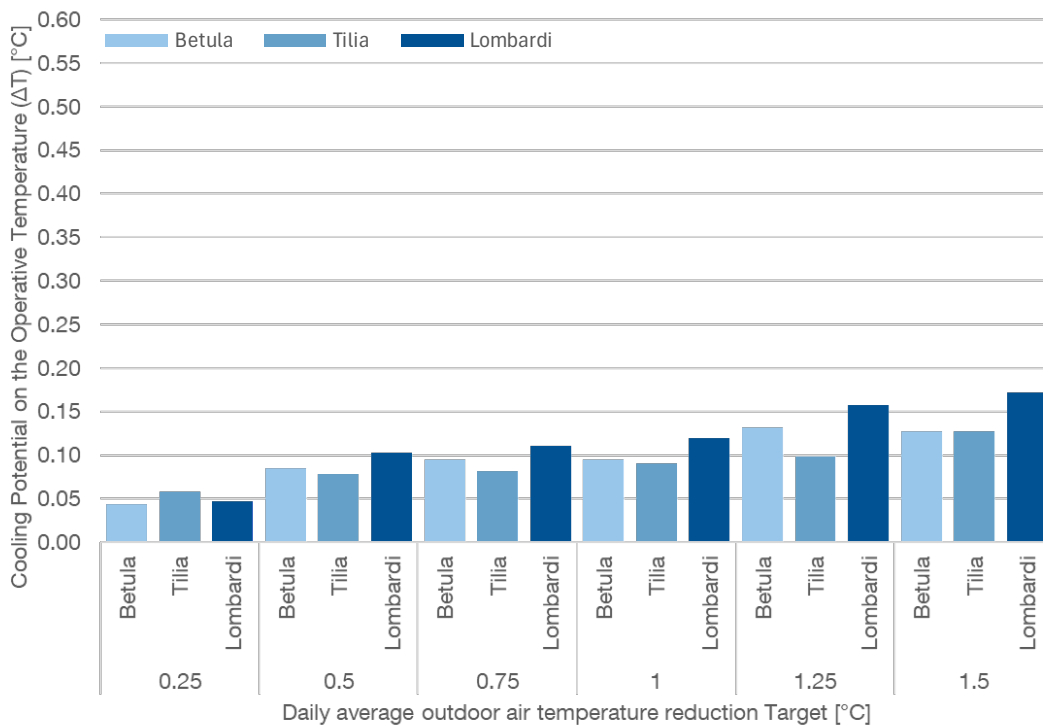


Figure 23 | Cooling potential through evapotranspiration per tree species per $T_{air↓,Target}$ | 2050 - RCP 4.5

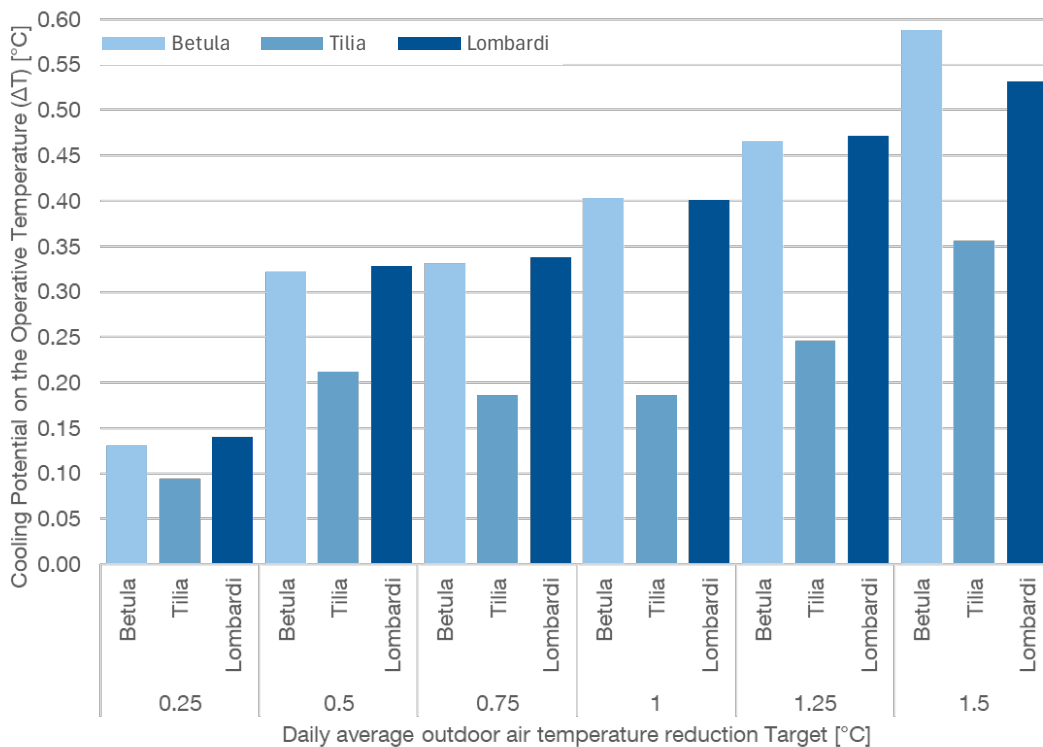


Figure 24 | Cooling potential through evapotranspiration per tree species per $T_{air↓,Target}$ | 2100 - RCP 4.5

Results

Office space | 2nd Floor | EPW RCP8.5

Contrary to the results with RCP4.5, differences on the operative temperature were more noticeable for RCP 8.5, keeping a better relationship between the changes on both the outdoor air temperature and the operative temperature. Figure 25 shows a box plot of the cooling potential through evapotranspiration per tree species at each $T_{air\downarrow,Target}$.

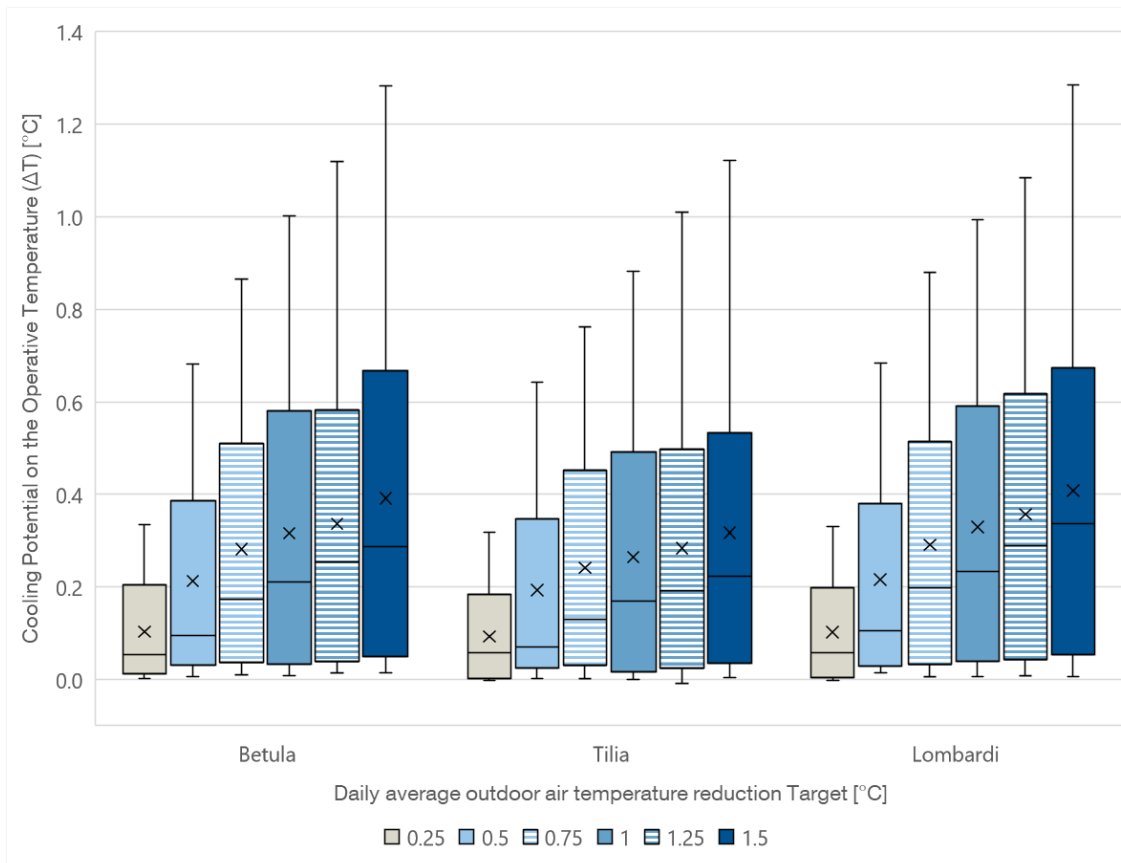


Figure 25 | Box plot of the cooling potential through evapotranspiration per tree species per $T_{air\downarrow,Target}$ | 2020-2100 in RCP 8.5

It can be observed a median cooling potential of about 2°C for the three tree species at $T_{air\downarrow,0.25^{\circ}C}$. On average, from $T_{air\downarrow,0.75^{\circ}C}$, as the $T_{air\downarrow,Target}$ increased, the median value increased, but at a lower rate. The median values of the cooling potential at $T_{air\downarrow,1.0^{\circ}C}$ and $T_{air\downarrow,1.25^{\circ}C}$ in all the scenarios were similar. These correspond to almost 0.6°C for Betula P. and Lombardi P. scenarios, and about 0.3 °C for Tilia C. trees. Betula P. and Lombardi P. showed the higher median cooling potential at $T_{air\downarrow,1.5^{\circ}C}$, i.e., almost 0.7°C. That from Tilia C. scenario was above 0.5°C.

As in the results with RCP 4.5, cooling potential through evapotranspiration was perceptible from 2050. Table 17 shows a summary of the cooling potential per tree

species between 2050 and 2100 at each $T_{air\downarrow,Target}$. In 2050 (see Figure 26), a slightly higher cooling potential was observed in the scenario with Lombardi P. trees. Its cooling potential ranged from 0.02 to 0.18°C between $T_{air\downarrow,0.25^{\circ}C}$ and $T_{air\downarrow,1.5^{\circ}C}$, respectively. Betula P. showed a similar performance, these were about 0.02°C to 0.15°C between $T_{air\downarrow,0.25^{\circ}C}$ and $T_{air\downarrow,1.5^{\circ}C}$, respectively. For the Tilia C. scenario, those corresponded to 0.01°C and 0.12°C, respectively. In 2100 (see Figure 27), Betula P. and Lombardi P. showed a similar cooling potential on each $T_{air\downarrow,Target}$. They showed the highest cooling potential. It was around 0.33 at $T_{air\downarrow,0.25^{\circ}C}$ and almost 1.3°C at $T_{air\downarrow,1.5^{\circ}C}$. Tilia C. showed a similar cooling potential from that from Betula P. and Lombardi P. at $T_{air\downarrow,0.25^{\circ}C}$, i.e., about 0.32°C. However, at $T_{air\downarrow,1.5^{\circ}C}$, it was about 1.12°C. Further information at each $T_{air\downarrow,Target}$ can be found in Appendix | Table XXV to Appendix | Table XXVII.

Table 17 | Cooling potential through evapotranspiration per tree species per $T_{air\downarrow,Target}$ | 2050 to 2100 in RCP 8.5

Cooling potential [°C]	0.25	0.5	0.75	1.0	1.25	1.5
Betula P.	0.02 to 0.34	0.06 to 0.68	0.09 to 0.87	0.12 to 1.00	0.12 to 1.12	0.15 to 1.28
Tilia C.	0.01 to 0.32	0.07 to 0.64	0.08 to 0.76	0.09 to 0.88	0.10 to 1.01	0.12 to 1.12
Lombardi P.	0.02 to 0.33	0.08 to 0.68	0.11 to 0.88	0.14 to 0.99	0.17 to 1.09	0.18 to 1.29

Results

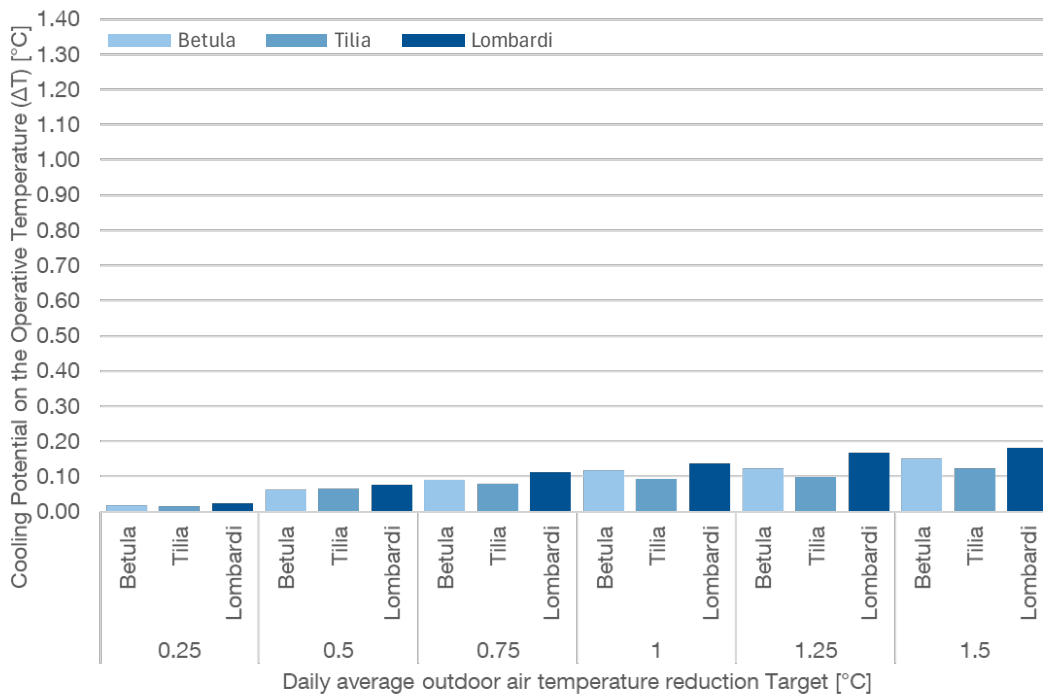


Figure 26 | Cooling potential through evapotranspiration per tree species per $T_{air\downarrow,Target}$ | 2050 - RCP 8.5

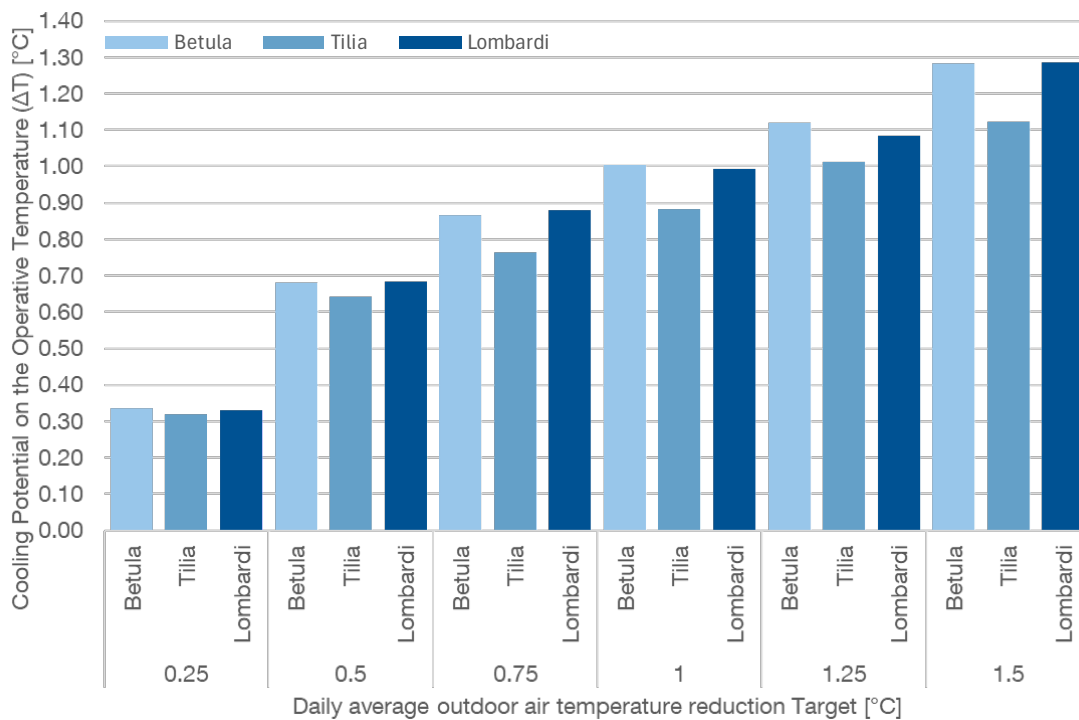


Figure 27 | Cooling potential through evapotranspiration per tree species per $T_{air\downarrow,Target}$ | 2100 - RCP 8.5

6.3 Cooling potential | Evapotranspiration and Shading

The cooling potential of trees through shading and evapotranspiration were combined to identify their contribution in a space. The presented results of the cooling potential refer to the summer average operative temperature reduction from the baseline scenario, i.e., without trees at each $T_{air\downarrow,Target}$ in 2050 and 2100.

6.3.1 Share on the cooling potential

Office space | 2nd Floor | RCP4.5

The shadow and evapotranspiration potential had a different share on the total cooling potential per tree species based on the $T_{air\downarrow,Target}$. Further information for each scenario can be found in the Appendix | Table XXVIII to Appendix | Table XXX.

In 2050, Lombardi P. scenario showed the greatest cooling potential on the summer average operative temperature through shadow and evapotranspiration considering the $T_{air\downarrow,0.25^{\circ}C}$ and $T_{air\downarrow,1.5^{\circ}C}$. A total cooling potential between 1.2°C and 1.4°C was observed, respectively. Betula P. showed a total cooling potential about 40% lower than the one from Lombardi P. trees. This was from 0.72°C to 0.80°C for $T_{air\downarrow,0.25^{\circ}C}$ and $T_{air\downarrow,1.5^{\circ}C}$, respectively. Tilia C. showed the lowest total cooling potential, about 70% lower than the one from Lombardi P. trees. It showed a total cooling potential between 0.34°C and 0.40°C for the $T_{air\downarrow,0.25^{\circ}C}$ and $T_{air\downarrow,1.5^{\circ}C}$, respectively.

The following distributions were observed in 2050 (see Figure 28):

- The shadow potential of Lombardi P. trees accounted from about 96% to 87% of the total cooling potential for $T_{air\downarrow,0.25^{\circ}C}$ to $T_{air\downarrow,1.5^{\circ}C}$, respectively. Evapotranspiration potential accounted for the remaining cooling potential, i.e., from about 6% to 13%.
- The shadow potential of Betula P. trees accounted from around 94% to 84% of the total cooling potential for $T_{air\downarrow,0.25^{\circ}C}$ to $T_{air\downarrow,1.5^{\circ}C}$, respectively.
- The shadow potential of Tilia C. trees ranged between 83% and 69% of the total cooling potential at $T_{air\downarrow,0.25^{\circ}C}$ and $T_{air\downarrow,1.5^{\circ}C}$, respectively. Evapotranspiration potential accounted from about 17% to 31% of the total cooling potential.

By 2100, the shadow potential of Betula P. and Lombardi P. trees accounted from about 94% to 80% of the total cooling potential for $T_{air\downarrow,0.25^{\circ}C}$ to $T_{air\downarrow,1.5^{\circ}C}$, respectively.

Results

Evapotranspiration represented around 6% to 20% of the total cooling potential (see Figure 29). Betula P. showed the greatest cooling potential, from about 2.35°C to 2.81°C for $T_{air\downarrow,0.25^\circ C}$ and $T_{air\downarrow,1.5^\circ C}$, respectively. That of the Lombardi P. scenario ranged from about 2.26°C to 2.65°C for $T_{air\downarrow,0.25^\circ C}$ to $T_{air\downarrow,1.5^\circ C}$, respectively. Tilia C. showed a total cooling potential from about 1.52°C to 1.78°C at $T_{air\downarrow,0.25^\circ C}$ and $T_{air\downarrow,1.5^\circ C}$, respectively. Its shadow potential represented 63% to 69% of the total cooling potential, respectively.

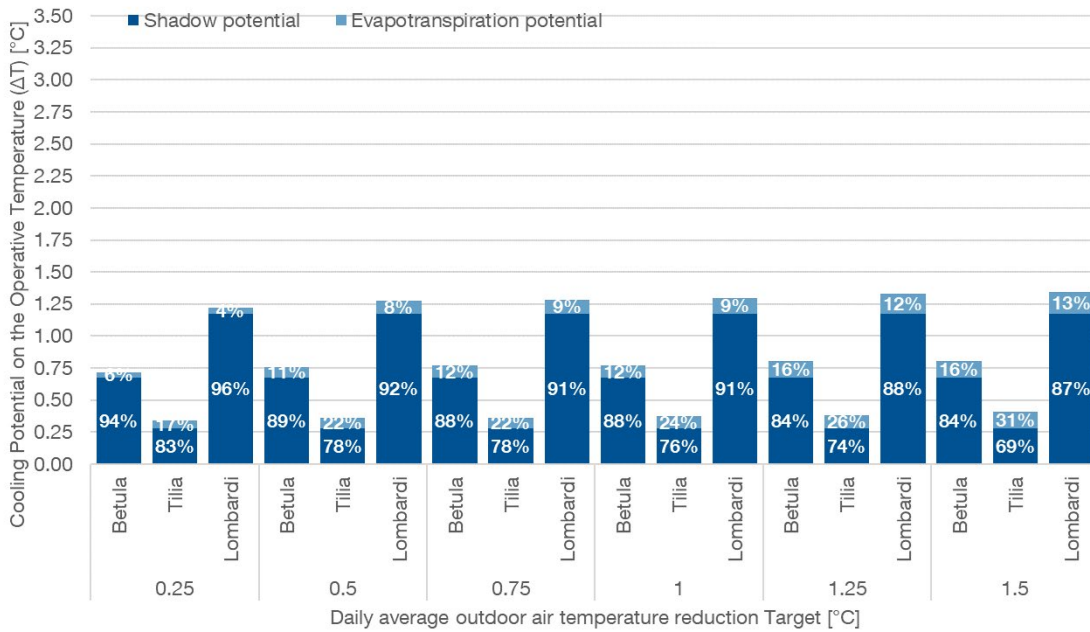


Figure 28 | Share of cooling potential per tree species | 2050 - RCP 4.5

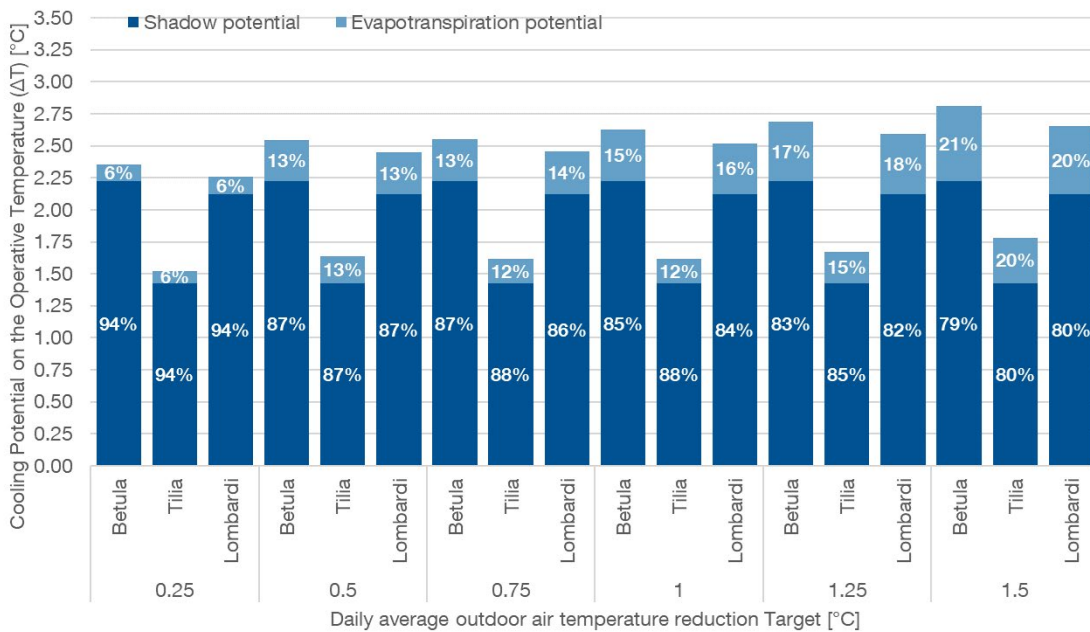


Figure 29 | Share of cooling potential per tree species | 2100 - RCP 4.5

Office space | 2nd Floor | RCP8.5

The share of the shading and evapotranspiration on the total cooling potential depended on the $T_{air\downarrow,Target}$ on each scenario. In 2050, Lombardi P. showed the highest total cooling potential for $T_{air\downarrow,0.25^{\circ}C}$ and $T_{air\downarrow,1.5^{\circ}C}$. It ranged from 1.22°C to 1.38°C, respectively. Betula P. showed a total cooling potential about 40% lower than the one from Lombardi P. trees. It corresponded to about 0.7°C to 0.84°C, respectively. The total cooling potential of Tilia C. was about 70% lower than the one of Lombardi P. It ranged from 0.34°C to 0.45°C, respectively. Further information regarding the cooling potential on the operative temperature for each scenario from 2020 to 2100 considering each $T_{air\downarrow,Target}$ can be found in the Appendix | Table XXXI to Appendix | Table XXXIII.

The following distributions were observed in 2050 for $T_{air\downarrow,0.25^{\circ}C}$ and $T_{air\downarrow,1.5^{\circ}C}$ (see Figure 30):

- The shadow potential of Lombardi P. trees accounted from about 98% to 87% of the total cooling potential between $T_{air\downarrow,0.25^{\circ}C}$ and $T_{air\downarrow,1.5^{\circ}C}$, respectively. Evapotranspiration potential ranged between 2% and 13%, respectively.
- The shadow potential of Betula P. represented from around 97% to 82% of the total cooling potential for $T_{air\downarrow,0.25^{\circ}C}$ and $T_{air\downarrow,1.5^{\circ}C}$, respectively. Evapotranspiration accounted for about 3% to 18%, respectively.
- Tilia C.'s shadow potential ranged between 96% and 72% of the total cooling potential for $T_{air\downarrow,0.25^{\circ}C}$ and $T_{air\downarrow,1.5^{\circ}C}$, respectively. Evapotranspiration had a share from about 4% to 28% of the total cooling potential.

It can be observed in the Figure 31 that, by 2100, the shadow potential of both Betula P. and Lombardi P. accounted from about 86% to around 60% of the total cooling potential for $T_{air\downarrow,0.25^{\circ}C}$ and $T_{air\downarrow,1.5^{\circ}C}$, respectively. Evapotranspiration potential accounted from about 14% to less than 40%, respectively. Tilia C. showed a lower share of the shadow potential. It represented about 81% to 54% of the total cooling potential for $T_{air\downarrow,0.25^{\circ}C}$ and $T_{air\downarrow,1.5^{\circ}C}$, respectively. The evapotranspiration potential accounted for around 19% to 46% of the total cooling potential, respectively.

Overall, Betula P. showed the highest cooling potential by 2100 (see Figure 31). It showed a cooling potential from about 2.41°C to 3.36°C for $T_{air\downarrow,0.25^{\circ}C}$ and $T_{air\downarrow,1.5^{\circ}C}$, respectively. That of Lombardi P. oscillated between 2.32°C and 3.28°C, respectively. Tilia C. showed the lowest total cooling potential. It ranged from about 1.65°C to 2.46°C, respectively.

Results

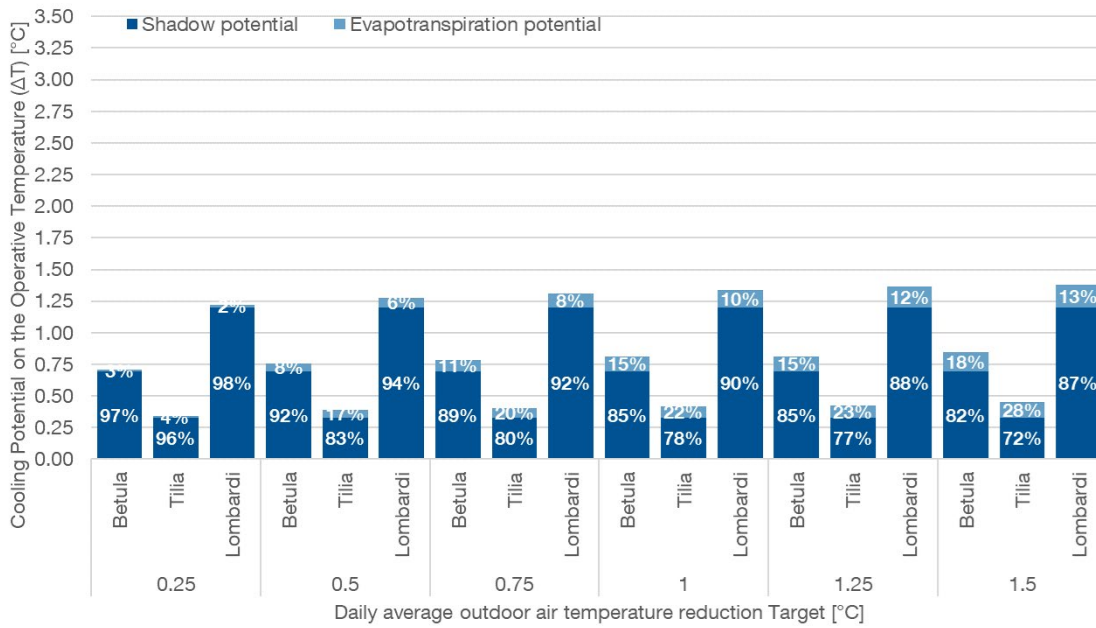


Figure 30 | Share of cooling potential per tree species | 2050 - RCP 8.5

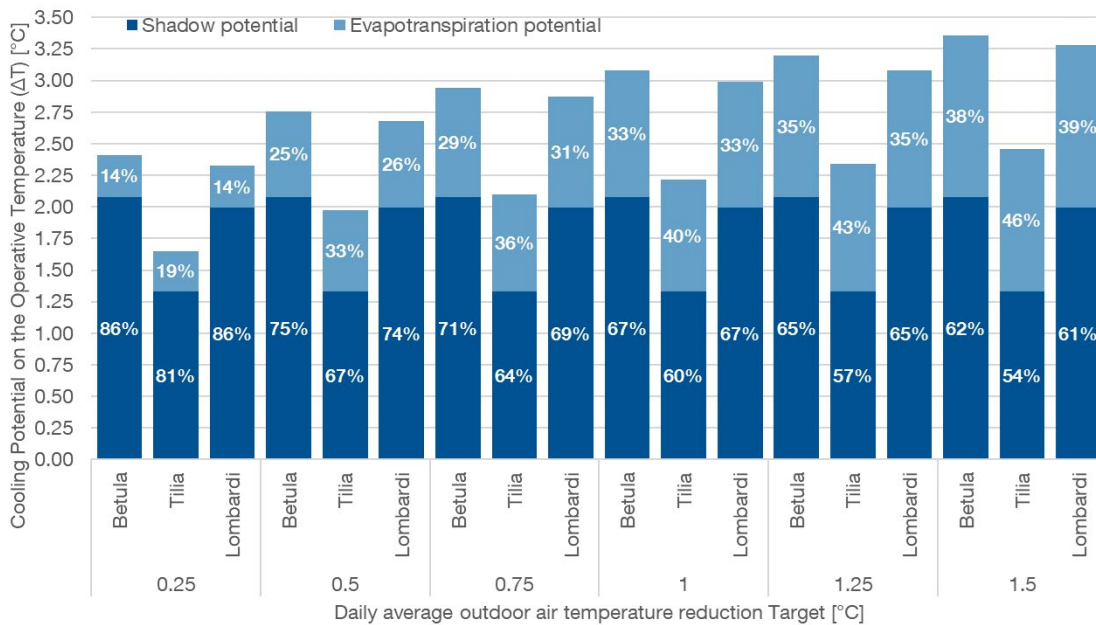


Figure 31 | Share of cooling potential per tree species | 2100 - RCP 8.5

6.3.2 Cooling potential through shadow and evapotranspiration at $T_{air\downarrow,1.5^\circ C}$

The presented results considered the shadow potential following the methodology described in Section 4.1 as well as the evapotranspiration potential with the $T_{air\downarrow,1.5^\circ C}$, as described in Section 4.2 for each tree species. The results refer to the cooling potential of trees, i.e., the summer average operative temperature reduction compared to the baseline scenario, i.e., without trees.

Office space | 2nd Floor | EPW RCP4.5

Figure 32 summarizes the cooling potential per tree species. Betula P. scenario showed the highest cooling potential in 2100. It was about 2.8°C, i.e., 9.5% lower than the scenario without trees. As presented in the Appendix | Table IV, the summer average operative temperature without trees was about 29.8°C by 2100. Thus, that was reduced from about 29.8°C to 27°C by the cooling potential through shadow and evapotranspiration of Betula P. trees. These accounted for 79% and 21%, respectively, of the total cooling potential. Overall, shadow and evapotranspiration potentials contributed to reducing the summer average operative temperature by about 2.2°C and 0.6°C, respectively.

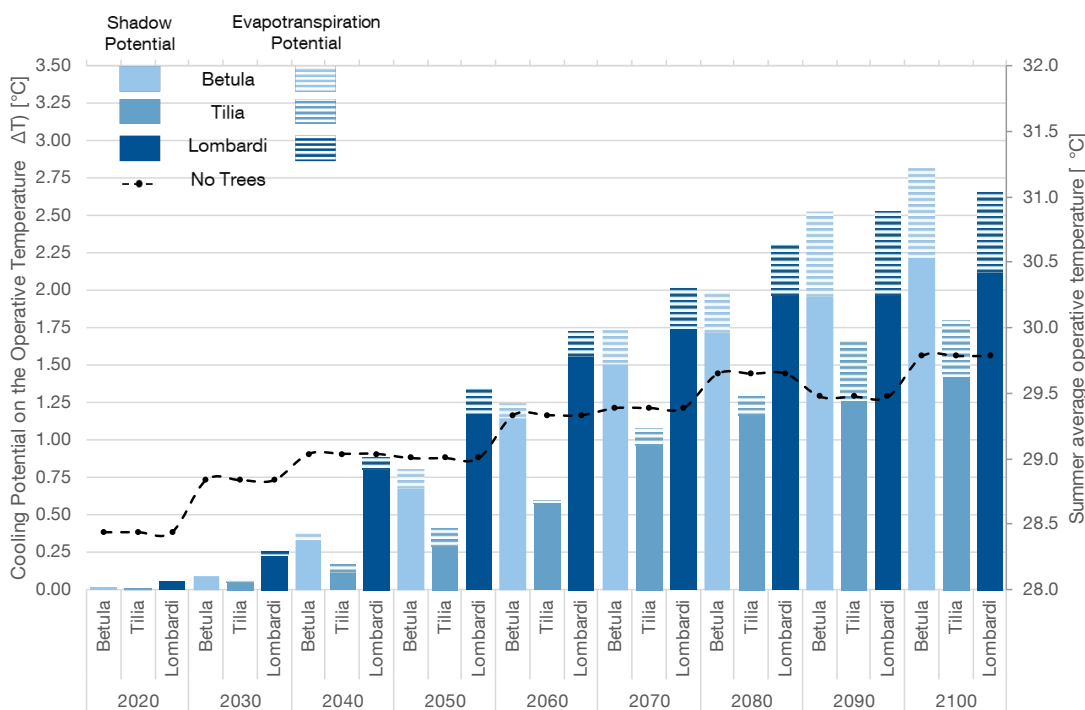


Figure 32 | Cooling Potential Shading and Evapotranspiration per Tree species at $T_{air\downarrow,1.5^\circ C}$ | Summer average operative temperature reduction per analysis year | 2nd Floor | RCP 4.5

Results

The cooling potential of Lombardi P. trees contributed to reducing the summer average operative temperature by about 2.7°C in 2100. This corresponded to an average operative temperature reduction of around 8.9% lower than the one without trees. Shading potential accounted for 80% of the total cooling potential, while evapotranspiration contributed to reducing the operative temperature by 20%. This corresponded to around 2.1°C and 0.6°C, respectively. Tilia C. showed the lowest contribution to the cooling potential. It showed a summer average operative temperature reduction of about 6%, about 1.8°C less than the one from the baseline scenario. Its shading potential accounted for 80% of the total cooling potential, while its evapotranspiration potential represented the remaining 20%. These represented a cooling potential of about 1.4°C and 0.4°C, respectively.

CDH per scenario | RCP 4.5

Table 18 summarizes the CDH per scenario. By 2100, the cooling potential of Betula P. trees contributed to reducing CDH up to 55%, i.e., about 4,790 Kh less than the baseline scenario. Compared to the results of cooling potential through shading from the section 6.1, evapotranspiration accounted for 18% of the total reduction of CDH. Those from Lombardi P. scenario were reduced by about 52%, i.e., about 4,507 Kh less than the ones without trees. Evapotranspiration contributed to reducing the total CDH by 15%, the rest was attributed to the shading potential (85%). Tilia C. contributed to reducing the CDH by about 36%, i.e., about 3,130 Kh less than the baseline scenario. Evapotranspiration and shading accounted for almost 10% and 90%, respectively, of the total reduction of CDH.

Table 18 | Cooling degree hours per analysis year per scenario | 2nd Floor | RCP 4.5

CDH26/26 [Kh]	2020	2030	2040	2050	2060	2070	2080	2090	2100
No Trees	6,350	7,313	7,588	6,976	7,718	7,901	8,398	8,232	8,701
Betula P. S+E	6,336	7,066	6,813	5,530	5,441	4,870	4,910	3,846	3,909
Tilia C. S+E	6,370	7,116	7,284	6,284	6,591	6,088	6,130	5,313	5,571
Lombardi P. S+E	6,267	6,777	5,997	4,630	4,697	4,383	4,410	3,809	4,194

S + E = Cooling potential through Shadow and Evapotranspiration

By 2100, operative temperatures in the Betula P. and Lombardi P. scenarios observed similar time frequency per operative temperature range. Operative temperatures were almost 30% of the occupancy time below 26°C. These corresponded to 17% and 16% more than those from the baseline scenario, respectively. Evapotranspiration accounted for almost 6% of the total time increase. Besides, operative temperatures above 32°C were observed between 6% and 7% of the occupancy time, respectively. Evapotranspiration contributed by 1% to reducing the time frequency. These were reduced to between 26% and 27% less than in the baseline scenario. Moreover, operative temperatures between 28°C and 30°C occurred almost 30% of the occupancy time. These were about 7% and 6%, respectively, more frequent than in the baseline scenario. Evapotranspiration accounted about 2% and 1%, respectively, of the increase (see Figure 33). For the Tilia C. scenario, the time frequency per operative temperature range was similar to those from the baseline scenario in 2020. Operative temperatures below 26°C were observed 24% of the occupancy time, 11% more than the baseline scenario from 2100. Evapotranspiration accounted for 5% of the time frequency increase. Besides, operative temperatures above 32°C were observed 14% of the occupancy time, i.e., about 19% less than the ones from the baseline scenario. Evapotranspiration accounted for 2% of the time frequency reduction (see Figure 33).

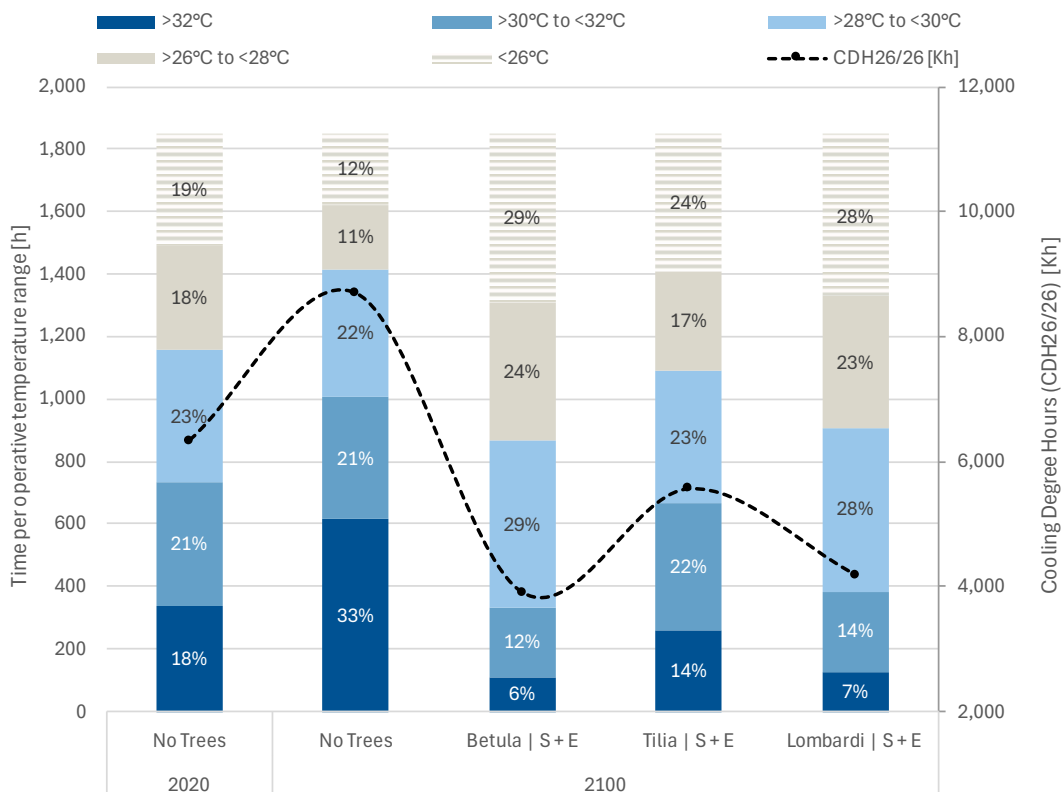


Figure 33 | Time per operative temperature range and CDH per scenario by 2100 | 2nd Floor | RCP 4.5

Results

Office space | 2nd Floor | EPW RCP8.5

The cooling potential per tree species for the summer average operative temperature of the office located on the second floor at $T_{air\downarrow,1.5^\circ C}$ can be consulted in the Figure 34. Betula P. showed the highest cooling potential in 2100 by reducing the summer average operative temperature about 3.4°C, i.e., 10.6% lower than the scenario without trees. The summer average operative temperature from the baseline scenario was reduced from 31.6°C to 28.2°C through cooling potential of Betula P. trees. Shading and evapotranspiration potentials accounted for 62% and 38%, respectively, of the total cooling potential. Overall, they contributed to reducing the summer average operative temperature by about 2.1°C and 1.3°C, respectively.

Lombardi P. trees showed a similar performance to that of Betula P. trees. They contributed to reducing the summer average operative temperature from the baseline scenario by about 10.4%. This corresponded to a summer average operative temperature reduction of around 3.3°C. Shading and evapotranspiration potentials contributed 61% and 39%, respectively, of the total cooling potential. This corresponded to around 2°C and 1.3°C, respectively.

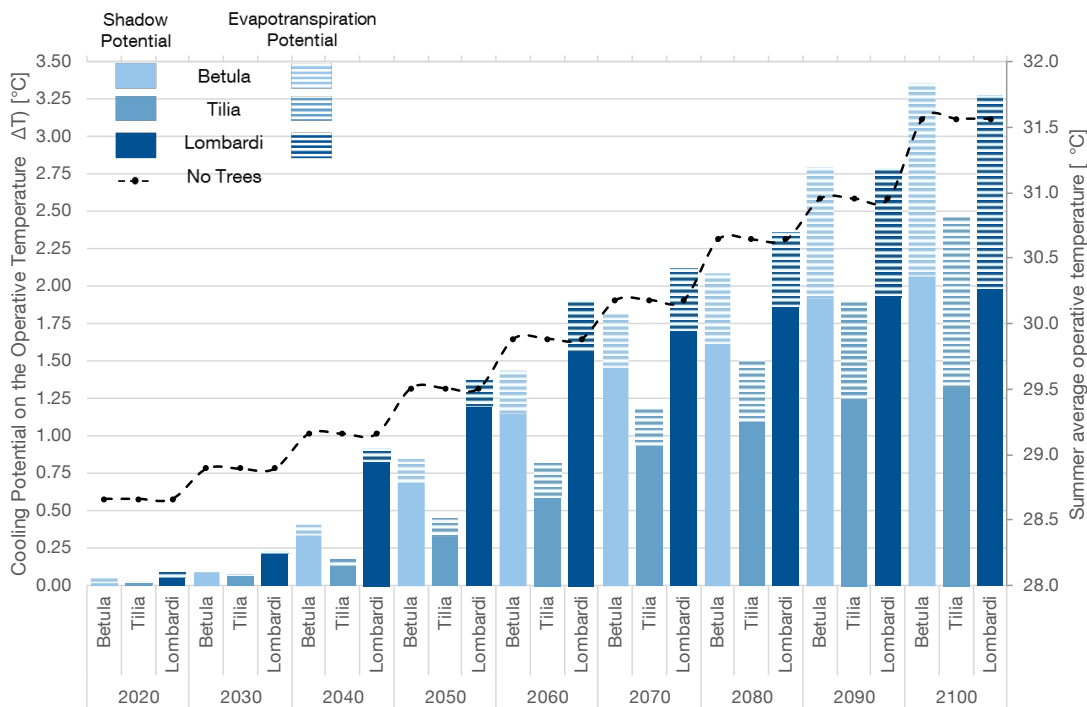


Figure 34 | Cooling Potential Shading and evapotranspiration per Tree species at $T_{air\downarrow,1.5^\circ C}$ | Summer average temperature reduction per analysis year | 2nd Floor | RCP 8.5

Tilia C. showed the lowest cooling potential. It showed a summer average operative temperature reduction of about 2.5°C, about 7.8% less than in the baseline scenario. Shading and evapotranspiration potentials accounted for 54% and 46%, respectively, of the total cooling potential. These represented a summer average operative temperature reduction of about 1.35°C and 1.15°C, respectively, less than the one without trees.

CDH per scenario | RCP 8.5

Table 17 summarizes the CDH per scenario. By 2100, Betula P. and Lombardi P. scenarios contributed to reducing the total CDH by more than 50% compared to the baseline scenario, i.e., 6,443 Kh and 6,363 Kh less than the baseline scenario. Evapotranspiration contributed to reducing the total CDH by more than 30%. Tilia C. contributed to reducing CDH about 41%, i.e., about 4,760 Kh less than the baseline scenario. About 25% of the total CDH reduction was attributed to the evapotranspiration potential.

Table 19 | Cooling degree hours per analysis year per scenario | 2nd Floor | RCP 8.5

CDH26/26 [Kh]	2020	2030	2040	2050	2060	2070	2080	2090	2100
No Trees	7,050	7,164	7,509	8,172	8,871	9,233	9,843	10,418	11,566
Betula P. S+E	6,979	6,900	6,729	6,483	6,138	5,641	5,858	5,089	5,123
Tilia C. S+E	7,018	6,943	7,163	7,223	7,254	6,721	6,909	6,667	6,806
Lombardi P. S+E	6,921	6,674	5,905	5,591	5,347	5,162	5,407	5,081	5,203

S + E = Cooling potential through Shadow and Evapotranspiration

The time per operative temperature range as well as the total CDH per scenario are illustrated in the Figure 35. The time frequency at each operative temperature range with Betula P. and Lombardi P. trees were similar. On average, operative temperature was more than 20% of the occupancy time below 26°C, i.e., about 15% and 13%,

Results

respectively, more than the scenario without trees. Evapotranspiration accounted for about 5% of the time increase. Besides, temperatures above 32°C were observed 9% of the occupancy time. Compared to the baseline scenario, these were reduced by about 35%. Evapotranspiration contributed to reducing the time frequency of those above 32°C by 21%. Regarding the Tilia C. scenario, like the observations with RCP 4.5, the time frequency at each temperature range was similar to those from the baseline scenario from 2020. Temperatures below 26°C were observed 17% of the occupancy time, i.e., about 10% more than the baseline scenario in 2100. Evapotranspiration accounted for 4% of the time increase. Besides, temperatures above 32°C were observed 21% of the occupancy time, i.e., about 22% less than the ones from the baseline scenario. Evapotranspiration contributed to reducing by 14% the time frequency from those above 32°C.

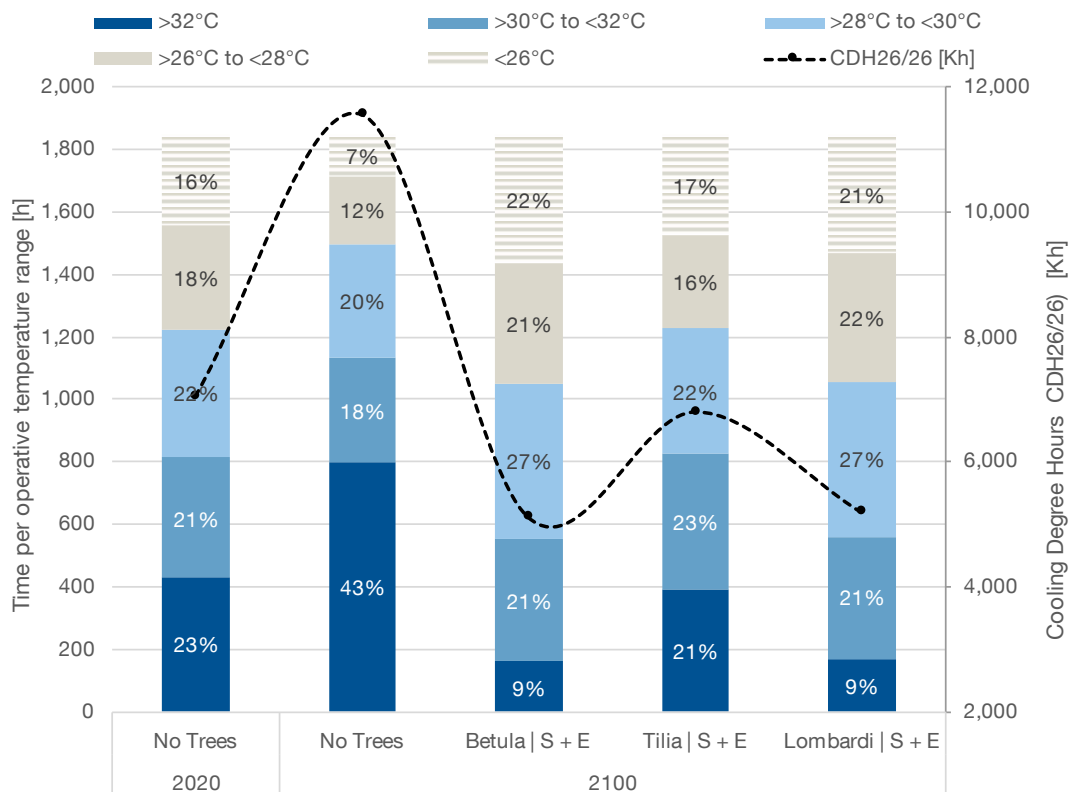


Figure 35 | Time per operative temperature range and CDH per scenario by 2100 | 2nd Floor | RCP 8.5

7 Discussion

The cooling potential through shading and evapotranspiration of trees increased over time and its rate depended on each tree species and their height related to the floor level of each interior space. In general, the impact of the cooling potential in the offices started between 2020 and 2040 and reached its maximum level by 2100. The cooling potential considering both climate change projections reported similar values.

7.1 Cooling potential through shading

Cooling potential through shading | RCP 4.5

The observed cooling potential between 2020 and 2040 in the office located on the first and ground floor provided by the different tree species was similar to the results of [13]. The summer average operative temperature of the office on the first and ground floor was reduced from 2020, particularly through Lombardi P. trees. It was about from 0.4°C to 0.7°C lower than the one from the baseline scenario between 2020 and 2040. In 2040, Lombardi P. scenario showed a cooling potential of 0.8°C for the office located on the second floor. Betula P. and Tilia C. contributed to reducing the summer average operative temperature of the office located on the first floor about 0.8°C and 0.7°C, respectively. Lombardi P. showed a cooling potential of about 1.4°C in both the office on the first and ground floor. From 2070, the cooling potential of the three tree species contributed to reducing the summer average operative temperature of the baseline scenario on the first and ground floors between 1.8°C and 2°C. Tilia C. reported a cooling potential of 2°C in the office on the first floor. In the office located on the ground floor, Tilia C. and Lombardi P. were the ones with the highest cooling potential. They contributed to reducing the summer average operative temperature of the baseline scenario by about 1.9°C. Betula P. showed a cooling potential of about 1.8°C. It must be noted that Lombardi P. trees contributed to keeping a summer average operative temperature of about 27.2°C +/- 2°C from 2050 to 2100 in the offices located on the ground and first floors. Besides, the summer average operative temperature of Tilia C. scenario for the office located on the ground floor remained almost the same from 2070 to 2100, about 27.1°C +/- 1°C. By 2100, both Betula P. and Lombardi P. showed the highest cooling potential through shadow in the office located on the second floor. These corresponded to about 2.2°C and 2.1°C, respectively, lower than the summer average operative temperature from the baseline scenario. On the first floor, the three species

Discussion

reported a summer average operative temperature about 2.4°C lower than the one from the baseline scenario. In the office on the ground floor, the three tree species showed a similar cooling potential. Contrary to the performance of Tilia C. on the second and first floors, it showed the highest cooling potential in the office located on the ground floor. It contributed to reducing the summer average operative temperature of the baseline scenario up to 2.3°C. The cooling potential of Betula P. and Lombardi P. corresponded to about 2°C and 2.2°C, respectively.

Cooling potential through shading | RCP 8.5

In 2020, the performance considering the climate change projections for RCP 8.5 was comparable to those from RCP 4.5. Lombardi P. showed the highest cooling potential in the office on the first and ground floor. It contributed to reducing the summer average operative temperature by about 0.3°C and 0.6°C, respectively. By 2040, cooling potential rates similar to the ones from the observations of [13] were registered. Lombardi P. showed a temperature reduction of about 0.8°C in the office located on the second floor. On the first floor, Betula P. and Tilia C. contributed to reducing the operative temperature of the baseline scenario by about 0.65°C. Cooling potentials between 0.8°C and 1.2°C were observed by the different tree species in the office on the ground floor, being Tilia C. the one with the higher contribution. From 2060, the cooling potential of Betula P. and Lombardi P. trees for the office on the second floor kept increasing at a rate of about 0.3°C and 0.15°C, respectively, per analysis year. Besides, in the office on the first floor, the three tree species contributed to reducing the summer average operative temperature of the baseline scenario above 1.4°C. By 2070, the three tree species showed almost the same cooling potential in the office located on the ground floor, about 1.8°C. Tilia C. showed the greatest contribution. This performance was comparable to the observations from RCP 4.5. In 2090, Tilia C. showed a cooling potential of 2.1°C in the office on the ground floor. Betula P. and Lombardi P. trees showed a cooling potential slightly lower than the one from Tilia C. The three tree species reported a cooling potential of about 2.1°C for the office located on the first floor. In 2100, Betula P. and Lombardi P. trees showed a cooling potential of around 2°C in the office on the second floor. As observed in the RCP 4.5 scenarios, Tilia C. showed the lowest cooling potential in the office on the second floor, about 1.3°C. Nonetheless, it showed the greatest value in the office on the ground floor, about 2.2°C lower than the summer average operative temperature from the baseline scenario. On

the first floor, the three tree species reached a cooling potential up to 2.2°C. *Tilia C.* showed a slightly lower cooling potential of 2.1°C.

Cooling potential through shading | Summary

The transparency rate per tree and analysis year was calculated considering the observations of [79] and [17]. The values varied from 2020 to 2100 and between the climate projections RCP 4.5 and RCP 8.5 (see Table 6). *Betula P.* showed a greater variation over time, about 21%. The transparency of *Tilia C.* increased about 15% and 17% on each climate projection. *Lombardi P.* showed a similar performance in both climate projections, about 15%. The calculated values were on average higher than the values from [80], providing less solar protection. However, the impact of transparency variations on the cooling potential through shading was not representative. On average, the cooling potential using the values from [80] was less than 1% higher than the one with the calculated values. Thus, the crown shape, size and tree height had a greater influence on the cooling potential.

In contrast to [49], the impact of shading potential on a space was not highly influenced by the tree morphology. On average, trees with half-ellipsoid and cylindrical shape, e.g., *Betula P.* and *Lombardi P.*, respectively (see Table 5), had a better performance. It was observed that tree height had the greatest impact on the first and second floors. Nonetheless, tree morphology of *Tilia C.* trees showed a greater impact on the ground floor. In the case of *Betula P.* tree, the position of the crown area related to the window surface of the office on the ground floor was displaced as it grew, causing the shading potential to slightly decrease.

Overall, the different tree species registered comparable cooling potentials to the one observed by [13] in the offices located on the different levels between 2020 and 2040 on both climate projections. However, those were much higher than the results from [76]. Despite the differences regarding tree morphology, number and distribution of trees between the *Betula P.* and *Lombardi P.* trees (see Table 3), their performance was similar on the different office levels. The morphology of *Tilia C.* tree played an important role in the office located on the ground floor. Nonetheless, it showed a lower cooling potential on the second floor because of its crown height related to the window height of the space.

On average, by 2100, trees contributed to reducing the summer average operative temperature of the baseline scenario more than 2°C. The greatest cooling potential was

Discussion

observed in the office on the first floor with climate change scenario RCP 4.5. Despite the morphological differences between the three tree species, they contributed to reducing the summer average operative temperature of the baseline scenario by 2.4°C. However, this value was less than half from the one observed by [14]. It must be noted that his investigation was performed in a city with different climatic conditions.

CDH | RCP 4.5

Without considering trees on the façade, the total CDH increased about 37% in the offices on the different analyzed floors between 2020 and 2100. By 2100, the baseline scenario reported the highest CDH in the office on the second floor, about 8,700 Kh. The ones from the office on the first and ground floor corresponded to more than 8,400 Kh and 7,900 Kh, respectively. On average, *Betula P.* and *Lombardi P.* provided the highest CDH reduction, about 45% and almost 50% less than those from the baseline scenario in the offices on the second and first floor, respectively. *Tilia C.* showed the highest contribution in those on the ground floor, about 50% less than the total CDH from the baseline scenario. On average, the CDH considering trees on the façade ranged from around 4,000 Kh on the ground floor to about 4,750 Kh on the second floor. *Tilia C.* showed the lowest CDH reduction for the office on the second floor. These were more than 6,000 Kh. Trees did not contribute to reducing the CDH to the levels required by DIN. However, it must be noted that the CDH from the scenarios with trees from 2100 were on average 20% to 30% lower than those from 2020 without trees. Furthermore, trees contributed to reducing operative temperatures above 32% between 23% to 25% less of the occupancy time than in the baseline scenario from 2100. It was observed that the temperatures between 26°C and 28°C increased between 9% and 13% more of the occupancy time than in the baseline scenario. Operative temperatures below 26°C occurred more than 20% of the occupancy time. This is twice the time frequency from the baseline scenario.

CDH | RCP 8.5

The total CDH without considering trees increased around 68% on the different levels from 2020 to 2100, i.e., from about 6,700 Kh to 11,300 Kh, respectively. In 2020, the CDH of the baseline scenario accounted for about 7,050 Kh and 6,300 Kh on the second floor and on the ground floor, respectively. On average, by 2100, the different tree species contributed to reducing the total CDH from the offices located on the different

levels between 31% and 35% less than those from the baseline scenario. CDH in all scenarios were greater than 7,000 Kh. With exception from those in the office on the second floor with Tilia C. trees, which reported CDH about 9,100 Kh, i.e., 20% less than those from the baseline scenario. Furthermore, by 2100, the different tree scenarios showed CDH 10% to 20% greater than those from the baseline scenario in 2020. Despite trees did not comply with DIN requirements, they did contribute to remaining CDH like those from 2020.

Despite the summer average operative temperature decreased from 1.5°C to 2.3°C by placing street trees, hourly operative temperatures above 32°C decreased considerably. For instance, in the scenario without trees, temperatures above 32°C were reported about 40% of the occupancy time. Betula P. and Lombardi P. scenarios contributed to decreasing these more than 10% less of the occupancy time compared to those from the baseline scenario. Furthermore, operative temperatures below 26°C occurred almost 20% of the occupancy time. This corresponded to more than double from those from the baseline scenario.

CDH | Summary

Despite the CDH calculation comprised only the period from April to October, by 2100, cooling potential of trees through shading did not contribute to complying with the requirements from DIN 4108-2 2013 [84]. Additional measures are required to achieve such levels. However, by 2100, the CDH results of the different tree species from the scenarios of RCP 4.5 were about 20% to 30% lower than the ones without trees from 2020. These from the scenarios of RCP 8.5 in 2100 were around 10% to 20% greater than those without trees in 2020. The reduction on the CDH and hourly operative temperatures above 32°C were more perceptible in the scenarios with RCP 4.5. On average, operative temperatures below 26°C occurred around 20% of the occupancy time in both climate change scenarios. This is twice as frequent as in the baseline scenario. It can be determined that, although trees could not suppress the totality of CDH, they could contribute to increasing the time frequency of operative temperatures below 26°C. At the same time, they could contribute to decreasing the time frequency of those above 32°C. Thus, they could contribute to reducing the operation time of an air conditioning system.

7.2 Cooling potential through evapotranspiration

The sensitivity analysis was performed for six different $T_{air\downarrow,Target}$. It must be noted that evapotranspiration of trees in urban environments depends on several environmental factors and weather conditions [5, 54–56]. The objective of this analysis was to study the cooling potential of evapotranspiration on the indoor temperature of a space. However, further research is still required to determine its cooling capacity and extension [58] and calculate the energy balance. Thus, it was assumed that the conditions were given for trees to transpire and contribute to reducing the daily average outdoor temperature at each $T_{air\downarrow,Target}$, as observed in several on-site measurements and simulation studies (see Table 1). As exposed by Federer [65], a single tree is not expected to influence the outdoor air temperature. The number of trees placed on each scenario is unrelated to their evapotranspiration potential. The described results correspond to the minimal and maximal $T_{air\downarrow,Target}$, i.e., $T_{air\downarrow,0.25^{\circ}C}$ and $T_{air\downarrow,1.5^{\circ}C}$, respectively. The results showed a correlation between the total leaf area density and the transpiration rate. However, according to the calculated data, the differences on the tree morphology related to a reduced leaf area density as a tree grows old described by [66] were not observed. Thus, the transpiration rate kept increasing over time, as the trees grew old. Further data related to the decrease in transpiration rate and to the ageing of trees would be required. PANDO calculations showed higher transpiration values for the projections of RCP 8.5 compared to those from RCP 4.5.

As observed by [7], differences between the transpiration rate of the three tree species were not representative in the outdoor air temperature reduction. The observed differences between the tree species ranged from $0.02^{\circ}C$ up to $0.06^{\circ}C$ (see Appendix | Table XVI to Appendix | Table XXI). On average, by 2060, the cooling potentials on the outdoor air temperature considering both climate change scenarios from RCP 4.5 and RCP 8.5 were comparable with the observations from Mohammad in [8] and the results from Kurn et. al. in [11]. By 2100, the observed cooling potential from both climate change scenarios were within the ranges measured by Mohammad in [10]. However, average outdoor air temperature reductions greater than $3^{\circ}C$, like those from the results of [6] and [7] were not reached.

Cooling potential through evapotranspiration | Limitations of the study

The initial goal was to analyze the impact of cooling potential of evapotranspiration of trees on the operative temperature of the office space without considering the one from shading potential. However, the first results were not consistent. It was observed that the outdoor air temperature reduction through evapotranspiration was not large enough to have an impact on the operative temperature. Because of the defined setpoints for natural ventilation from the simulation described in the Section 5.2, the windows got closed when the outdoor temperature was below the specified setpoint. Meanwhile, the space remained exposed to solar radiation, causing it to overheat, and, as the outdoor temperature was below the setpoint, the windows would not be opened to dissipate the heat. Thus, the operative temperature increased at lower outdoor air temperatures, instead of decreasing. The setpoints were not modified to maintain consistency with the shadow potential study and the baseline scenario. Further configurations in the setpoints are suggested to study the impact of evapotranspiration. Consequently, the evapotranspiration was analyzed considering the shading of trees. The results were contrasted with those from shadow potential and the difference was considered as the cooling potential through evapotranspiration. It should also be noted that the initial goal was to compare the impact of evapotranspiration in 2060, as it was the reference age for the transpiration calculation of trees (see Section 4.2). However, reductions on the outdoor air temperature from 2060 with RCP 4.5 showed the same behavior with the ventilation setpoint previously described. In the case of Tilia C. scenario, since the tree was not high enough to cover the window surface of the office on the second floor, operative temperature increased at lower outdoor air temperature levels. Therefore, 2050 was selected as the reference analysis year for the comparison of results. Partial greater impact of the evapotranspiration on the operative temperature in the scenarios with RCP 8.5 was observed because the reduced outdoor air temperatures were above the setpoint for ventilation control, which allowed operable windows to remain opened.

Cooling potential through shadow and evapotranspiration

On average, by 2050, both climate change projections with RCP 4.5 and RCP 8.5 showed an equivalent performance between $T_{air\downarrow,0.25^{\circ}C}$ and $T_{air\downarrow,1.5^{\circ}C}$. The evapotranspiration of Betula P. and Lombardi P. trees accounted for about 3% to 18% and from around 2% to 13%, respectively, of the total cooling potential. The total summer average operative temperature reduction of Lombardi P. trees was about 1.2°C and 1.4°C, respectively, lower than the one from the baseline scenario. Betula P. showed a

Discussion

total cooling potential of around 0.7°C to 0.8°C. Greater differences in the share of cooling potential through shadow and evapotranspiration of *Tilia C.* trees were observed between the climate change scenarios. For RCP 4.5, evapotranspiration accounted for 17% to about 30% of the total cooling potential. For RCP 8.5, it represented 4% to 28% of the total cooling potential. The ratio of shading and cooling potential were within the ranges observed by the author in [48], with the difference that the observations correspond to an exterior space. In both climate scenarios, it represented an average operative temperature reduction from about 0.34°C to 0.41°C (+/-4°C) lower than the one from the baseline scenario.

By 2100, a similar share through evapotranspiration of *Betula P.* and *Lombardi P.* trees was observed on each climate change scenario. *Betula P.* showed a cooling potential slightly higher than the one from *Lombardi P.* trees. For the scenarios with RCP 4.5, their cooling potential ranged from about 2.3°C to about 2.8°C. Like the observed shading potential of *Tilia C.*, it reported the lowest total cooling potential. It accounted from 1.5°C to about 1.8°C. Evapotranspiration of all tree species accounted for 6% to 20% of the total cooling potential. These were comparable to the observations from [48], with the exception that those refer to an exterior space. For the scenarios with RCP 8.5, the cooling potential of *Betula P.* and *Lombardi P.* oscillated between 2.3°C and about 3.4°C. The evapotranspiration potential of both tree species accounted for 14% to almost 40% of the total cooling potential. *Tilia C.* showed a cooling potential from about 1.7°C to about 2.5°C. Evapotranspiration accounted for about 20% to 46% of the total cooling potential.

The latter showed the highest share of evapotranspiration potential, about 46% of the total cooling potential. However, this representative share of evapotranspiration does not necessarily represent a greater operative temperature reduction compared to the other tree species. Shading and evapotranspiration potential of *Tilia C.* contributed to reducing the summer average operative temperature about 1.3°C and around 1.1°C, respectively. While that of *Betula P.* was about 2.1°C and 1.3°C through shadow and evapotranspiration potential, respectively. Besides, cooling potential with RCP8.5 was on average twice as those with RCP 4.5 in part because of the findings related to the ventilation setpoint previously described. At higher outdoor air temperatures, the modified outdoor air temperature through evapotranspiration remained above the ventilation setpoint, allowing to dissipate the heat from the space. Thus, lower operative temperatures were observed.

Cooling potential through shadow and evapotranspiration | CDH

Overall, as observed in the results of cooling potential through shading of trees, the combination of evapotranspiration and shading did not comply with the DIN requirements. However, in the scenario with RCP 4.5 from 2100 at $T_{air\downarrow,1.5^\circ C}$, the total cooling potential of Betula P. and Lombardi P. trees contributed to reducing the total CDH from the baseline scenario above 50%. Evapotranspiration contributed to reducing the total CDH about 18% and 15%, respectively. Furthermore, hourly operative temperatures below 26°C occurred less than 30% of the occupancy time. This corresponded to a time frequency twice as high as without trees. Those above 32°C were observed around 7% of the occupancy time, about 26% less frequent than in the baseline scenario. More than 50% of the CDH were concentrated on the ranges from 26°C to 28°C and 28°C to 30°C. Tilia C. reported CDH 36% less than those from the baseline scenario. Operative temperatures above 32°C were reduced about 14% of the occupancy time. About 45% of the operative temperatures occurred between the ranges 28°C to 30°C and 30°C to 32°C.

By 2100, in the climate change scenario from RCP 8.5, CDH from Betula P. and Lombardi P. were more than 30% less than those from the baseline scenario. Hourly operative temperatures below 26°C were observed more than 20% of the occupancy time. The time frequency was two times higher than without trees. Those above 32°C were observed less than 10% of the occupancy time. Almost 50% of the total CDH occurred between the ranges 26°C to 28°C and 28°C to 30°C. Tilia C. showed about 25% less CDH than the baseline scenario. Temperatures above 32°C were observed 21% of the occupancy time. And similar to the scenario with RCP 4.5, operative temperatures were observed more than 45% of the occupancy time within the ranges 28°C to 30°C and 30°C to 32°C.

Thus, cooling potential through shading and evapotranspiration of trees could contribute to reducing the total CDH by up to 55% less than without trees. The time frequency of the operative temperatures below 26°C could be increased between 20% and 30% for RCP 4.5 and RCP 8.5, respectively. That means that those above 26°C could be less than 80% and 70% of the occupancy time, respectively. Particularly those above 32°C, which could occur up to less 10% of the occupancy time under both climate change scenarios. This could represent a significant reduction in the operating time of an air conditioning system. The next step should consist of investigating its impact on the cooling energy demand.

7.3 General

From the selected tree species, *Betula P.* showed the best performance. *Lombardi P.* showed a performance like the one from *Betula P.* However, *Betula P.* and *Tilia C.* may require constant maintenance and pruning as they grow to prevent any damage to the building façade, as well as to assure a proper tree development. In contrast with *Lombardi P.* tree, *Betula P.* is not suitable for urban climates [82]. Thus, *Lombardi P.* could be a suitable tree species for this case study. Besides, *Lombardi P.*'s maintenance may be less intensive because of its morphology.

Limitations of the study

Typical and extreme hot weeks for each analysis year were studied to show representative changes between tree species. However, the results based on this type of analysis period were not consistent. For instance, the hottest week in 2020 did not correspond to the one from 2070. The operative temperature from one specific period was found to be lower than the one from a previous analysis year. Thus, average operative temperature from April to October results were used to compare the scenarios.

Limitations for the selected tree species

The selection of tree species was influenced by the availability of information. Even though CityTree [19] and PANDO [81] allow the user to add new species in their database, it would have been required additional time for the research and validation data process. Thus, it was decided to work with the available information. It is to be noted that the tree species used in PANDO were not the same as the ones selected for the analysis. Nonetheless, the tree geometry was the same as CityTree. The transpiration rate calculation was based on tree morphology and leaf development over time. Tree development deficiencies related to transplantation [55], water needs [55], influence of urban conditions on their grow development [56] and evapotranspiration rate [5, 12, 41], as well as tree mortality [56] were not considered in the study. The existing vegetation located in the adjacent park was not included in the study. 10-year-old tree species were considered for the first analysis period. Although younger trees may be easier to transplant, they would have taken longer to grow and see actual impact in the interior space. Similar tree species were identified in Munich, Germany, to support its selection and the morphology data calculated with CityTree (see Appendix | Table I).

8 Conclusions

The impact of cooling potential of trees through shading and evapotranspiration in the operative temperature of a space was studied. An indoor adaptive thermal comfort considering trees as shading elements with different transparency values allowed to investigate the shading potential of trees. The impact of evapotranspiration potential in the interior of a space was analyzed through a sensitivity analysis considering outdoor air temperature reduction through evapotranspiration of trees. Both ecosystem services were combined to identify synergies. Between 2020 and 2040, most of the cooling potential through shading of the different tree species were comparable to the observations from Szkordilis in [13] for the offices located the different levels with both RCP 4.5 and RCP 8.5.

On average, in 2020, 10-year-old street trees between 9 m to 14 m high placed to the southwest of the building's façade contributed to reducing the summer average operative temperature of an office space located on the ground and first floor. Summer average operative temperature reductions between 0.4°C and 0.7°C were observed. On lower levels, tree shape and leaf area density were more representative. For instance, a tree with ovoid shape, i.e., *Tilia C.*, showed the highest cooling potential over time. It took about 20 years for trees to prevent solar radiation into the space located on the second floor. Tree height played a more important role than tree shape. At first, trees with cylindrical shape had a better performance than those with half-ellipsoid shape. Differences on the total leaf density area between tree species was not as representative as its height related to the office space. The disposition of the windows was somehow part of the influence on the results. By 2100, trees with greater crown size and lower height, i.e., *Tilia C.*, had the greatest cooling potential in an office on the ground floor. It was about 2.3°C. On the first floor, tree shape and leaf area density were not as representative as on other levels. The cooling potential between the different tree species was quite similar. On the second floor, trees with half-ellipsoid shape had a cooling potential about 0.1°C higher than those with cylindrical shape. On average, *Betula P.* and *Lombardi P.* trees showed the highest cooling potentials on the different levels. Those ranged between 2.2 and 2.4°C for RCP 4.5, and between 2.0°C and 2.2°C for RCP 8.5. Despite it would be required to plant more *Lombardi P.* trees than *Betula P.* trees to achieve similar temperature reductions, *Betula P.* trees could require more maintenance than *Lombardi P.* trees [82] because of its morphology and proximity to the building facade. Besides, considering climate change, *Lombardi P.* trees have a

Conclusions

better resistance to urban environments [82]. On average, the greatest shading potential was observed in the office on the first floor. Trees contributed to reducing the operative temperature by about 2.4°C and 2.2°C for the RCP 4.5 and RCP 8.5, respectively.

Cooling potential through evapotranspiration under ideal conditions considering $T_{air\downarrow,1.5^\circ C}$ showed perceptible contributions from 2040. By 2050, it accounted from 5% to almost 15% of the total cooling potential. By 2100, trees contributed to reducing the summer average operative temperature about 2.8°C and 3.4°C for the climate change scenarios RCP 4.5 and RCP 8.5, respectively. Evapotranspiration accounted for about 21% and 38%, respectively, of the total cooling potential. The rest was attributed to the shading potential. The study and simulation configuration showed a dependency between the shadow and evapotranspiration potential. Without shadow protection, cooling potential of trees was not representative in the operative temperature of a space. It was also observed a greater cooling potential through evapotranspiration at higher outdoor air temperatures. Nonetheless, this performance was influenced by the setpoint for ventilation control defined in the simulation.

Although trees may require more than 30 years to contribute to reducing the operative temperature in a space about 11 m above the sidewalk, the benefits on a long-term in both exterior [5–10, 18, 48, 51] and interior spaces [13–15, 17, 49] are representative. Trees can provide benefits to spaces located on the ground and first floor from the first decade. Temporary shading devices could be installed on levels without direct shading from the trees, which could be removed once the tree has reached the required height. Climbing plants and green walls can also contribute to such end [67, 76].

Despite cooling potential of trees did not contribute to reducing CDH to the required levels from DIN, by 2100, *Betula P.* and *Lombardi P.* tree scenarios contributed to reducing these from the baseline scenario with RCP 4.5 by up to 50%. Evapotranspiration potential accounted for more than 15% of the CDH reduction. Operative temperatures above 32°C were observed about 7% of the operating time. For RCP 8.5, those were reduced up to 55%. Evapotranspiration potential accounted for more than 30% of the CDH reduction. Temperatures above 32°C occurred 10% of the occupancy time through both *Betula P.* and *Lombardi P.* trees. By 2100, CDH similar and in some cases, lower than those from the baseline scenario in 2020 were observed. Thus, by placing trees on a building's façade, their cooling potential could contribute to reducing the operating time of an air conditioning system. It is suggested to integrate the cooling potential of trees in a hybrid cooling simulation to investigate its contribution to reducing the cooling energy demand.

9 Acknowledgements

The author expresses his gratitude to the Mexican National Council for Humanities, Science and Technology (CONAHCYT) for their financial support through the international scholarship “Becas CONACYT Cultura: Creadores del futuro 2021” to study the Master of Science “Resource-efficient and Sustainable Building” at the Technical University of Munich, Germany.

He also thanks Roland Reitberger and the Chair of Energy Efficient and Sustainable Design and Building for their assistance and support with the required information for this paper; to Prof. Dr. Thomas Rötzer for providing the Excel-Tool CityTree; and to Dr. Ing. Ata Chokhachian for providing further data for the implementation of PANDO components. These tools and data were key elements for this paper.

Acknowledgements

10 References

- [1] United Nations, *Causes and Effects of Climate Change*. [Online]. Available: <https://www.un.org/en/climatechange/science/causes-effects-climate-change> (accessed: Nov. 30 2023).
- [2] International Energy Agency (IEA), *The future of Cooling: Opportunities for energy-efficient air conditioning*. [Online]. Available: <https://www.iea.org/reports/the-future-of-cooling> (accessed: Nov. 4 2023).
- [3] UN Environmental Programme, *Partners announce new ambition on sustainable cooling for COP28*. [Online]. Available: <https://www.unep.org/news-and-stories/press-release/partners-announce-new-ambition-sustainable-cooling-cop28> (accessed: Nov. 4 2023).
- [4] H. Taha, H. Akbari, and A. Rosenfeld, "Heat island and oasis effects of vegetative canopies: Micro-meteorological field-measurements," *Theoretical and Applied Climatology*, vol. 44, no. 2, pp. 123–138, 1991, doi: 10.1007/BF00867999.
- [5] J. Konarska *et al.*, "Transpiration of urban trees and its cooling effect in a high latitude city," *International journal of biometeorology*, vol. 60, no. 1, pp. 159–172, 2016, doi: 10.1007/s00484-015-1014-x.
- [6] L. O. Myrup, "A Numerical Model of the Urban Heat Island," *Journal of Applied Meteorology*, vol. 8, no. 6, pp. 908–918, 1969, doi: 10.1175/1520-0450(1969)008<0908:ANMOTU>2.0.CO;2.
- [7] A. Dimoudi and M. Nikolopoulou, "Vegetation in the urban environment: microclimatic analysis and benefits," *Energy and Buildings*, vol. 35, no. 1, pp. 69–76, 2003, doi: 10.1016/S0378-7788(02)00081-6.
- [8] M. A. Rahman, A. Moser, T. Rötzer, and S. Pauleit, "Within canopy temperature differences and cooling ability of *Tilia cordata* trees grown in urban conditions," *Building and Environment*, vol. 114, pp. 118–128, 2017, doi: 10.1016/j.buildenv.2016.12.013.
- [9] M. A. Rahman, A. Moser, A. Gold, T. Rötzer, and S. Pauleit, "Vertical air temperature gradients under the shade of two contrasting urban tree species during different types of summer days," *Science of The Total Environment*, vol. 633, pp. 100–111, 2018, doi: 10.1016/j.scitotenv.2018.03.168.
- [10] M. A. Rahman *et al.*, "Tree cooling effects and human thermal comfort under contrasting species and sites," *Agricultural and Forest Meteorology*, vol. 287, p. 107947, 2020, doi: 10.1016/j.agrformet.2020.107947.
- [11] D. M. Kurn, S. E. Bretz, B. Huang, and H. Akbari, "The potential for reducing urban air temperatures and energy consumption through vegetative cooling," United States, 1994. [Online]. Available: <https://www.osti.gov/biblio/10180633>

References

- [12] N. Meili *et al.*, "Tree effects on urban microclimate: Diurnal, seasonal, and climatic temperature differences explained by separating radiation, evapotranspiration, and roughness effects," *Urban Forestry & Urban Greening*, vol. 58, p. 126970, 2021, doi: 10.1016/j.ufug.2020.126970.
- [13] F. Szkordilisz and M. Kiss, "Potential of Vegetation in Improving Indoor Thermal Comfort and Natural Ventilation," *Applied Mechanics and Materials*, vol. 824, pp. 278–287, 2016, doi: 10.4028/www.scientific.net/AMM.824.278.
- [14] M. Chagolla, G. Álvarez-García, E. Simá, R. Tovar, and G. Huelsz, "Effect of Tree Shading on the Thermal Load of a House in a Warm Climate Zone in Mexico," in 2012.
- [15] H. Akbari and H. Taha, "The impact of trees and white surfaces on residential heating and cooling energy use in four Canadian cities," *Energy*, vol. 17, no. 2, pp. 141–149, 1992, doi: 10.1016/0360-5442(92)90063-6.
- [16] H. Akbari, D. M. Kurn, S. E. Bretz, and J. W. Hanford, "Peak power and cooling energy savings of shade trees," *Energy and Buildings*, vol. 25, no. 2, pp. 139–148, 1997, doi: 10.1016/S0378-7788(96)01003-1.
- [17] G. M. Heisler, "Effects of individual trees on the solar radiation climate of small buildings," *Urban Ecology*, vol. 9, no. 3, pp. 337–359, 1986, doi: 10.1016/0304-4009(86)90008-2.
- [18] H. Taha, H. Akbari, A. Rosenfeld, and J. Huang, "Residential cooling loads and the urban heat island—the effects of albedo," *Building and Environment*, vol. 23, no. 4, pp. 271–283, 1988, doi: 10.1016/0360-1323(88)90033-9.
- [19] T. Rötzer, *CityTree*: Technical University of Munich, 2023.
- [20] F. Tardieu and T. Simonneau, "Variability among species of stomatal control under fluctuating soil water status and evaporative demand: Modelling isohydric and anisohydric behaviours," *Journal of Experimental Botany*, vol. 49, pp. 419–432, 1998, doi: 10.1093/jexbot/49.suppl_1.419.
- [21] American Meteorological Society (AMS), *Glossary of Meteorology*. [Online]. Available: https://glossarytest.ametsoc.net/wiki/Anthropogenic_heat (accessed: Apr. 27 2024).
- [22] P. U. Pimpalkhute, S. Rao, and T. V. Ramachandra, "Carbon Sequestration Potential of Urban Trees," in 2010.
- [23] U.S. Energy Information Administration (EIA), *Units and calculators explained: Degree days*. 1000 Independence Ave., SW, Washington, DC 20585. [Online]. Available: <https://www.eia.gov/energyexplained/units-and-calculators/degree-days.php> (accessed: Mar. 29 2024).
- [24] cli-MATE Database, *Degree days description*. [Online]. Available: https://mrcc.purdue.edu/CLIMATE/Station/Daily/degreeday_description.html#:~:text=temperature%20and%2065,-,For%20example%2C%20if%20the%20high%20temperature%20for%20the%20day%20was,80%20%2D%2065%20%3D%2015%20CDD. (accessed: Mar. 29 2024).

- [25] M. Dardir, K. Panchabikesan, F. Haghghat, M. El Mankibi, and Y. Yuan, "Opportunities and challenges of PCM-to-air heat exchangers (PAHXs) for building free cooling applications—A comprehensive review," *Journal of Energy Storage*, vol. 22, pp. 157–175, 2019, doi: 10.1016/j.est.2019.02.011.
- [26] M. Thambidurai, K. Panchabikesan, K. Mohan N., and V. Ramalingam, "Review on phase change material based free cooling of buildings—The way toward sustainability," *Journal of Energy Storage*, vol. 4, pp. 74–88, 2015, doi: 10.1016/j.est.2015.09.003.
- [27] Portland Gov., *How to measure a tree*. [Online]. Available: <https://www.portland.gov/trees/tree-care-and-resources/how-measure-tree#:~:text=Guide,4.5%20feet%20above%20the%20ground>. (accessed: Nov. 22 2023).
- [28] NatureScot, *Ecosystem services - nature's benefits*. [Online]. Available: <https://www.nature.scot/scotlands-biodiversity/scottish-biodiversity-strategy-and-cop15/ecosystem-approach/ecosystem-services-natures-benefits#:~:text=Ecosystem%20Services%20are%20the%20direct,as%20reducing%20stress%20and%20anxiety>. (accessed: Jun. 30 2024).
- [29] Britannica, *Evapotranspiration*. [Online]. Available: <https://www.britannica.com/science/evapotranspiration>
- [30] *Thermal Environmental Conditions for Human Occupancy*, ANSI/ASHRAE Standard 55-2020.
- [31] H. Lieth and American Institute of Biological Sciences, *Phenology and seasonality modeling*. New York: Springer-Verlag New York, 1974.
- [32] Britannica, *Phenology*. [Online]. Available: <https://www.britannica.com/science/phenology>
- [33] M. David, M. Donn, F. Garde, and A. Lenoir, "Assessment of the thermal and visual efficiency of solar shades," *Building and Environment*, vol. 46, no. 7, pp. 1489–1496, 2011, doi: 10.1016/j.buildenv.2011.01.022.
- [34] *AZ of tree terms: A companion to british arboriculture*. [Online]. Available: <https://treeterms.co.uk/files/definitions/street-tree>
- [35] C. Park, J. Ha, and S. Lee, "Association between Three-Dimensional Built Environment and Urban Air Temperature: Seasonal and Temporal Differences," *Sustainability*, vol. 9, p. 1338, 2017, doi: 10.3390/su9081338.
- [36] Britannica, *Transpiration*. [Online]. Available: <https://www.britannica.com/science/transpiration>
- [37] Collins Dictionary, *Transpiration*. [Online]. Available: <https://www.collinsdictionary.com/dictionary/english/transpiration>
- [38] EU, *Regulation of the European Parliament and of The Council on nature restoration*. [Online]. Available: <https://eur-lex.europa.eu/legal-content/EN/TXT/PDF/?uri=CELEX:52022PC0304> (accessed: Nov. 7 2023).

References

- [39] DWD, *Urban climate - urban heat islands*. [Online]. Available: https://www.dwd.de/EN/research/climateenvironment/climate_impact/urbanism/urban_heat_island/urbanheatisland_node.html
- [40] J. P. Ortiz Partida, *California's Thirsty Future: The Role of Vapor Pressure Deficit in Our Changing Climate and Droughtwildfires?* [Online]. Available: <https://blog.ucsusa.org/pablo-ortiz/californias-thirsty-future-the-role-of-vapor-pressure-deficit-in-our-changing-climate-and-drought/> (accessed: Nov. 12 2023).
- [41] C. Phillips, *What is Vapor Pressure Deficit (VPD) and what is its connection to wildfires?* [Online]. Available: <https://blog.ucsusa.org/carly-phillips/what-is-vapor-pressure-deficit-vpd-and-what-is-its-connection-to-wildfires/#:~:text=what%20is%20VPD%3F,moisture%20is%20in%20the%20air.> (accessed: Nov. 12 2023).
- [42] International Energy Agency (IEA), *IEA - Energy systems - Buildings*. [Online]. Available: <https://www.iea.org/energy-system/buildings> (accessed: Nov. 3 2023).
- [43] United Nations, *Sustainable Development Goals (SDG)*. [Online]. Available: <https://www.un.org/sustainabledevelopment/> (accessed: Nov. 3 2023).
- [44] International Energy Agency (IEA), *IEA - Tracking Clean Energy Progress 2023*. [Online]. Available: <https://www.iea.org/reports/tracking-clean-energy-progress-2023> (accessed: Nov. 3 2023).
- [45] Intergovernmental Panel on Climate Change (IPCC), *AR6 Synthesis Report: Climate Change 2023*. [Online]. Available: <https://www.ipcc.ch/report/ar6/syr/> (accessed: Nov. 4 2023).
- [46] International Energy Agency (IEA), *IEA - Energy systems - Buildings - Space Cooling*. [Online]. Available: <https://www.iea.org/energy-system/buildings/space-cooling> (accessed: Nov. 3 2023).
- [47] European Environmental Agency (EEA), *Proposal for a Common International Classification of Ecosystem Goods and Services (CICES) for Integrated Environmental and Economic Accounting*. [Online]. Available: <https://www.nottingham.ac.uk/CEM/pdf/UNCEEA-5-7-Bk1.pdf> (accessed: Nov. 13 2023).
- [48] L. Shashua-Bar and M. Hoffman, "Vegetation as a climatic component in the design of an urban street," *Energy and Buildings - ENERG BLDG*, vol. 31, pp. 221–235, 2000, doi: 10.1016/S0378-7788(99)00018-3.
- [49] J. R. Simpson and McPherson, "Potential of tree shade for reducing residential energy use in California," *Journal of Arboriculture*, 22(1): 10-18, 1996. [Online]. Available: <https://www.fs.usda.gov/research/treesearch/61736>
- [50] Y. Lin, T. Huang, W. Yang, X. Hu, and C. Li, "A Review on the Impact of Outdoor Environment on Indoor Thermal Environment," *Buildings*, vol. 13, no. 10, 2023, doi: 10.3390/buildings13102600.
- [51] L. Manickathan, T. Defraeye, J. Allegrini, D. Derome, and J. Carmeliet, "Parametric study of the influence of environmental factors and tree properties on the transpirative cooling effect of trees," *Agricultural and Forest Meteorology*, vol. 248, pp. 259–274, 2018, doi: 10.1016/j.agrformet.2017.10.014.

- [52] M. A. Rahman, D. Armson, and A. R. Ennos, "A comparison of the growth and cooling effectiveness of five commonly planted urban tree species," *Urban Ecosystems*, vol. 18, no. 2, pp. 371–389, 2015, doi: 10.1007/s11252-014-0407-7.
- [53] L. Pastore, R. Corrao, and P. K. Heiselberg, "The effects of vegetation on indoor thermal comfort: The application of a multi-scale simulation methodology on a residential neighborhood renovation case study," *Energy and Buildings*, vol. 146, pp. 1–11, 2017, doi: 10.1016/j.enbuild.2017.04.022.
- [54] E. B. Peters, J. P. McFadden, and R. A. Montgomery, "Biological and environmental controls on tree transpiration in a suburban landscape," *Journal of Geophysical Research: Biogeosciences*, vol. 115, G4, 2010, doi: 10.1029/2009JG001266.
- [55] R. Kjelgren and T. Montague, "Urban tree transpiration over turf and asphalt surfaces," *Atmospheric Environment*, vol. 32, no. 1, pp. 35–41, 1998, doi: 10.1016/S1352-2310(97)00177-5.
- [56] R. K. Kjelgren and J. R. Clark, "Microclimates and Tree Growth in Three Urban Spaces," *Journal of Environmental Horticulture*, vol. 10, no. 3, pp. 139–145, 1992, doi: 10.24266/0738-2898-10.3.139.
- [57] T. R. Oke and G. B. Maxwell, "Urban heat island dynamics in Montreal and Vancouver," *Atmospheric Environment (1967)*, vol. 9, no. 2, pp. 191–200, 1975, doi: 10.1016/0004-6981(75)90067-0.
- [58] D. E. Bowler, L. Buyung-Ali, T. M. Knight, and A. S. Pullin, "Urban greening to cool towns and cities: A systematic review of the empirical evidence," *Landscape and Urban Planning*, vol. 97, no. 3, pp. 147–155, 2010, doi: 10.1016/j.landurbplan.2010.05.006.
- [59] TUM Graduate School, *Research Training Group 2679 - Urban Green Infrastructure*. [Online]. Available: <https://www.gs.tum.de/en/grk/urban-green-infrastructure/> (accessed: Apr. 21 2024).
- [60] EU, *The European Green Deal: Delivering on our targets*. [Online]. Available: https://ec.europa.eu/commission/presscorner/detail/en/fs_21_3688 (accessed: Nov. 7 2023).
- [61] EU, *Biodiversity Strategy for 2030*. [Online]. Available: https://environment.ec.europa.eu/strategy/biodiversity-strategy-2030_en (accessed: Nov. 7 2023).
- [62] International Energy Agency (IEA), *IEA - In a hotter world, energy efficiency is more important than ever*. [Online]. Available: <https://www.iea.org/spotlights/in-a-hotter-world-energy-efficiency-is-more-important-than-ever> (accessed: Nov. 3 2023).
- [63] N. E. Klepeis *et al.*, "The National Human Activity Pattern Survey (NHAPS): a resource for assessing exposure to environmental pollutants," *Journal of Exposure Science & Environmental Epidemiology*, vol. 11, no. 3, pp. 231–252, 2001, doi: 10.1038/sj.jea.7500165.

References

- [64] EU, *Indoor air pollution: new EU research reveals higher risks than previously thought* (accessed: Nov. 7 2023).
- [65] C. A. Federer, "Trees Modify the Urban Microclimate," *Arboriculture & Urban Forestry (AUF)*, vol. 2, no. 7, pp. 121–127, 1976, doi: 10.48044/jauf.1976.028.
- [66] T. Rötzer, A. Moser-Reischl, S. Pauleit, and H. Pretzsch, "Process based simulation of tree growth and ecosystem services of urban trees under present and future climate conditions," *Science of The Total Environment*, vol. 676, pp. 651–664, 2019, doi: 10.1016/j.scitotenv.2019.04.235.
- [67] R. Berry, S. J. Livesley, and L. Aye, "Tree canopy shade impacts on solar irradiance received by building walls and their surface temperature," *Building and Environment*, vol. 69, pp. 91–100, 2013, doi: 10.1016/j.buildenv.2013.07.009.
- [68] H. Swaid, "Urban climate effects of artificial heat sources and ground shadowing by buildings," *International Journal of Climatology*, vol. 13, no. 7, pp. 797–812, 1993, doi: 10.1002/joc.3370130707.
- [69] J. Pan and J. A. Jakubiec, "Simulating the Impact of Deciduous Trees on Energy, Daylight, and Visual Comfort: Impact Analysis and a Practical Framework for Implementation," in *Proceedings of eSim 2022: 12th Conference of IBPSA-Canada, 2022*. [Online]. Available: https://publications.ibpsa.org/conference/paper/?id=esim2022_251
- [70] K. Nice, A. Coutts, and N. Tapper, "Development of the VTUF-3D v1.0 urban micro-climate model to support assessment of urban vegetation influences on human thermal comfort," *Urban Climate*, vol. 24, 2018, doi: 10.1016/j.uclim.2017.12.008.
- [71] R. Reitberger, K. Theilig, M. Vollmer, I. Takser, and W. Lang, "Connecting building density and vegetation to investigate synergies and trade-offs between thermal comfort and energy demand – a parametric study in the temperate climate of Germany," *IOP Conference Series: Earth and Environmental Science*, vol. 1196, p. 12034, 2023, doi: 10.1088/1755-1315/1196/1/012034.
- [72] R. Reitberger, N. Palm, H. Palm, and W. Lang, "Urban systems exploration: A generic process for multi-objective urban planning to support decision making in early design phases," *Building and Environment*, vol. 254, p. 111360, 2024, doi: 10.1016/j.buildenv.2024.111360.
- [73] F. S. Chapin III, P. A. Matson, and H. A. Mooney, *Principles of Terrestrial Ecosystem Ecology*, 2002.
- [74] S. Cheval *et al.*, "A systematic review of urban heat island and heat waves research (1991–2022)," *Climate Risk Management*, vol. 44, p. 100603, 2024, doi: 10.1016/j.crm.2024.100603.
- [75] M. A. Rahman, A. Moser, T. Rötzer, and S. Pauleit, "Below-canopy Surface and Air Cooling Effect of Two Contrasting Tree Species in Urban Street Conditions: Cited from Mohammad A. Rahman; Astrid Moser; Anna, Vertical air temperature gradients under the shade of two contrasting urban tree species during different types of summer days," 2018.

- [76] D. Marx, R. Reitberger, and W. Lang, "Automated workflow for simulating the effect of green façades on indoor thermal comfort," Institute of Energy Efficient and Sustainable Design and Building, TUM | ENPB, Munich, Germany, 2023. [Online]. Available: <https://mediatum.ub.tum.de/doc/1728650/llwukuq1vnywvj5qr2l7ayuly.MA%20Fassadenbegru%CC%88nung%20und%20Innenraum%20David%20Marx%20Bildschirmfassung.pdf>
- [77] *Meteonorm*. Computer Software: Meteotest AG.
- [78] C. Mackey, *Discourse Ladybug: Outdoor comfort UTCI microclimat map | Vegetation limitations*. [Online]. Available: <https://discourse.ladybug.tools/t/outdoor-comfort-utci-microclimat-map-vegetation-limitations/3263/4> (accessed: Nov. 9 2023).
- [79] T. Rötzer, A. Moser-Reischl, M. Rahman, R. Grote, S. Pauleit, and H. Pretzsch, "Modelling Urban Tree Growth and Ecosystem Services: Review and Perspectives," in 2020, pp. 405–464.
- [80] R. Helliwell, "Site Layout Planning for Daylight and Sunlight. A guide to good practice (2nd edition)," *Arboricultural Journal*, vol. 34, 2012, doi: 10.1080/03071375.2012.692505.
- [81] A. Chokhachian and M. Hiller, "PANDO: Parametric Tool for Simulating Soil-Plant Atmosphere of Tree Canopies in Grasshopper," in *SimAUD '20: Proceedings of the 11th Annual Symposium on Simulation for Architecture and Urban Design*, 2020. Accessed: Nov. 7 2023. [Online]. Available: <https://simaud.org/2020/proceedings/105.pdf>
- [82] GALK (Deutsche Gartenamtsleiterkonferenz) e.V., *GALK Straßenbaumliste: Arbeitskreis Stadtbäume*. [Online]. Available: <https://galk.de/arbeitskreise/stadtbaeume/themenuuebersicht/strassenbaumliste/galk-strassenbaumliste> (accessed: Mar. 30 2024).
- [83] Intergovernmental Panel on Climate Change (IPCC), *Climate Change 2014 Synthesis Report: Topic 2: Future Climate Changes, Risks and Impacts*. [Online]. Available: https://ar5-syr.ipcc.ch/topic_futurechanges.php (accessed: Jan. 9 2024).
- [84] *Thermal protection and energy economy in buildings: Part 2: Minimum requirements to thermal insulation*, DIN 4108-2:2013.
- [85] team für technik, "General Report: TUM", Aug. 2010.
- [86] *Bekanntmachung der Regeln zur Datenaufnahme und Datenverwendung im Wohngebäudebestand: BAnz AT 04.12.2020 B1*, 2020. Accessed: Apr. 3 2024. [Online]. Available: <https://www.bundesanzeiger.de/pub/publication/qzQUGd8A3unSCCbVMcf?0>
- [87] Ingenieurbüro Junge, *Energie sparen, Einsatz erneuerbarer Energien Effiziente Anlagentechnik: Kennwerte von Fenstern*. [Online]. Available: <https://www.xn--ingbro-junge-0ob.de/html/fenster.html#Kennwerte-Fenster>
- [88] G. Hausladen, P. Liedl, and M. de Saldanha, *Climate responsive building, a handbook*.

References

- [89] R. Pongrácz, J. Bartholy, and Z. Dezső, "Application of remotely sensed thermal information to urban climatology of Central European cities," *Physics and Chemistry of the Earth, Parts A/B/C*, vol. 35, no. 1, pp. 95–99, 2010, doi: 10.1016/j.pce.2010.03.004.
- [90] DWD, *Climate data Center (CDC)*. Open Data Server: The Deutscher Wetterdienst (DWD), 2023.
- [91] DWD, *Stadtklima-Studie: Zukünftige Wärmebelastung und Alpines Pumpen*. [Online]. Available: https://www.dwd.de/DE/presse/pressemitteilungen/DE/2020/20200626_stadtklima_muenchen.pdf?__blob=publicationFile&v=3 (accessed: May 18 2024).
- [92] F. Banihashemi, M. Weber, and W. Lang, "Deep learning for predictive window operation modeling in open-plan offices," *Energy and Buildings*, vol. 310, p. 114109, 2024, doi: 10.1016/j.enbuild.2024.114109.
- [93] DWD, *Climate data Center (CDC)*. Open Data Server: The Deutscher Wetterdienst (DWD), 2022.
- [94] Bayerische Vermessungsverwaltung, *Bayern Atlas*. [Online]. Available: <https://geoportal.bayern.de/bayernatlas/?lang=de&topic=ba&catalogNodes=11&bgLayer=atkis>
- [95] Landeshauptstadt München Mobilitätsreferat, *Die Mobilitätsstrategie der Stadt München 2035*. [Online]. Available: https://cdn.muenchenunterwegs.de/live/static-content/2035_web_final.pdf

List of figures

Figure 1 Simulation process - Shading potential	33
Figure 2 Simulation process - Evapotranspiration potential	36
Figure 3 Case Study - Site location	39
Figure 4 Data Validation Monthly average indoor air temperature On-site measurements and simulation results.	43
Figure 5 CDH for Data Validation On-site measurements and Simulation results	45
Figure 6 Cooling Potential per Tree – Summer average temperature reduction per analysis year 2nd Floor RCP 4.5.....	53
Figure 7 Time per operative temperature range and CDH per scenario by 2100 2nd Floor RCP 4.5	55
Figure 8 Cooling Potential per Tree – Summer average temperature reduction per analysis year 1st Floor RCP 4.5	56
Figure 9 Time per operative temperature range and CDH per scenario by 2100 1st Floor RCP 4.5	57
Figure 10 Cooling Potential per Tree – Summer average temperature reduction per analysis year Ground Floor RCP 4.5.....	58
Figure 11 Time per operative temperature range and CDH per scenario by 2100 Ground Floor RCP 4.5.....	60
Figure 12 Cooling Potential per Tree – Summer average temperature reduction per analysis year 2nd Floor RCP 8.5.....	61
Figure 13 Time per operative temperature range and CDH per scenario by 2100 2nd Floor RCP 8.5	63
Figure 14 Cooling Potential per Tree – Summer average temperature reduction per analysis year 1st Floor RCP 8.5	64
Figure 15 Time per operative temperature range and CDH per scenario by 2100 1st Floor RCP 8.5	65
Figure 16 Cooling Potential per Tree – Summer average temperature reduction per analysis year Ground Floor RCP 8.5.....	66
Figure 17 Time per operative temperature range and CDH per scenario by 2100 Ground Floor RCP 8.5.....	67
Figure 18 Box plot of the cooling potential through evapotranspiration per tree species in the summer average outdoor air temperature at each $T_{air \downarrow}$, T_{target} 2020-2100 RCP 4.5	69

List of figures

Figure 19 | Evapotranspiration potential on the outdoor air temperature per tree species | 2050 -2100 | RCP 4.570

Figure 20 | Box plot of the cooling potential through evapotranspiration per tree species in the summer average outdoor air temperature at each $T_{air\downarrow,Target}$ | 2020-2100 | RCP 8.5.....71

Figure 21 | Evapotranspiration potential on the outdoor air temperature per tree species | 2050 -2100 | RCP 8.572

Figure 22 | Box plot of the cooling potential through evapotranspiration per tree species in the summer average operative temperature of the office at each $T_{air\downarrow,Target}$ | 2020-2100 | RCP 4.573

Figure 23 | Cooling potential through evapotranspiration per tree species per $T_{air\downarrow,Target}$ | 2050 - RCP 4.575

Figure 24 | Cooling potential through evapotranspiration per tree species per $T_{air\downarrow,Target}$ | 2100 - RCP 4.575

Figure 25 | Box plot of the cooling potential through evapotranspiration per tree species per $T_{air\downarrow,Target}$ | 2020-2100 in RCP 8.576

Figure 26 | Cooling potential through evapotranspiration per tree species per $T_{air\downarrow,Target}$ | 2050 - RCP 8.578

Figure 27 | Cooling potential through evapotranspiration per tree species per $T_{air\downarrow,Target}$ | | 2100 - RCP 8.578

Figure 28 | Share of cooling potential per tree species | 2050 - RCP 4.580

Figure 29 | Share of cooling potential per tree species | 2100 - RCP 4.580

Figure 30 | Share of cooling potential per tree species | 2050 - RCP 8.582

Figure 31 | Share of cooling potential per tree species | 2100 - RCP 8.582

Figure 32 | Cooling Potential Shading and Evapotranspiration per Tree species at $T_{air\downarrow},1.5^{\circ}C$ | Summer average operative temperature reduction per analysis year | 2nd Floor | RCP 4.5.....83

Figure 33 | Time per operative temperature range and CDH per scenario by 2100 | 2nd Floor | RCP 4.585

Figure 34 | Cooling Potential Shading and evapotranspiration per Tree species at $T_{air\downarrow},1.5^{\circ}C$ | Summer average temperature reduction per analysis year | 2nd Floor | RCP 8.5.....86

Figure 35 | Time per operative temperature range and CDH per scenario by 2100 | 2nd Floor | RCP 8.5.....88

List of Tables

Table 1 Cooling potential through evapotranspiration Outdoor air temperature reduction related to transpiration rate of trees	25
Table 2 Building construction specifications	40
Table 3 Average monthly indoor air temperature per scenario	44
Table 4 CDH results for Data Validation On-site measurements and Simulation results	45
Table 5 Morphology per tree species from 2020 to 2100	47
Table 6 Leaf development and seasonal transparency per tree species for the climate change projections RCP 4.5 and RCP 8.5	48
Table 7 Data for average air temperature calculations Daily average air temperature reduction target of 0.25°C ($T_{air} \downarrow, 0.25^{\circ}C$) RCP 4.5	49
Table 8 Cooling degree hours per analysis year per scenario 2nd Floor RCP 4.5	54
Table 9 Cooling degree hours per analysis year per scenario 1st Floor RCP 4.5	57
Table 10 Cooling degree hours per analysis year per scenario Ground Floor RCP 4.5	59
Table 11 Cooling degree hours per analysis year per scenario 2nd Floor RCP 8.5	62
Table 12 Cooling degree hours per analysis year per scenario 1st Floor RCP 8.5	64
Table 13 - Cooling degree hours per analysis year per scenario Ground Floor RCP 8.5	67
Table 14 Summary - Evapotranspiration rate in the summer average outdoor air temperature per tree species at each $T_{air} \downarrow, Target$ between 2050 and 2100 RCP 4.5	70
Table 15 Summary - Evapotranspiration rate in the summer average outdoor air temperature per tree species at each $T_{air} \downarrow, Target$ between 2050 and 2100 RCP 8.5	72
Table 16 Cooling potential through evapotranspiration per tree species per $T_{air} \downarrow, Target$ 2050 to 2100 with RCP 4.5	74
Table 17 Cooling potential through evapotranspiration per tree species per $T_{air} \downarrow, Target$ 2050 to 2100 in RCP 8.5	77
Table 18 Cooling degree hours per analysis year per scenario 2nd Floor RCP 4.5	84

List of Tables

Table 19 | Cooling degree hours per analysis year per scenario | 2nd Floor | RCP
8.587

Appendix

Table of content

1 Case study Architectural and schematic plans.....	118
2 Trees species data	121
3 Weather of Munich Climate Change Projections.....	123
4.1 Results Cooling potential Shading Operative temperature reduction per tree species between 2020 and 2100.....	125
5.1 Results Cooling potential Evapotranspiration Outdoor air temperature reduction per tree species for each Tair ↓, Target between 2020 and 2100	131
5.2 Results Cooling potential Evapotranspiration Operative temperature reduction per tree species for each Tair ↓, Target. between 2020 and 2100	137
5.3 Results Cooling potential Shading + Evapotranspiration Operative temperature reduction per tree species for each Tair ↓, Target between 2020 and 2100.....	143
5.4 Results Cooling potential Shading + Evapotranspiration CDH per tree scenario at Tair ↓ ,1.5°C between 2020 and 2100.....	149

List of Tables

Appendix Table I Height of tree species in Munich, Germany.....	121
Appendix Table II Average annual outdoor air temperature per year RCP 4.5 ...	123
Appendix Table III Average annual outdoor air temperature per year RCP 8.5 ..	124
Appendix Table IV Cooling Potential per Tree Summer average operative temperature reduction per analysis year 2nd Floor RCP 4.5.....	125
Appendix Table V Cooling Potential per Tree Summer average operative temperature reduction per analysis year 1st Floor RCP 4.5.....	125
Appendix Table VI Cooling Potential per Tree Summer average operative temperature reduction per analysis year Ground Floor RCP 4.5.....	126
Appendix Table VII Cooling Potential per Tree Summer average operative temperature reduction per analysis year 2nd Floor RCP 8.5.....	126
Appendix Table VIII Cooling Potential per Tree Summer average operative temperature reduction per analysis year 1st Floor RCP 8.5.....	127
Appendix Table IX Cooling Potential per Tree Summer average operative temperature reduction per analysis year Ground Floor RCP 8.5.....	127

Appendix

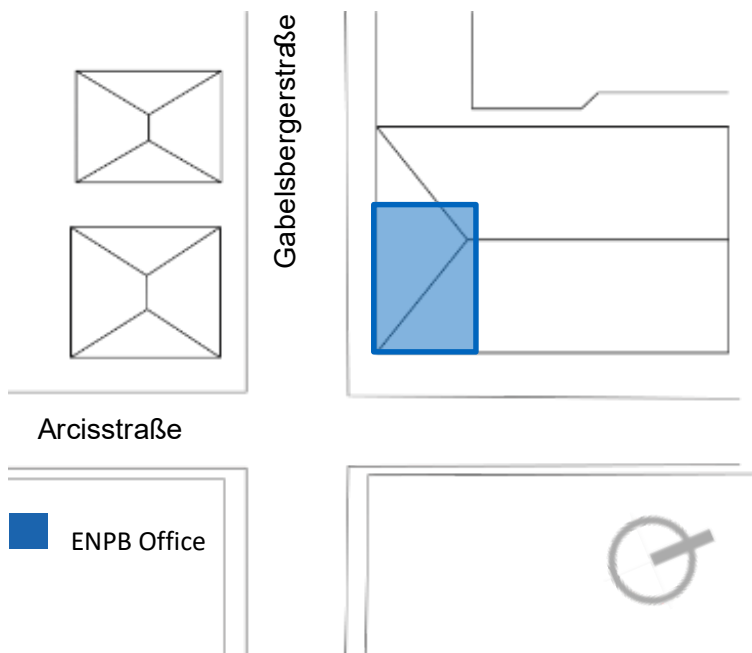
Appendix Table X Cooling degree hours per analysis year per scenario 2nd Floor RCP 4.5.....	128
Appendix Table XI Cooling degree hours per analysis year per scenario 1st Floor RCP 4.5.....	128
Appendix Table XII Cooling degree hours per analysis year per scenario Ground Floor RCP 4.5.....	129
Appendix Table XIII Cooling degree hours per analysis year per scenario 2nd Floor RCP 8.5.....	129
Appendix Table XIV - Cooling degree hours per analysis year per scenario 1st Floor RCP 8.5.....	130
Appendix Table XV - Cooling degree hours per analysis year per scenario Ground Floor RCP 8.5.....	130
Appendix Table XVI Cooling potential through evapotranspiration on the outdoor air temperature Betula P. with RCP 4.5	131
Appendix Table XVII Cooling potential through evapotranspiration on the outdoor air temperature Tilia C. with RCP 4.5.....	132
Appendix Table XVIII Cooling potential through evapotranspiration on the outdoor air temperature Lombardi P. with RCP 4.5	133
Appendix Table XIX Cooling potential through evapotranspiration on the outdoor air temperature Betula P. with RCP 8.5	134
Appendix Table XX Cooling potential through evapotranspiration on the outdoor air temperature Tilia C. with RCP 8.5.....	135
Appendix Table XXI Cooling potential through evapotranspiration on the outdoor air temperature Lombardi P. with RCP 8.5.....	136
Appendix Table XXII Total Cooling potential through evapotranspiration on the operative temperature Betula P. scenario 2nd floor with RCP 4.5	137
Appendix Table XXIII Total Cooling potential through evapotranspiration on the operative temperature Tilia C. scenario 2nd floor with RCP 4.5	138
Appendix Table XXIV Total Cooling potential through evapotranspiration on the operative temperature Lombardi P. scenario 2nd floor with RCP 4.5	139
Appendix Table XXV Total Cooling potential through evapotranspiration on the operative temperature Betula P. scenario 2nd floor with RCP 8.5	140
Appendix Table XXVI Total Cooling potential through evapotranspiration on the operative temperature Tilia C. scenario 2nd floor with RCP 8.5	141
Appendix Table XXVII Total Cooling potential through evapotranspiration on the operative temperature Lombardi P. scenario 2nd floor with RCP 8.5	142
Appendix Table XXVIII Total Cooling potential on the operative temperature Betula P. scenario 2 nd floor with RCP 4.5.....	143

Appendix Table XXIX Total Cooling potential on the operative temperature Tilia C. scenario 2 nd floor with RCP 4.5	144
Appendix Table XXX Total Cooling potential on the operative temperature Lombardi P. scenario 2 nd floor with RCP 4.5	145
Appendix Table XXXI Total Cooling potential on the operative temperature Betula P. scenario 2 nd floor with RCP 8.5	146
Appendix Table XXXII Total Cooling potential on the operative temperature Tilia C. scenario 2 nd floor with RCP 8.5	147
Appendix Table XXXIII Total Cooling potential on the operative temperature Lombardi P. scenario 2 nd floor with RCP 8.5	148
Appendix Table XXXIV Cooling degree hours per analysis year per scenario 2nd Floor RCP 4.5	149
Appendix Table XXXV Cooling degree hours per analysis year per scenario 2nd Floor RCP 8.5	149

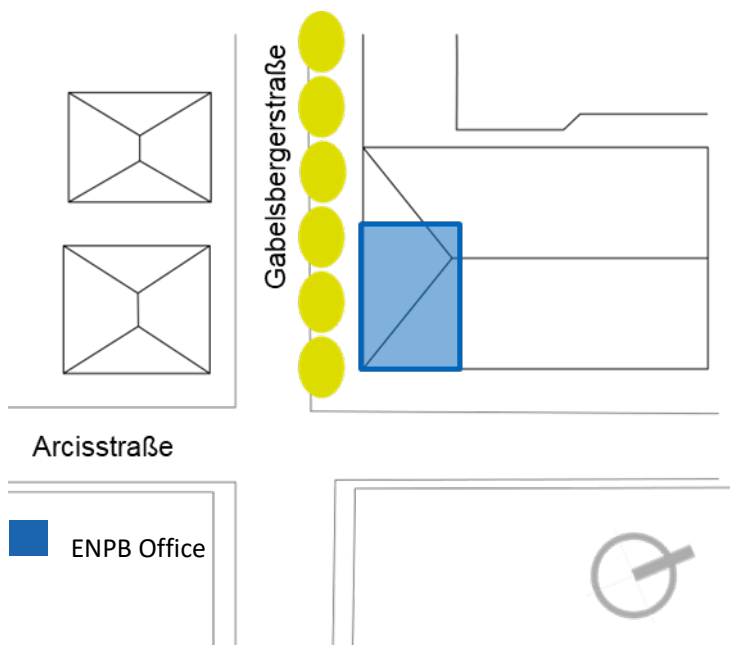
List of Figures

Appendix Figure I Site plan Baseline scenario	118
Appendix Figure II Site plan Proposal scenario (Lombardi P. trees)	118
Appendix Figure III Floor plan ENPB Office	119
Appendix Figure IV ENPB Office Cross Section and interior views.....	119
Appendix Figure V ENPB Office Longitudinal section	119
Appendix Figure VI Schematic Side view Arcisstraße Baseline	120
Appendix Figure VII Schematic Side view Arcisstraße Proposal scenario (Lombardi P. trees) ENPB Office 2 nd Floor in 2020.....	120
Appendix Figure VIII Schematic Side view Arcisstraße Proposal scenario (Lombardi P. trees) Hypothetical office 1st Floor in 2020.....	120
Appendix Figure IX Schematic Side view Arcisstraße Proposal scenario (Lombardi P. trees) Hypothetical office Ground Floor in 2020.....	120

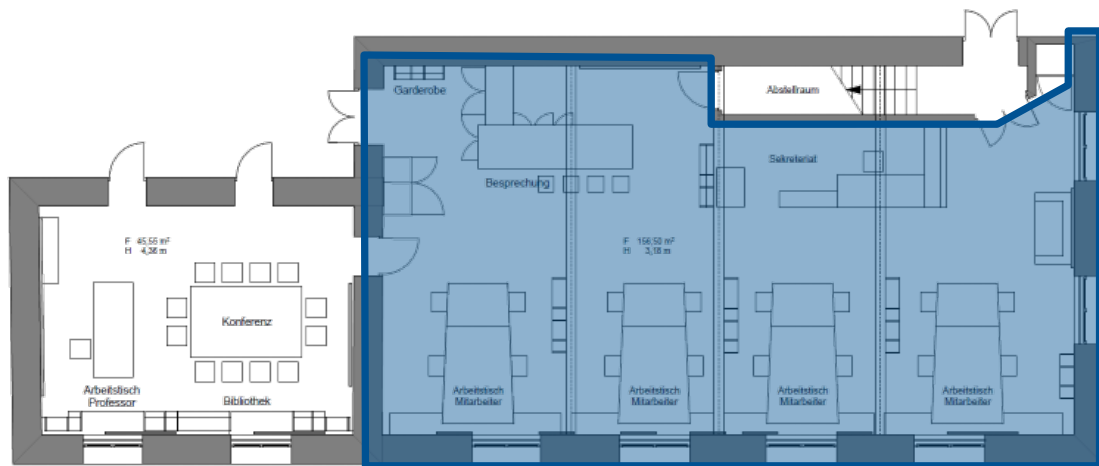
1 | Case study | Architectural and schematic plans



Appendix | Figure I | Site plan | Baseline scenario

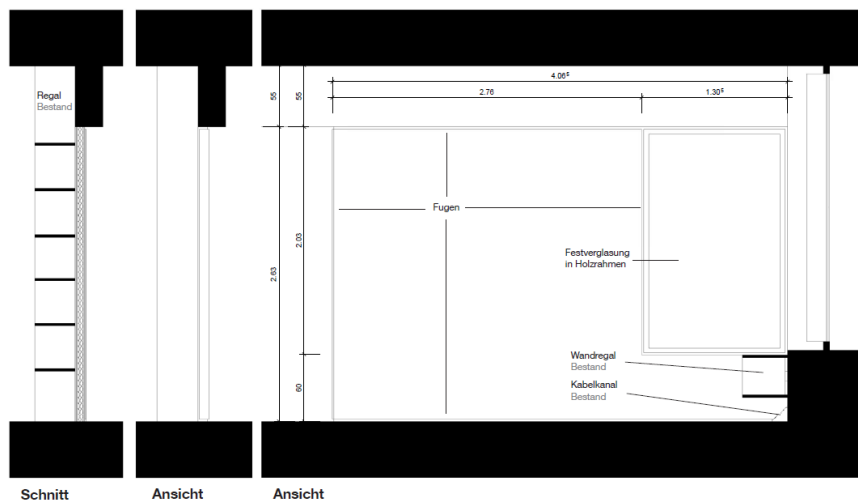


Appendix | Figure II | Site plan | Proposal scenario (Lombardi P. trees)

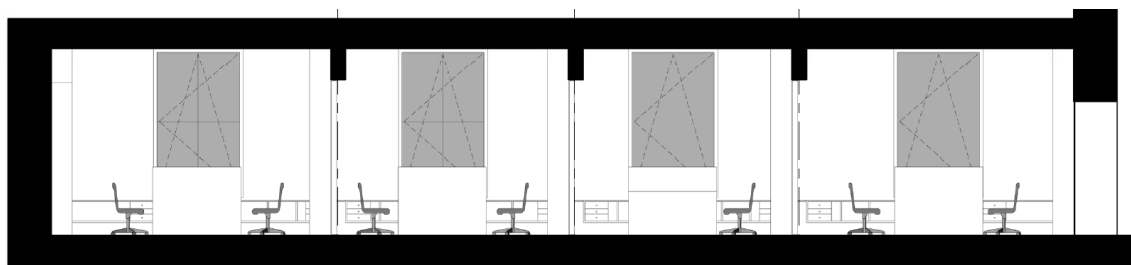


ENPB Open office – 2F

Appendix | Figure III | Floor plan | ENPB Office

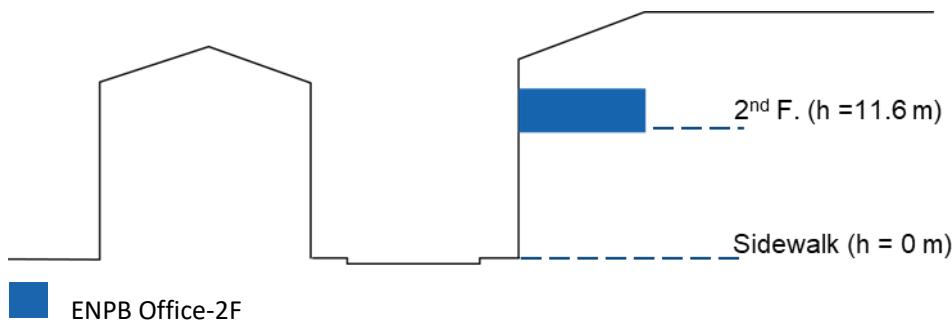


Appendix | Figure IV | ENPB Office | Cross Section and interior views

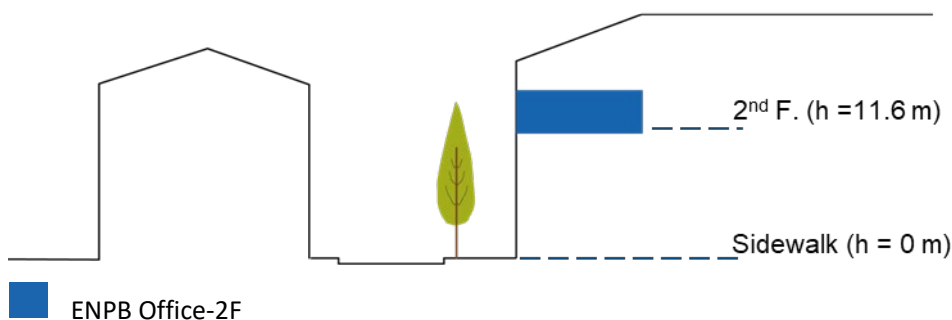


Appendix | Figure V | ENPB Office | Longitudinal section

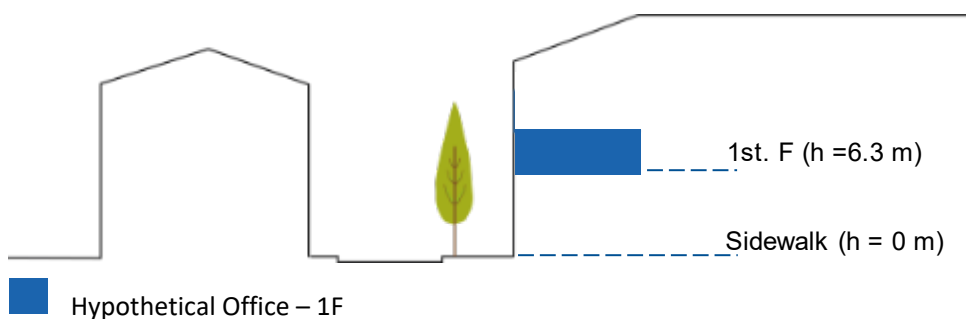
Appendix



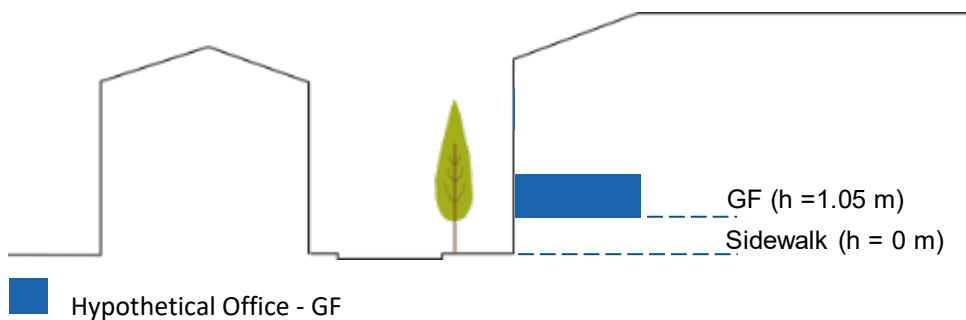
Appendix | Figure VI | Schematic Side view Arcisstraße | Baseline



Appendix | Figure VII | Schematic Side view Arcisstraße | Proposal scenario (Lombardi P. trees) | ENPB Office | 2nd Floor in 2020




Appendix | Figure VIII | Schematic Side view Arcisstraße | Proposal scenario (Lombardi P. trees) | Hypothetical office | 1st Floor in 2020




Appendix | Figure IX | Schematic Side view Arcisstraße | Proposal scenario (Lombardi P. trees) | Hypothetical office | Ground Floor in 2020

2 | Trees species data

Appendix | Table I | Height of tree species in Munich, Germany

Tree species	Image
<p data-bbox="309 548 590 638">Betula P. Approx. Height: 16 m</p> <p data-bbox="309 712 619 855">Location: Milbertshofener Str. 47, 80807 Munich</p>	
<p data-bbox="309 1265 590 1355">Tilia C. Approx. Height: 16 m</p> <p data-bbox="309 1429 587 1563">Location: Bordeauxplatz, Wörthstraße, Munich</p>	

Tree species	Image
<p>Lombardi P. Approx. Height: 28 m</p> <p>Location: TUM Main Campus, north site, building N3 Heißstraße 30, 80799 München</p>	 A photograph showing a tall, slender Lombardi tree (Lombardi P.) standing next to a modern building with a grid of windows. The tree is green and reaches a height of approximately 28 meters. The building is multi-storied with a light-colored facade and dark window frames. A white van is parked on the street in front of the building. The sky is blue with some light clouds.

3 | Weather of Munich | Climate Change Projections

Appendix | Table II | Average annual outdoor air temperature per year | RCP 4.5

Period	Average	Maximum
2020	11.8	33.8
2030	12.1	34.1
2040	12.5	34.7
2050	12.9	35.2
2060	13.1	35.3
2070	13.3	35.4
2080	13.5	35.6
2090	13.7	35.6
2100	13.9	35.8

Appendix | Table III | Average annual outdoor air temperature per year | RCP 8.5

Period	Average	Maximum
2020	11.8	33.6
2030	12.2	34.1
2040	12.8	34.9
2050	13.4	35.7
2060	14.0	36.5
2070	14.7	37.4
2080	15.4	38.4
2090	16.1	39.3
2100	16.8	40.2

4.1 | Results | Cooling potential | Shading | Operative temperature reduction per tree species between 2020 and 2100

Appendix | Table IV | Cooling Potential per Tree | Summer average operative temperature reduction per analysis year | 2nd Floor | RCP 4.5

Analysis Year		2020	2030	2040	2050	2060	2070	2080	2090	2100
Operative Temperature No Trees ¹ [°C]		28.4	28.8	29.0	29.0	29.3	29.4	29.7	29.5	29.8
Cooling Potential Reduction ² [°C]	Betula P.	0.02	0.08	0.33	0.68	1.14	1.50	1.71	1.96	2.22
	Tilia C.	-0.01	0.05	0.12	0.28	0.58	0.97	1.16	1.26	1.43
	Lombardi P.	0.05	0.23	0.80	1.18	1.56	1.75	1.97	1.96	2.12

1- Summer average Operative Temperature

2- Summer average Operative Temperature reduction related to the scenario without trees

Appendix | Table V | Cooling Potential per Tree | Summer average operative temperature reduction per analysis year | 1st Floor | RCP 4.5

Analysis Year		2020	2030	2040	2050	2060	2070	2080	2090	2100
Operative Temperature No Trees ¹ [°C]		28.3	28.7	28.9	29.0	29.2	29.3	29.6	29.4	29.7
Cooling Potential Reduction ² [°C]	Betula P.	0.12	0.40	0.78	1.17	1.53	1.89	2.04	2.17	2.41
	Tilia C.	0.09	0.31	0.68	1.16	1.48	1.86	2.12	2.18	2.36
	Lombardi P.	0.36	0.86	1.36	1.64	1.85	2.04	2.24	2.17	2.35

1- Summer average Operative Temperature

2- Summer average Operative Temperature reduction related to the scenario without trees

Appendix | Table VI | Cooling Potential per Tree | Summer average operative temperature reduction per analysis year | Ground Floor | RCP 4.5

Analysis Year		2020	2030	2040	2050	2060	2070	2080	2090	2100
Operative Temperature No Trees ¹ [°C]		28.1	28.5	28.7	28.8	29.0	29.0	29.3	29.2	29.4
Cooling Potential Reduction ² [°C]	Betula P.	0.31	0.62	0.89	1.24	1.49	1.78	1.92	1.87	2.02
	Tilia C.	0.23	0.83	1.18	1.46	1.64	1.91	2.18	2.20	2.33
	Lombardi P.	0.66	1.05	1.36	1.63	1.74	1.89	2.09	2.03	2.18

- 1- Summer average Operative Temperature
- 2- Summer average Operative Temperature reduction related to the scenario without trees

Appendix | Table VII | Cooling Potential per Tree | Summer average operative temperature reduction per analysis year | 2nd Floor | RCP 8.5

Analysis Year		2020	2030	2040	2050	2060	2070	2080	2090	2100
Operative Temperature No Trees ¹ [°C]		28.7	28.9	29.2	29.5	29.9	30.2	30.6	31.0	31.6
Cooling Potential Reduction ² [°C]	Betula P.	0.02	0.09	0.34	0.70	1.16	1.47	1.63	1.93	2.08
	Tilia C.	0.01	0.07	0.13	0.33	0.60	0.95	1.11	1.26	1.34
	Lombardi P.	0.06	0.22	0.84	1.20	1.58	1.72	1.88	1.94	2.00

- 1- Summer average Operative Temperature
- 2- Summer average Operative Temperature reduction related to the scenario without trees

Appendix | Table VIII | Cooling Potential per Tree | Summer average operative temperature reduction per analysis year | 1st Floor | RCP 8.5

Analysis Year		2020	2030	2040	2050	2060	2070	2080	2090	2100
Operative Temperature No Trees ¹ [°C]		28.5	28.7	29.0	29.3	29.7	30.0	30.5	30.8	31.4
Cooling Potential Reduction ² [°C]	Betula P.	0.02	0.29	0.70	1.07	1.45	1.77	1.87	2.07	2.18
	Tilia C.	-0.02	0.21	0.60	1.06	1.41	1.72	1.93	2.10	2.14
	Lombardi P.	0.28	0.76	1.26	1.56	1.79	1.93	2.06	2.07	2.16

1- Summer average Operative Temperature

2- Summer average Operative Temperature reduction related to the scenario without trees

Appendix | Table IX | Cooling Potential per Tree | Summer average operative temperature reduction per analysis year | Ground Floor | RCP 8.5

Analysis Year		2020	2030	2040	2050	2060	2070	2080	2090	2100
Operative Temperature No Trees ¹ [°C]		28.2	28.5	28.7	29.1	29.4	29.8	30.3	30.6	31.2
Cooling Potential Reduction ² [°C]	Betula P.	0.22	0.51	0.79	1.12	1.40	1.68	1.74	1.78	1.87
	Tilia C.	0.16	0.74	1.09	1.34	1.57	1.81	2.02	2.14	2.18
	Lombardi P.	0.60	0.98	1.25	1.53	1.66	1.80	1.93	1.93	2.04

1- Summer average Operative Temperature

2- Summer average Operative Temperature reduction related to the scenario without trees

4.2 | Results | Shading potential | CDH per tree species between 2020 and 2100

Appendix | Table X | Cooling degree hours per analysis year per scenario | 2nd Floor | RCP 4.5

CDH26/26 [Kh]	2020	2030	2040	2050	2060	2070	2080	2090	2100
No Trees	6,350	7,313	7,588	6,976	7,718	7,901	8,398	8,232	8,701
Betula P.	6,320	7,155	6,932	5,698	5,612	5,068	5,300	4,694	4,744
Tilia C.	6,368	7,225	7,359	6,463	6,612	6,065	6,230	5,877	6,046
Lombardi P.	6,259	6,898	6,131	4,871	4,967	4,656	4,897	4,693	4,915

Appendix | Table XI | Cooling degree hours per analysis year per scenario | 1st Floor | RCP 4.5

CDH26/26 [Kh]	2020	2030	2040	2050	2060	2070	2080	2090	2100
No Trees	6,146	7,114	7,385	6,863	7,501	7,713	8,210	8,045	8,468
Betula P.	5,945	6,351	5,945	4,763	4,839	4,263	4,610	4,243	4,284
Tilia C.	6,003	6,556	6,150	4,797	4,949	4,349	4,507	4,256	4,354
Lombardi P.	5,532	5,530	4,993	4,016	4,369	4,025	4,312	4,250	4,365

Appendix | Table XII | Cooling degree hours per analysis year per scenario | Ground Floor | RCP 4.5

CDH26/26 [Kh]	2020	2030	2040	2050	2060	2070	2080	2090	2100
No Trees	5,791	6,677	6,973	6,513	7,111	7,285	7,740	7,693	7,921
Betula P.	5,245	5,532	5,378	4,355	4,588	4,053	4,389	4,378	4,444
Tilia C.	5,399	5,188	4,927	4,024	4,392	3,870	4,009	3,930	3,993
Lombardi P.	4,632	4,783	4,614	3,747	4,227	3,876	4,131	4,166	4,208

Appendix | Table XIII | Cooling degree hours per analysis year per scenario | 2nd Floor | RCP 8.5

CDH26/26 [Kh]	2020	2030	2040	2050	2060	2070	2080	2090	2100
No Trees	7,050	7,164	7,509	8,172	8,871	9,233	9,843	10,418	11,566
Betula P.	7,032	7,005	6,845	6,852	6,716	6,601	6,788	6,891	7,801
Tilia C.	7,042	7,046	7,255	7,566	7,739	7,505	7,747	8,045	9,109
Lombardi P.	6,955	6,763	6,035	6,010	6,020	6,216	6,359	6,896	7,945

Appendix

Appendix | Table XIV - Cooling degree hours per analysis year per scenario | 1st Floor | RCP 8.5

CDH26/26 [Kh]	2020	2030	2040	2050	2060	2070	2080	2090	2100
No Trees	6,691	6,790	7,142	7,822	8,500	8,946	9,496	10,112	11,264
Betula P.	6,665	6,240	5,882	5,884	5,886	5,876	6,076	6,448	7,392
Tilia C.	6,737	6,408	6,089	5,935	5,970	5,975	6,009	6,416	7,496
Lombardi P.	6,177	5,475	5,011	5,067	5,329	5,612	5,757	6,436	7,429

Appendix | Table XV - Cooling degree hours per analysis year per scenario | Ground Floor | RCP 8.5

CDH26/26 [Kh]	2020	2030	2040	2050	2060	2070	2080	2090	2100
No Trees	6,329	6,437	6,802	7,458	8,064	8,579	9,156	9,756	10,970
Betula P.	5,899	5,540	5,444	5,446	5,588	5,718	6,015	6,614	7,617
Tilia C.	6,036	5,167	4,986	5,097	5,313	5,527	5,577	6,086	7,136
Lombardi P.	5,236	4,741	4,709	4,775	5,158	5,521	5,693	6,374	7,346

5.1 | Results | Cooling potential | Evapotranspiration | Outdoor air temperature reduction per tree species for each $T_{air\downarrow,Target}$ between 2020 and 2100

Appendix | Table XVI | Cooling potential through evapotranspiration on the outdoor air temperature | Betula P. with RCP 4.5

Analysis Year		2020	2030	2040	2050	2060	2070	2080	2090	2100
Outdoor Air Temperature ¹ [°C]		16.88	17.32	17.69	18.06	18.39	18.52	18.77	18.97	19.14
Cooling Potential Reduction ² [°C]	0.25	0.02	0.03	0.06	0.11	0.18	0.26	0.29	0.38	0.43
	0.5	0.03	0.06	0.12	0.22	0.35	0.51	0.58	0.75	0.85
	0.75	0.05	0.09	0.18	0.32	0.53	0.77	0.87	1.13	1.28
	1	0.07	0.12	0.24	0.43	0.71	1.02	1.16	1.50	1.71
	1.25	0.08	0.15	0.30	0.54	0.88	1.28	1.45	1.88	2.13
	1.5	0.10	0.18	0.36	0.65	1.06	1.54	1.74	2.26	2.56

1- Summer average outdoor air temperature

2- Summer average outdoor air temperature reduction related to the initial outdoor air temperature per daily average outdoor air temperature reduction target

Appendix | Table XVII | Cooling potential through evapotranspiration on the outdoor air temperature | Tilia C. with RCP 4.5

Analysis Year		2020	2030	2040	2050	2060	2070	2080	2090	2100
Outdoor Air Temperature ¹ [°C]		16.88	17.32	17.69	18.06	18.39	18.52	18.77	18.97	19.14
Cooling Potential Reduction ² [°C]	0.25	0.00	0.01	0.04	0.09	0.16	0.24	0.28	0.37	0.41
	0.5	0.02	0.05	0.11	0.20	0.34	0.50	0.57	0.75	0.83
	0.75	0.03	0.08	0.17	0.31	0.52	0.76	0.86	1.13	1.26
	1	0.05	0.11	0.23	0.42	0.70	1.02	1.15	1.51	1.68
	1.25	0.07	0.14	0.29	0.53	0.88	1.27	1.44	1.89	2.10
	1.5	0.08	0.17	0.35	0.64	1.06	1.53	1.73	2.27	2.53

- 1- Summer average outdoor air temperature
- 2- Summer average outdoor air temperature reduction related to the initial outdoor air temperature per daily average outdoor air temperature reduction target

Appendix | Table XVIII | Cooling potential through evapotranspiration on the outdoor air temperature | Lombardi P. with RCP 4.5

Analysis Year		2020	2030	2040	2050	2060	2070	2080	2090	2100
Outdoor Air Temperature ¹ [°C]		16.88	17.32	17.69	18.06	18.39	18.52	18.77	18.97	19.14
Cooling Potential Reduction ² [°C]	0.25	0.00	0.01	0.04	0.09	0.16	0.24	0.27	0.36	0.41
	0.5	0.02	0.05	0.11	0.20	0.34	0.49	0.56	0.73	0.84
	0.75	0.03	0.08	0.17	0.31	0.51	0.75	0.85	1.10	1.27
	1	0.00	0.01	0.04	0.09	0.16	0.24	0.27	0.36	0.41
	1.25	0.07	0.14	0.29	0.52	0.87	1.26	1.43	1.85	2.12
	1.5	0.08	0.17	0.35	0.63	1.04	1.52	1.72	2.23	2.55

1- Summer average outdoor air temperature

2- Summer average outdoor air temperature reduction related to the initial outdoor air temperature per daily average outdoor air temperature reduction target

Appendix | Table XIX | Cooling potential through evapotranspiration on the outdoor air temperature | Betula P. with RCP 8.5

Analysis Year		2020	2030	2040	2050	2060	2070	2080	2090	2100
Outdoor Air Temperature ¹ [°C]		16.89	17.41	18.03	18.58	19.29	20.05	20.81	21.55	22.32
Cooling Potential Reduction ² [°C]	0.25	0.02	0.03	0.06	0.11	0.18	0.26	0.30	0.39	0.45
	0.5	0.03	0.06	0.12	0.22	0.36	0.53	0.60	0.77	0.90
	0.75	0.05	0.09	0.18	0.32	0.54	0.79	0.90	1.16	1.36
	1	0.06	0.12	0.24	0.43	0.72	1.05	1.20	1.54	1.81
	1.25	0.08	0.15	0.30	0.54	0.90	1.31	1.50	1.93	2.26
	1.5	0.09	0.18	0.36	0.65	1.07	1.58	1.80	2.31	2.71

1- Summer average outdoor air temperature

2- Summer average outdoor air temperature reduction related to the initial outdoor air temperature per daily average outdoor air temperature reduction target

Appendix | Table XX | Cooling potential through evapotranspiration on the outdoor air temperature | Tilia C. with RCP 8.5

Analysis Year		2020	2030	2040	2050	2060	2070	2080	2090	2100
Outdoor Air Temperature ¹ [°C]		16.89	17.41	18.03	18.58	19.29	20.05	20.81	21.55	22.32
Cooling Potential Reduction ² [°C]	0.25	0.02	0.03	0.06	0.11	0.18	0.26	0.30	0.39	0.46
	0.5	0.03	0.06	0.12	0.22	0.36	0.53	0.61	0.78	0.92
	0.75	0.05	0.09	0.18	0.33	0.55	0.79	0.91	1.17	1.37
	1	0.06	0.12	0.24	0.43	0.73	1.06	1.21	1.55	1.83
	1.25	0.08	0.15	0.30	0.54	0.91	1.32	1.51	1.94	2.29
	1.5	0.09	0.18	0.36	0.65	1.09	1.59	1.82	2.33	2.75

1- Summer average outdoor air temperature

2- Summer average outdoor air temperature reduction related to the initial outdoor air temperature per daily average outdoor air temperature reduction target

Appendix | Table XXI | Cooling potential through evapotranspiration on the outdoor air temperature | Lombardi P. with RCP 8.5

Analysis Year		2020	2030	2040	2050	2060	2070	2080	2090	2100
Outdoor Air Temperature ¹ [°C]		16.89	17.41	18.03	18.58	19.29	20.05	20.81	21.55	22.32
Cooling Potential Reduction ² [°C]	0.25	0.02	0.03	0.06	0.11	0.18	0.26	0.30	0.38	0.45
	0.5	0.03	0.06	0.12	0.22	0.36	0.53	0.60	0.76	0.90
	0.75	0.05	0.09	0.18	0.32	0.54	0.79	0.90	1.15	1.35
	1	0.06	0.12	0.24	0.43	0.72	1.05	1.19	1.53	1.79
	1.25	0.08	0.15	0.30	0.54	0.89	1.31	1.49	1.91	2.24
	1.5	0.09	0.18	0.36	0.65	1.07	1.58	1.79	2.29	2.69

- 1- Summer average outdoor air temperature
- 2- Summer average outdoor air temperature reduction related to the initial outdoor air temperature per daily average outdoor air temperature reduction target

5.2 | Results | Cooling potential | Evapotranspiration | Operative temperature reduction per tree species for each $T_{air\downarrow,Target}$ between 2020 and 2100

Appendix | Table XXII | Total Cooling potential through evapotranspiration on the operative temperature | Betula P. scenario | 2nd floor with RCP 4.5

Analysis Year		2020	2030	2040	2050	2060	2070	2080	2090	2100
Operative Temperature ¹ [°C]		28.44	28.84	29.04	29.01	29.34	29.39	29.65	29.48	29.79
Cooling Potential Reduction ² [°C]	0.25	-0.003	0.01	0.01	0.04	0.04	0.05	0.10	0.18	0.13
	0.5	-0.017	0.02	0.02	0.08	0.09	0.10	0.13	0.30	0.32
	0.75	-0.005	0.03	0.03	0.09	0.09	0.12	0.17	0.38	0.33
	1	-0.008	0.03	0.06	0.09	0.06	0.19	0.18	0.47	0.40
	1.25	-0.004	0.03	0.06	0.13	0.09	0.18	0.17	0.51	0.47
	1.5	-0.005	0.02	0.06	0.13	0.10	0.23	0.27	0.56	0.59

1- Summer average operative temperature

2- Summer average operative temperature reduction related to the baseline operative temperature at each daily average outdoor air temperature reduction target

Appendix | Table XXIII | Total Cooling potential through evapotranspiration on the operative temperature | Tilia C. scenario | 2nd floor with RCP 4.5

Analysis Year		2020	2030	2040	2050	2060	2070	2080	2090	2100
Operative Temperature ¹ [°C]		28.44	28.84	29.04	29.01	29.34	29.39	29.65	29.48	29.79
Cooling Potential Reduction ² [°C]	0.25	0.002	0.02	0.01	0.06	0.04	0.03	0.09	0.15	0.09
	0.5	-0.011	0.03	0.02	0.08	0.05	0.04	0.08	0.24	0.21
	0.75	-0.007	0.04	0.03	0.08	0.05	0.05	0.10	0.31	0.19
	1	-0.007	0.03	0.04	0.09	0.00	0.12	0.07	0.36	0.19
	1.25	-0.006	0.02	0.05	0.10	0.04	0.08	0.08	0.35	0.25
	1.5	0.000	0.02	0.05	0.13	0.02	0.11	0.14	0.39	0.36

- 1- Summer average operative temperature
- 2- Summer average operative temperature reduction related to the baseline operative temperature at each daily average outdoor air temperature reduction target

Appendix | Table XXIV | Total Cooling potential through evapotranspiration on the operative temperature | Lombardi P. scenario | 2nd floor with RCP 4.5

Analysis Year		2020	2030	2040	2050	2060	2070	2080	2090	2100
Operative Temperature ¹ [°C]		28.44	28.84	29.04	29.01	29.34	29.39	29.65	29.48	29.79
Cooling Potential Reduction ² [°C]	0.25	-0.002	0.01	0.02	0.05	0.05	0.06	0.13	0.18	0.14
	0.5	-0.005	0.02	0.03	0.10	0.10	0.13	0.15	0.31	0.33
	0.75	-0.005	0.03	0.05	0.11	0.12	0.16	0.18	0.36	0.34
	1	-0.009	0.04	0.07	0.12	0.09	0.24	0.21	0.44	0.40
	1.25	0.000	0.04	0.08	0.16	0.13	0.24	0.22	0.52	0.47
	1.5	-0.004	0.03	0.07	0.17	0.16	0.28	0.33	0.56	0.53

1- Summer average operative temperature

2- Summer average operative temperature reduction related to the baseline operative temperature at each daily average outdoor air temperature reduction target

Appendix | Table XXV | Total Cooling potential through evapotranspiration on the operative temperature | Betula P. scenario | 2nd floor with RCP 8.5

Analysis Year		2020	2030	2040	2050	2060	2070	2080	2090	2100
Operative Temperature ¹ [°C]		28.66	28.90	29.16	29.51	29.89	30.18	30.65	30.96	31.58
Cooling Potential Reduction ² [°C]	0.25	0.002	0.01	0.01	0.02	0.05	0.09	0.15	0.25	0.34
	0.5	0.006	0.02	0.04	0.06	0.09	0.23	0.31	0.47	0.68
	0.75	0.009	0.02	0.06	0.09	0.17	0.30	0.38	0.64	0.87
	1	0.011	0.01	0.05	0.12	0.21	0.28	0.44	0.72	1.00
	1.25	0.025	0.01	0.05	0.12	0.25	0.27	0.41	0.75	1.12
	1.5	0.034	0.01	0.06	0.15	0.29	0.35	0.46	0.87	1.28

- 1- Summer average operative temperature
- 2- Summer average operative temperature reduction related to the baseline operative temperature at each daily average outdoor air temperature reduction target

Appendix | Table XXVI | Total Cooling potential through evapotranspiration on the operative temperature | Tilia C. scenario | 2nd floor with RCP 8.5

Analysis Year		2020	2030	2040	2050	2060	2070	2080	2090	2100
Operative Temperature ¹ [°C]		28.66	28.90	29.16	29.51	29.89	30.18	30.65	30.96	31.58
Cooling Potential Reduction ² [°C]	0.25	-0.003	0.003	-0.0005	0.01	0.06	0.08	0.13	0.23	0.32
	0.5	0.002	0.011	0.04	0.07	0.07	0.21	0.28	0.41	0.64
	0.75	0.001	0.008	0.05	0.08	0.13	0.23	0.34	0.57	0.76
	1	0.003	0.000	0.03	0.09	0.17	0.22	0.36	0.63	0.88
	1.25	0.012	-0.008	0.04	0.10	0.19	0.22	0.36	0.63	1.01
	1.5	0.023	0.004	0.05	0.12	0.22	0.25	0.41	0.66	1.12

1- Summer average operative temperature

2- Summer average operative temperature reduction related to the baseline operative temperature at each daily average outdoor air temperature reduction target

Appendix | Table XXVII | Total Cooling potential through evapotranspiration on the operative temperature | Lombardi P. scenario | 2nd floor with RCP 8.5

Analysis Year		2020	2030	2040	2050	2060	2070	2080	2090	2100
Operative Temperature ¹ [°C]		28.66	28.90	29.16	29.51	29.89	30.18	30.65	30.96	31.58
Cooling Potential Reduction ² [°C]	0.25	0.004	0.005	-0.002	0.02	0.06	0.10	0.14	0.26	0.33
	0.5	0.013	0.016	0.040	0.08	0.10	0.25	0.30	0.46	0.68
	0.75	0.009	0.006	0.058	0.11	0.20	0.33	0.41	0.62	0.88
	1	0.013	0.006	0.065	0.14	0.23	0.33	0.46	0.72	0.99
	1.25	0.025	0.009	0.062	0.17	0.29	0.34	0.51	0.73	1.09
	1.5	0.029	0.007	0.079	0.18	0.34	0.40	0.48	0.86	1.29

- 1- Summer average operative temperature
- 2- Summer average operative temperature reduction related to the baseline operative temperature at each daily average outdoor air temperature reduction target

5.3 | Results | Cooling potential | Shading + Evapotranspiration | Operative temperature reduction per tree species for each $T_{air\downarrow,Target}$ between 2020 and 2100

Appendix | Table XXVIII | Total Cooling potential on the operative temperature | Betula P. scenario | 2nd floor with RCP 4.5

Analysis Year		2020	2030	2040	2050	2060	2070	2080	2090	2100
Operative Temperature ¹ [°C]		28.44	28.84	29.04	29.01	29.34	29.39	29.65	29.48	29.79
Cooling Potential Reduction ² [°C]	0.25	0.02	0.09	0.34	0.72	1.18	1.55	1.82	2.14	2.35
	0.5	0.00	0.10	0.35	0.76	1.23	1.60	1.84	2.26	2.54
	0.75	0.01	0.11	0.36	0.77	1.23	1.62	1.88	2.33	2.55
	1	0.01	0.12	0.39	0.77	1.20	1.69	1.90	2.43	2.62
	1.25	0.02	0.11	0.39	0.81	1.23	1.69	1.89	2.47	2.69
	1.5	0.01	0.10	0.39	0.80	1.25	1.73	1.98	2.52	2.81

1- Summer average operative temperature

2- Summer average operative temperature reduction related to the baseline operative temperature at each daily average outdoor air temperature reduction target

Appendix | Table XXIX | Total Cooling potential on the operative temperature | Tilia C. scenario | 2nd floor with RCP 4.5

Analysis Year		2020	2030	2040	2050	2060	2070	2080	2090	2100
Operative Temperature ¹ [°C]		28.44	28.84	29.04	29.01	29.34	29.39	29.65	29.48	29.79
Cooling Potential Reduction ² [°C]	0.25	-0.01	0.06	0.13	0.34	0.61	1.00	1.25	1.42	1.52
	0.5	-0.02	0.08	0.14	0.36	0.63	1.01	1.25	1.50	1.64
	0.75	-0.01	0.08	0.15	0.36	0.62	1.02	1.26	1.58	1.61
	1	-0.01	0.08	0.16	0.37	0.58	1.10	1.24	1.62	1.61
	1.25	-0.01	0.07	0.17	0.38	0.62	1.05	1.24	1.62	1.67
	1.5	-0.01	0.07	0.16	0.41	0.59	1.08	1.30	1.65	1.78

- 1- Summer average operative temperature
- 2- Summer average operative temperature reduction related to the baseline operative temperature at each daily average outdoor air temperature reduction target

Appendix | Table XXX | Total Cooling potential on the operative temperature | Lombardi P. scenario | 2nd floor with RCP 4.5

Analysis Year		2020	2030	2040	2050	2060	2070	2080	2090	2100
Operative Temperature ¹ [°C]		28.44	28.84	29.04	29.01	29.34	29.39	29.65	29.48	29.79
Cooling Potential Reduction ² [°C]	0.25	0.05	0.24	0.83	1.22	1.61	1.81	2.09	2.14	2.26
	0.5	0.05	0.25	0.83	1.28	1.66	1.88	2.11	2.27	2.45
	0.75	0.05	0.26	0.85	1.29	1.68	1.90	2.14	2.33	2.46
	1	0.05	0.26	0.88	1.29	1.65	1.98	2.17	2.41	2.52
	1.25	0.05	0.26	0.88	1.33	1.70	1.99	2.19	2.48	2.59
	1.5	0.05	0.25	0.88	1.35	1.72	2.02	2.30	2.52	2.65

1- Summer average operative temperature

2- Summer average operative temperature reduction related to the baseline operative temperature at each daily average outdoor air temperature reduction target

Appendix | Table XXXI | Total Cooling potential on the operative temperature | Betula P. scenario | 2nd floor with RCP 8.5

Analysis Year		2020	2030	2040	2050	2060	2070	2080	2090	2100
Operative Temperature ¹ [°C]		28.66	28.90	29.16	29.51	29.89	30.18	30.65	30.96	31.58
Cooling Potential Reduction ² [°C]	0.25	0.02	0.10	0.35	0.71	1.21	1.55	1.78	2.18	2.41
	0.5	0.03	0.11	0.38	0.75	1.25	1.69	1.93	2.39	2.76
	0.75	0.03	0.10	0.40	0.78	1.33	1.76	2.00	2.57	2.94
	1	0.03	0.09	0.39	0.81	1.36	1.74	2.06	2.65	3.08
	1.25	0.04	0.10	0.40	0.82	1.41	1.73	2.04	2.68	3.20
	1.5	0.05	0.10	0.40	0.84	1.44	1.81	2.09	2.80	3.36

- 1- Summer average operative temperature
- 2- Summer average operative temperature reduction related to the baseline operative temperature at each daily average outdoor air temperature reduction target

Appendix | Table XXXII | Total Cooling potential on the operative temperature | Tilia C. scenario | 2nd floor with RCP 8.5

Analysis Year		2020	2030	2040	2050	2060	2070	2080	2090	2100
Operative Temperature ¹ [°C]		28.66	28.90	29.16	29.51	29.89	30.18	30.65	30.96	31.58
Cooling Potential Reduction ² [°C]	0.25	0.00	0.07	0.13	0.34	0.65	1.02	1.24	1.49	1.65
	0.5	0.01	0.08	0.17	0.39	0.66	1.15	1.38	1.67	1.98
	0.75	0.01	0.08	0.18	0.40	0.72	1.17	1.44	1.82	2.10
	1	0.01	0.07	0.16	0.42	0.76	1.17	1.46	1.88	2.21
	1.25	0.02	0.06	0.17	0.43	0.79	1.16	1.46	1.89	2.34
	1.5	0.03	0.07	0.18	0.45	0.82	1.19	1.51	1.91	2.46

1- Summer average operative temperature

2- Summer average operative temperature reduction related to the baseline operative temperature at each daily average outdoor air temperature reduction target

Appendix | Table XXXIII | Total Cooling potential on the operative temperature | Lombardi P. scenario | 2nd floor with RCP 8.5

Analysis Year		2020	2030	2040	2050	2060	2070	2080	2090	2100
Operative Temperature ¹ [°C]		28.66	28.90	29.16	29.51	29.89	30.18	30.65	30.96	31.58
Cooling Potential Reduction ² [°C]	0.25	0.06	0.23	0.83	1.22	1.63	1.81	2.01	2.19	2.32
	0.5	0.07	0.24	0.87	1.27	1.67	1.96	2.18	2.38	2.68
	0.75	0.06	0.23	0.89	1.31	1.77	2.04	2.29	2.55	2.87
	1	0.07	0.23	0.90	1.34	1.80	2.04	2.33	2.65	2.99
	1.25	0.08	0.23	0.90	1.37	1.86	2.05	2.38	2.66	3.08
	1.5	0.08	0.23	0.91	1.38	1.91	2.11	2.36	2.79	3.28

- 1- Summer average operative temperature
- 2- Summer average operative temperature reduction related to the baseline operative temperature at each daily average outdoor air temperature reduction target

5.4 | Results | Cooling potential | Shading + Evapotranspiration | CDH per tree scenario at $T_{air\downarrow,1.5^\circ C}$ between 2020 and 2100

Appendix | Table XXXIV | Cooling degree hours per analysis year per scenario | 2nd Floor | RCP 4.5

CDH26/26 [Kh]	2020	2030	2040	2050	2060	2070	2080	2090	2100
No Trees	6,350	7,313	7,588	6,976	7,718	7,901	8,398	8,232	8,701
Betula P. S+E	6,336	7,066	6,813	5,530	5,441	4,870	4,910	3,846	3,909
Tilia C. S+E	6,370	7,116	7,284	6,284	6,591	6,088	6,130	5,313	5,571
Lombardi P. S+E	6,267	6,777	5,997	4,630	4,697	4,383	4,410	3,809	4,194

S + E = Cooling potential through Shadow + Evapotranspiration

Appendix | Table XXXV | Cooling degree hours per analysis year per scenario | 2nd Floor | RCP 8.5

CDH26/26 [Kh]	2020	2030	2040	2050	2060	2070	2080	2090	2100
No Trees	7,050	7,164	7,509	8,172	8,871	9,233	9,843	10,418	11,566
Betula P. S+E	6,979	6,900	6,729	6,483	6,138	5,641	5,858	5,089	5,123
Tilia C. S+E	7,018	6,943	7,163	7,223	7,254	6,721	6,909	6,667	6,806
Lombardi P. S+E	6,921	6,674	5,905	5,591	5,347	5,162	5,407	5,081	5,203

S + E = Cooling potential through Shadow + Evapotranspiration

